Test of Cracked Prestressed Concrete T-Beam Retrofitted for Shear using CFRP L-Shaped Plates

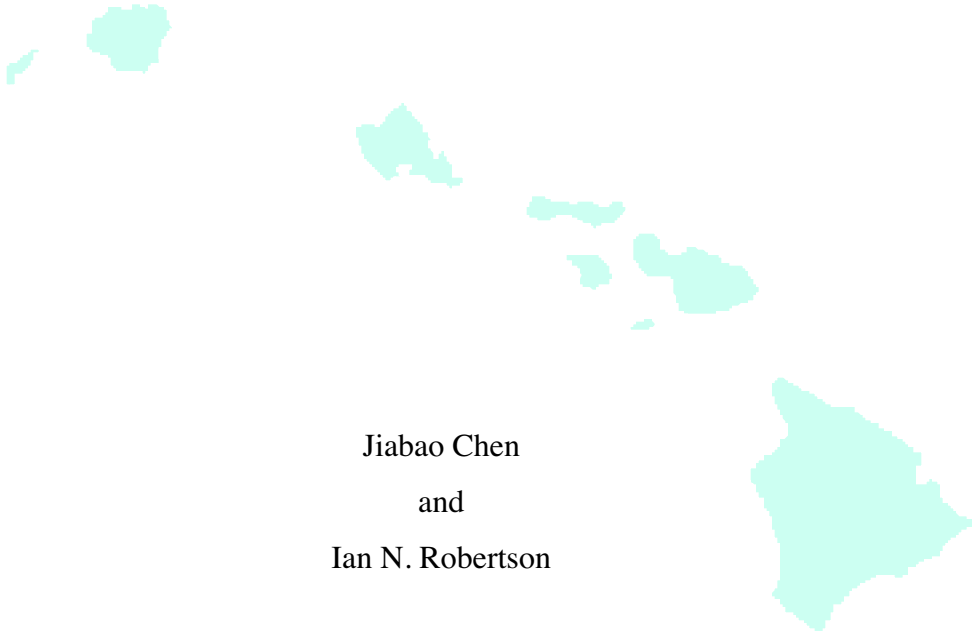

Jiabao Chen

and

Ian N. Robertson

Prepared in Cooperation with:

State of Hawaii, Department of Transportation, Highways Division

and

U.S. Department of Transportation, Federal Highway Administration

UNIVERSITY OF HAWAII
COLLEGE OF ENGINEERING

DEPARTMENT OF CIVIL AND ENVIRONMENTAL ENGINEERING

Research Report UHM/CEE/04-06
June 2004

Technical Report Documentation Page

1. Report No. HWY-L-2001-01	2. Government Accession No	3. Recipient's Catalog No
4. Title and Subtitle TEST OF CRACKED PRESTRESSED CONCRETE T-BEAM RETROFITTED FOR SHEAR USING CFRP L-SHAPED PLATES		5. Report Date June 16, 2004 6. Performing Organization Code
7. Authors Jiabao Chen, Ian N. Robertson		8. Performing Organization Report No.
9. Performing Organization Name and Address Department of Civil and Environmental Engineering University of Hawaii at Manoa 2540 Dole St. Holmes Hall 383 Honolulu, HI 96822		10. Work Unit No. (TRAIS) 11. Contract or Grant No. 47770
12. Sponsoring Agency Name and Address Hawaii Department of Transportation Highways Division 869 Punchbowl St. Honolulu, HI 96813		13. Type of Report and Period Covered Final – Phase 2 – Volume 2 5/01 – 4/04 14. Sponsoring Agency Code

15. Supplementary Notes

Prepared in cooperation with the U.S. Department of Transportation, Federal Highway Administration

16. Abstract

This research study involved a series of tests performed on a prestressed T-Beam recovered from the Ala Moana Shopping Center Parking Structure. The objective of this study was to evaluate the performance of CFRP L-shaped stirrups as a shear retrofit applied over existing shear cracks, particularly under cyclic loading conditions. The research was performed to provide guidance for the shear retrofit to be performed on cracked AASHTO girders in the Salt Lake Boulevard Bridge. In addition, the instrumentation system used in this study is evaluated for potential use in the field instrumentation of the Salt Lake Boulevard Bridge during and after application of the shear retrofit.

The left end of the T-Beam was tested to determine the shear capacity of the original beam (T-Beam 3C). The nominally identical right hand end of the beam was then subjected to a series of shear tests to induce shear cracks similar to those noted in the Salt Lake Boulevard Bridge girders. The right hand end of the beam was then retrofitted for shear with CarboShear-L stirrups applied over the cracked beam without epoxy injection of the existing cracks. Cementitious filler blocks were installed in the web of the beam to provide a smooth profile for installation of the vertical legs of the CarboShear-L stirrups. The final Shear Retrofit Test (T-Beam 3S) was performed to evaluate the effect of the retrofit on the crack widths under cyclic loading. The beam was then loaded monotonically to failure, which resulted from delamination of the flexural Carbodur strips bonded to the soffit of the beam.

The CarboShear-L stirrups prevented shear failure in the retrofitted right end shear span. They were effective at controlling the width of the existing shear cracks and prevented further growth of the cracks during cyclic loading. The anchorage at top and bottom of the CarboShear-L stirrups was effective even after delamination of the full vertical leg of the stirrup. Strain gages on the surface of the CFRP stirrups were effective for monitoring delamination of the stirrup.

17. Key Words	18. Distribution Statement
Fiber reinforced polymer (FRP) Prestressed girder Shear crack repair	No restriction. This document is available to the public through the National Technical Information Service 5285 Port Royal Road, Springfield VA 22161

19. Security Classif.(of this report)	20. Security Classif. (of this page)	21. No. of Pages	22. Price
Unclassified	Unclassified	188	

ABSTRACT

This research study involved a series of tests performed on a prestressed T-Beam recovered from the Ala Moana Shopping Center Parking Structure. The objective of this study was to evaluate the performance of CarboShear-L shear stirrup retrofit applied over existing shear cracks, particularly under cyclic loading conditions. The research was performed to provide guidance for the shear retrofit to be performed on the Salt Lake Boulevard Bridge. In addition, the instrumentation system used in this study is evaluated for potential use in the field instrumentation of the Salt Lake Boulevard Bridge during and after application of the shear retrofit.

The left hand end of the T-Beam was tested to determine the shear capacity of the original beam (T-Beam 3C). The nominally identical right hand end of the beam was then subjected to a series of shear tests to induce shear cracks similar to those noted in the Salt Lake Boulevard Bridge girders. The right hand end of the beam was then retrofitted for shear with CarboShear-L stirrups applied over the cracked beam without epoxy injection of the existing cracks. Cementitious filler blocks were installed in the web of the beam to provide a smooth profile for installation of the vertical legs of the CarboShear-L stirrups. The final Shear Retrofit Test (T-Beam 3S) was performed to evaluate the effect of the retrofit on the crack widths under cyclic loading. The beam was then loaded monotonically to failure, which resulted from delamination of the flexural Carbodur strips bonded to the soffit of the beam.

The CarboShear-L stirrups prevented shear failure in the retrofitted right end shear span. They were effective at controlling the width of the existing shear cracks and prevented further growth of the cracks during cyclic loading.

ACKNOWLEDGEMENTS

This report is based on a Master of Science thesis prepared by Jiabao Chen under the direction of Dr. Ian Robertson. The authors wish to express their gratitude to Drs. H. Ronald Riggs, Si-Hwan Park and Gregor Fischer for their effort in reviewing this report.

The authors are extremely grateful to Adriano "A. B." Bortolin of Sika Corporation, USA, for donating all of the CFRP materials required for laboratory shear retrofit of the test beam. The authors are also indebted to Chandler Rowe and his colleagues at Plas-Tech Ltd., Honolulu, Hawaii, for donating their labor and expertise in the repair of the beams and for installation of the flexural retrofit materials.

The authors would also like to thank Andrew Oshita and Miles Wagner, the laboratory technicians, for their assistance during this project. Thanks also to Gaur Johnson for his help throughout the tests. Thanks to Yuhai Yan for his help in the preparation of the beam, coring the slots in the top slab, and recording manual strain gage readings. Thanks to Kainoa Aki for programming the Labview data acquisition system and to Huiyun Zhang for helping record crack widths. Thanks also to Dr. Fischer for his advice regarding the FRCC filler blocks, and to Cori-Ann Gum for mixing the FRCC.

This research project was funded by the Federal Highway Administration (FHWA) and Hawaii Department of Transportation (HDOT), research contract No.47770. This financial support is grateful acknowledged. The contents of this report reflect the view of the authors, who are responsible for the facts and the accuracy of the data presented herein. The contents do not necessarily reflect the official views or policies of the State of Hawaii, Department of Transportation or the Federal Highway Administration. This report does not constitute a standard, specification or regulation.

TABLE OF CONTENTS

LIST OF FIGURES

LIST OF TABLES

CHAPTER 1

1 INTRODUCTION

1.1 Background

The Salt Lake Boulevard Bridge over Halawa Stream is a three-span structure consisting of prestressed AASHTO girders supporting a reinforced concrete top slab. The girders are supported on end abutments and two interior bents all oriented at 45 degrees to the bridge longitudinal axis (Figure 1.1). The 2001 biennial inspection identified a number of shear cracks at the ends of certain girders. An investigation of the theoretical shear capacity of the existing prestressed girders showed that they are inadequate based on current AASHTO LRFD bridge design requirements. A report from KAI Hawaii, Inc (2003) indicated that sixteen of the AASHTO girders have visually detectable shear cracks, with the maximum crack size approximately 0.02 inches (0.5 mm). The majority of the shear cracks are within 7 ft (twice the depth of the girder) from the end support. The average shear crack inclination is 25.1^{o} from the horizontal (Figure 1.2, KAI Hawaii, 2003). As a result, the City and County of Honolulu plans to strengthen the girders in shear. The design consultant (KAI Hawaii, Inc.) is considering a strengthening system of Carbon Fiber Reinforced Polymer L-Shaped Plates (CarboShear-L) combined with external steel stirrups. The objective of this study was to evaluate the performance of CarboShear-L shear retrofit applied over existing shear cracks, especially under cyclic loading. In addition, the instrumentation system proposed for installation in the field application will be evaluated prior to deployment on the Salt Lake Boulevard Bridge during application of the shear retrofit.

The prestressed T-Beam used in this study was salvaged from the Ala Moana Shopping Center Parking Structure. In 2000, when the old parking garage was demolished to make way for a new multilevel parking garage, this T-Beam, along with two nominally identical T-Beams, were salvaged and transported to the University of Hawaii at Manoa Structural Testing Laboratory (UHM-STL). Under a prior Hawaii Department of Transportation (HDOT) funded program, Agapay and Robertson (2003) tested one un-strengthened T-Beam as the control specimen (T-Beam 1). The second T-Beam was strengthened in flexure in the field in 1997 with CFRP Carbodur strips. Testing of T-Beam 2 indicated that the CFRP strengthening provided a 70% increase in the beam flexural capacity. Both beams were also used to evaluate shear retrofit using wet lay-up CFRP sheets as shear stirrups. These tests were reported in detail by Agapay and Robertson (2003). T-Beam 3 used in this study was nominally identical to T-Beam 1.

The research program reported here involved a series of tests performed on the prestressed concrete T-Beam 3. The left hand end of the beam was tested to determine the shear capacity of the original unstrengthened beam. The right hand end of the beam was then preloaded cyclically to induce shear cracks similar to those in the Salt Lake Boulevard Bridge girders. The beam was then unloaded and retrofitted for shear using CarboShear-L stirrups. The T-Beam with shear retrofit was then tested under the same cyclic loading conditions used to induce the shear cracks. The beam was then loaded to failure.

Figure 1.1: Salt Lake Boulevard Bridge over Halawa Stream

Figure 1.2: Multiple shear cracks in girder web (highlighted with chalk)

1.2 Overview

Carbon Fiber Reinforced Polymer (CFRP) is being used increasingly for the rehabilitation of existing concrete structures because of its high tensile strength, light weight, and relatively high modulus of elasticity. Numerous research studies have shown that CFRP sheets or strips bonded to the concrete surface can substantially increase shear strength of concrete members. Because of the disadvantages of handling wet lay-up CFRP fabric on site, and concerns over the need for end anchorage of shear reinforcement, a relatively new shear strengthening system using CarboShear-L pre-cured stirrups has been developed by Sika Corporation. The literature review in Chapter 2 provides summaries of prior research studies related to shear retrofit using CFRP.

The top slab of the T-Beam was removed during extraction from the parking structure to facilitate shipping of the salvaged beams to the University of Hawaii structures laboratory. In order to replicate the T-Beam behavior of the in-situ beam, a concrete flange was reconstructed on T-Beam 3 in the laboratory. In addition, in order to increase the flexural capacity of the beam, personnel from Plas-Tech Ltd., Hawaii, installed six pre-cured CFRP Carbodur strips on the soffit of the beam as flexural retrofit. They also repaired small surface spalls on the beam using a Sika epoxy mortar (Sikadur-30) patching system. The details of this beam preparation are provided in Chapter 3.

The precise test setup and the layout of instrumentation for each test are presented in detail in Chapter 4. Material properties for the beam and CFRP materials are presented in Chapter 5. In Chapter 6, the theoretical shear strength predictions for the control and strengthened beams are presented. The test procedure and results of each test are presented in Chapter 7. Chapter 8 presents comparisons of the predicted strengths with

the observed strengths, and the comparison of related beam tests. Finally Chapter 9 presents a summary, conclusions and recommendations based on this research program.

1.3 Objective

The primary objective of this research program was to evaluate the performance of CarboShear-L shear retrofit applied over existing shear cracks, especially under cyclic loading. In addition, the instrumentation system used in this study was evaluated for potential deployment on the Salt Lake Boulevard Bridge during application of the shear retrofit. Because of the similarities between the Ala Moana beams and typical prestressed AASHTO bridge girders, the results of this research program should provide valuable insight into the likely performance of the bridge girders.

1.3.1 Use of CarboShear-L for Shear Strengthening

Shear strengthening using CFRP wet lay-up fabrics has proven effective in a number of prior experimental studies (Chapter 2 Literature Review). However, wet lay-up applications have a number of disadvantages such as poor anchorage at the top and bottom of the section, difficult handling on site, and variations in application technique and potential variability in material properties. Sika Corporation recently developed a shear strengthening system using CFRP L-Shaped plates (CarboShear-L). The most important features of these CarboShear-L stirrups are that they are lightweight, have consistent material properties, are easy to handle on site, and are designed for effective anchorage at the top and bottom of the beam.

In order to install the CarboShear-L stirrups to the sides of the T-Beam section, pre-cast filler blocks were added to the web area to provide a vertical surface at each stirrup. The filler blocks are intended to transfer the tension from the web concrete to the

CarboShear-L stirrups. Three different cementitious mixtures were used for the filler blocks as discussed in Chapter 4.

The shear strengthening was installed on the right hand end of T-Beam 3. The CarboShear-L stirrups were placed 12" on center, between the internal 3/8" (10 mm) diameter steel stirrups. A detailed description of the shear retrofit of the T-Beam is provided in Chapter 4. Before the shear retrofit was installed, cyclic shear loading was applied to the right end of T-Beam 3 to induce shear cracks similar to those in the Salt Lake Boulevard Bridge girders. The contribution of the CarboShear-L is evaluated based on the performance of the T-Beam before and after shear retrofit.

1.3.2 Validation of Instrumentation System

An important objective of this research program was to evaluate potential sensors for use in the instrumentation system to be deployed on the Salt Lake Boulevard Bridge during application of the shear retrofit.

In this study, various sensors were used to monitor the beam response during each test. An LVDT (linear variable displacement transducer) was used to record the vertical deflection of T-Beam 3 at the location of the applied load; two types of crack extensometer were used to monitor changes in the existing shear cracks during load cycling; surface mounted stain gages were used to monitor potential delamination of the CarboShear-L stirrups; and LVDTs were used to monitor anchorage slip of the CarboShear-L stirrups. A detailed description of the layout of sensors for each test is provided in Chapter 4. The results of the instrumentation output are presented in Chapter 7 and discussed in Chapter 8.

1.3.3 Summary

The objectives and outcomes of this research program are summarized below:

1. To evaluate the performance of CarboShear-L shear retrofit applied over existing shear cracks in a prestressed concrete beam. The behavior of the beam section with shear retrofit is compared with the tests prior to retrofit.

2. The control beam test result is compared with the strengths predicted by the ACI 318-02, "Building Code Requirements for Structural Concrete" (ACI 318 2002), and the AASHTO, "LRFD Bridge Design Specifications" (AASHTO 1999).

3. The retrofit shear test results are compared with the strength predicted by the ACI 440.2R-02 committee report, "Guide for the Design and Construction of Externally Bonded FRP Systems for Strengthening Concrete Structures" (ACI440 2002).

4. The instrumentation system used in this study, including LVDTs, crack extensometers and strain gages, is evaluated to provide insight into the instrumentation to be selected for the Salt Lake Boulevard Bridge project.

5. Recommendations are made regarding appropriate shear retrofit with CarboShear-L for cracked prestressed concrete bridge girders.

CHAPTER 2

2 LITERATURE REVIEW

2.1 Overview

Shear failure of concrete beams is often catastrophic and can occur with little or no advance warning. Existing concrete beams with known shear deficiencies must be strengthened to safely support the design loads. Numerous research programs have shown that externally bonded CFRP fabrics (in the form of sheets or stirrups) can increase beam shear capacity significantly. The CFRP shear strengthening can be installed as wet lay-up fabric sheets or pre-cured CFRP stirrups. Wet lay-up fabrics have a number of disadvantages including poor anchorage at the top and bottom of the beam web, variability in field applied material properties and awkward handling on site. A recently developed shear strengthening system using pre-cured CFRP L-Shaped plates is also commercially available (Sika Corporation, 2002). The most important features of the CarboShear-L stirrups are their lightweight, well-established material properties, superior anchorage at top and bottom of the beam web, and the ease of installation on site.

This chapter presents some of the recent published research on the use of CFRP fabrics and CarboShear-L stirrups for shear strengthening of concrete beams. A research program involving externally mounted steel stirrups will also be presented because the design consultant, KAI Hawaii, Inc., is considering a strengthening system of CarboShear-L combined with external steel stirrups for the Salt Lake Boulevard Bridge project. Additional discussion of many of these research studies is presented by Nakashima and Robertson (2003).

2.2 CFRP Shear Retrofit for Reinforced Concrete (RC) Beams

2.2.1 Introduction

Most of the prior research on CFRP shear strengthening was performed on reinforced concrete (RC) beams. These studies considered different strengthening systems, including CFRP fabrics (sheets or stirrups) and CarboShear-L stirrups.

For CFRP fabric systems, research studies have considered different wrapping schemes. In general, completely wrapping a rectangular beam section on all four sides is the most effective shear-strengthening scheme. Research studies also show that shear strength can be improved by wrapping the bottom and both sides of the member (three-sided wrap) or bonding to only the two vertical sides of the web (two-sided wrap). Some of these studies investigated different anchorage systems to provide better attachment between the CFRP and concrete substrate.

For the CarboShear-L system, the EMPA (Swiss Federal Laboratories for Material Testing and Research, Dübendorf, Switzerland) performed tests on RC T-Beams with CarboShear-L stirrups in 1998 (EMPA, 1998). The tests showed that the CarboShear-L system is an effective solution for shear strengthening.

2.2.2 CFRP Fabric Systems

Sheikh, DeRose & Mardukhi (2002) investigated two 5/6th-scale models of the beams of a building that was damaged by unexpected loads during the first two years of service. The beams were cast with a haunch to simulate being framed into the walls and to force shear failure to occur within the shallow section of the beam. The beams had internal steel shear reinforcement as contained in the original beams. The repaired beam was completely wrapped on all sides of the shallow section to prevent shear failure. The

beams were subjected to a single point load at the edge of the haunch section. The control beam failed in shear at a load of 1,700 kN (382 kips) while the retrofitted beam failed in flexure at a load of 2,528 kN (568 kips) a 48% increase. The failure of the beam changed from a brittle shear failure to a more ductile flexural failure. The mid-span deflection of the repaired specimen was 10 times greater than that of the control specimen. No premature delamination of FRP was observed in the test specimens.

Chaallal, Nollet and Perraton (1998) tested reinforced concrete beams retrofitted with pre-cured CFRP strips bonded to the sides of the beam at various angles. Three groups of beams were tested. The first group was designed with sufficient internal shear reinforcement to prevent shear failure. The second group was designed with a reduced shear strength. The last group was identical to group two but with external CFRP reinforcement at 90 degrees to the horizontal and 45 degrees to the horizontal. The CFRP retrofit was applied to the two vertical faces of the beams. All specimens were subjected to four-point bending. Repaired beams showed an increase in strength of about 70% and increased stiffness over the group two beams, however, they did not support the same load as the group 1 beams. The 45-degree CFRP stirrups performed better than the 90-degree CFRP stirrups. Failure occurred due to delamination of the CFRP stirrups from the surface of the concrete. For more extreme loading, U-shaped retrofit stirrups were suggested.

Triantafillou (1998) tested eleven reinforced concrete beams strengthened with CFRP stirrups at various angles on the vertical sides of the beam. Two beams were used as control specimens. Three of the beams were fitted with CFRP stirrups oriented at 45 degrees to the horizontal. The rest of the beams were fitted with CFRP stirrups oriented at

90 degrees to the horizontal. Internal steel shear reinforcement was not included in order to force shear failure in each specimen. The one-meter (3.28 ft) beams were loaded in four-point bending with a shear span of 0.32 meter (12.6 in). Results showed an increase in shear strength between 65% and 95% over the control specimens. Failure was initiated by shear cracking followed by peeling of the CFRP shear stirrups. Results also showed that the 45 degree CFRP shear reinforcement was more effective than the vertical CFRP shear reinforcement due to the fibers being more perpendicular to the shear cracks.

Al-Sulaimani et al. (1994) conducted research on sixteen reinforced concrete beams with various configurations of CFRP shear reinforcement. These beams had no internal steel shear reinforcement. The beams were divided into four groups. The first group was used as the control. All of the retrofitted beams were preloaded until hairline shear cracks formed. The load was then released and the beams were repaired. The first retrofit method consisted of bonding wet lay-up CFRP stirrups to the sides of the beam in the shear span. The second retrofit method consisted of CFRP sheets bonded to the entire side faces of the beam. The final retrofit method consisted of CFRP sheets that continuously wrapped both sides and the bottom of the beam along the full span length. Of the four beams in each group, two were retrofitted for flexure and the other two were not. All specimens were tested monotonically in four-point loading. Results showed that the stirrups and sheets bonded to the sides of the beams produced a similar increase in strength. They also had similar failure modes where both delaminated at the bottom of the member. The CFRP sheets that wrapped the bottom of the beam prevented shear failure and caused the specimens to fail in flexure. The continuity of the wrap repair

reduced the bond stress concentrations that caused delamination of the stirrups and sheets. All forms of shear repair also increased the beam stiffness.

Chaallal, Shahawy and Hassan (2002) presented results of an experimental investigation on the performance of 20 ft long reinforced concrete T-girders strengthened in shear using epoxy-bonded bi-directional CFRP fabrics. The study considered four series of tests corresponding to the following four stirrup spacings: 5.5, 8, 16 and 24 in. Each series of girders included control specimens with no CFRP wrap and specimens retrofitted in shear with one, two, and three layers of CFRP wrap. Results showed that for unwrapped specimens, the values for nominal shear predicted by ACI underestimated the test results by 40% to 80%. For wrapped specimens, the maximum shear force, as well as the midspan deflection, generally increased with the number of the CFRP layers. The optimum number of layers to achieve the maximum gain in shear resistance was found to depend on the internal shear steel reinforcement provided. Retrofitting RC girders in shear with CFRP wrap also increased the ductility. The experimental evidence indicated that an optimum combination of CFRP layers and steel stirrups exists for a maximum increase in ductility.

Khalifa et al. (1999) investigated the shear behavior and modes of failure of two-span continuous RC beams strengthened with CFRP sheets. The experimental program consisted of nine full-scale, two-span, continuous beams with rectangular cross sections. The tested beams were grouped into three series. Three beams, one from each series, were not strengthened and taken as control beams, whereas six beams were strengthened using different schemes. The variables investigated in this study included the amount of steel shear reinforcement, amount of FRP, wrapping schemes, and $90^{o}/0^{o}$ ply

combination. The experimental results indicated that the contribution of externally bonded CFRP to the shear capacity of continuous RC beams was significant (ranged from 22 to 135%), depending on the tested variables. Test results also indicated that the CFRP contribution was greater for beams without stirrups than for beams with adequate internal steel shear reinforcement.

2.2.3 Anchorage of CFRP Shear Strengthening

Schuman and Karbhari (2003) conducted research on half-scale cantilever RC T-Beams retrofitted for shear with wet lay-up CFRP fabric. They investigated the effect and benefits of anchoring the CFRP shear stirrups to the side of the beam. Two types of CFRP retrofit were considered. The first consisted of U-Shaped CFRP fabric stirrups bonded to the bottom and sides of the beam. The second consisted of L-Shaped CFRP fabric stirrups that were placed in an offset configuration so as not to overlap on the bottom of the beam. Five specimens were tested with different anchorage configurations. The first specimen was the control with no CFRP retrofit. The second specimen was retrofitted with the U-Shaped CFRP fabrics without anchorage at the top of the web. The third specimen was retrofitted with offset L-Shaped CFRP fabric stirrups with steel anchor plates and 3/8" diameter anchor bolts extending 4" into the top slab. This anchor embedment did not extend past the internal steel stirrups. The fourth specimen was also retrofitted with the offset L-Shaped CFRP fabric stirrups using 3/8" diameter anchor bolts extending 6" into the top slab. The embedment of the anchors was now deep enough to pass the internal steel stirrups and slab reinforcement. The last specimen was also retrofitted with offset L-Shaped CFRP fabric stirrups but using ½" diameter anchor bolts extending 6" into the top slab. The second test specimen results showed that there is little

or no benefit in using CFRP shear stirrups without anchorage. The third specimen only showed a slight increase in strength and ductility. The fourth and fifth specimens showed considerable increase in strength, ductility, and stiffness. The test showed that there was a strong dependence on both the anchor size and embedment depth of the anchorage system.

2.2.4 CarboShear-L Shear Strengthening System

Czaderski (2002) reports that the shear strengthening of a reinforced concrete T-Beam with CFRP L-shaped plates (CarboShear-L) could increase the shear ultimate limit state as well as serviceability. A total of five specimens were tested of which two were control specimens. One control specimen was a beam that had internal steel shear reinforcement while the other did not have internal steel shear reinforcement. The remaining three specimens were retrofitted with CarboShear-L stirrups spaced equally along the length of the shear span and overlapped on the bottom of the beam. The specimens were subjected to increasing static loading until failure. The test results showed an increase in shear strength for beams retrofitted with the CarboShear-L stirrups. The retrofitted specimens also exhibited greater ductility than the control specimens. The brittle "shear failure" mode changed to a ductile behavior with yielding of the internal flexural reinforcement. The tests also indicated that the bottom overlapped ends of the CarboShear-L stirrups tended to separate from one another at failure.

Basler, White and Desroches (2003) report that the CarboShear-L system is an innovative solution for shear strengthening. They indicate that the important features of CarboShear-L stirrups are their lightweight, clearly defined material properties, and ease of handling on site. Systematic testing undertaken by Sika AG, Switzerland, in co-

operation with the independent laboratories of EMPA showed the potential of this new shear strengthening composite system. Three different preliminary tests on the CarboShear-L are described, which determined the mechanical properties of CarboShear-L and behavior when installed. The suitability of CarboShear-L was verified in tests by EMPA in which RC beams without internal shear reinforcement were strengthened with CarboShear-L. The contribution of CarboShear-L to increase the load-bearing capacity of the beams was clearly shown.

2.3 CFRP Shear Retrofit for Prestressed Concrete (PC) Beams

Most of the prior research on CFRP shear strengthening was performed on reinforced concrete (RC) beams. These studies considered different strengthening systems, including CFRP fabrics (sheets or stirrups) and CarboShear-L stirrups.

All of the studies described above considered shear retrofit applied to reinforced concrete (RC) beams, most without internal steel shear reinforcement. However, for the current study, the T-Beam is a prestressed concrete (PC) beam with internal steel shear reinforcement. The following research programs consider CFRP shear strengthening performed on PC beams.

As mentioned in Chapter 1, the prestressed T-Beam used in this study was salvaged from the Ala Moana shopping Center parking structure along with two nominally identical T-Beams. Under another Hawaii Department of Transportation (HDOT) funded program, Robertson, Agapay and Nakashima (2003) tested one un-strengthened T-Beam as the control specimen (T-Beam 1). The second T-Beam was strengthened in flexure in the field in 1997 with CFRP Carbodur strips. Flexural testing of T-Beam 2 showed that the CFRP strengthening provided a 70% increase in the flexural capacity. Both beams

were also used to evaluate the use of wet lay-up CFRP sheets for shear strengthening. The shear capacity of the prestressed T-Beam without CFRP shear strengthening exceeded the ACI318-02 predicted strength by 33%. The two T-Beam shear tests with CFRP sheets produced 7% and 16% increases in shear capacity.

Hutchinson et al. (2003) provide a review of four recent field applications in Western Canada, utilizing externally bonded CFRP for the repair and strengthening of bridges. Two of them were shear strengthening of I-shaped prestressed concrete AASHTO girders for the Maryland Bridge in Winnipeg, Manitoba, and the John Hart Bridge in Prince George, British Columbia. In both cases, the fact that the bridges remained completely accessible to traffic during strengthening was a major factor in selecting CFRP as the retrofit scheme. The configuration of the CFRP sheets selected for the Maryland Bridge girders included vertical sheets on either side of the beam web with horizontal layers at the top and bottom of the web as anchorage. Based on experimental test results and recommended design procedures, the shear capacity of the girders was increased by 20 to 25%. The John Hart Bridge was retrofitted using a single diagonal layer of CFRP sheets applied over a 4 m length at each end of all 42 girders, resulting in a theoretical increase in shear capacity of about 15 to 20%.

Hutchinson and Rizkalla (1999) summarized research findings on the use of CFRP sheets for shear strengthening of pretensioned AASHTO bridge girders. Seven pretensioned concrete girders were tested to failure at each end. The ten-meter long beams are 1:3.5 scale models of the I-shaped bridge girders. The beams were divided into 2 series, with different forms of internal steel stirrups. One beam from each series was tested as a control beam. The remaining beams were strengthened using three types of

CFRP sheets. The test results showed the effectiveness of each configuration of CFRP was different. The increase of shear capacity ranged from 9% to 36%. A rational model was introduced to define the contribution of the CFRP sheets to the shear resistance in addition to the contribution provided by the stirrups and the concrete for I-shaped pretensioned concrete members. The model is shown to be in good agreement with their test results.

2.4 Externally Mounted Steel Stirrups

The design consultant (KAI Hawaii, Inc.) of the Salt Lake Boulevard Bridge strengthening project is considering a shear retrofit system of CarboShear-L stirrups combined with external steel stirrups. A research program on the performance of externally mounted steel stirrups is summarized below.

Altin et al. (2003) conducted experiments to investigate the behavior of RC T-beams with external steel clamps designed to behave as shear stirrups. A total of 13 T-beams with differing levels of shear reinforcement deficiency were tested. These beams were strengthened by external clamps and then experiments were performed on two groups in which the ratio of the shear span to the effective height of the beam is equal to 4.5 and 3.3, respectively. Experimental results showed that this strengthening method is effective and the specimens' strength, rigidity and ductility were improved. The external steel clamps controlled any shear cracks and helped to ensure ductile flexural behavior of the members. The tests also indicated that the strengthening procedure would be more effective if the clamps are tied together over the beam top flange with steel strips. The authors note that steel clamps attached to the outside of the beam must be protected from external effects such as fire and corrosion.

2.5 Chapter Summary

Numerous research programs have shown that externally bonded CFRP shear reinforcement can increase the shear capacity of RC and PC beams. A retrofit system using externally mounted steel stirrups is also effective and contributes to improve the specimens' strength, rigidity and ductility. However, the steel retrofit requires corrosion protection and effective anchorage to the structure. CFRP fabrics have the disadvantage of being difficult to anchor, especially in the peel zones. The newly developed system of CarboShear-L stirrups tested at EMPA overcomes many of these problems.

Based on the literature review, the retrofit system of CarboShear-L stirrups was considered for this test program. The proposed CarboShear-L stirrups combine easy installation on site with the unique advantages of FRP materials. In order to install the CarboShear-L stirrups around the T-Beam section, pre-cast filler blocks were added in the web area. The filler blocks are expected to transfer the tension from the beam web to the CarboShear-L stirrups. The shear strengthening was installed on the right hand end of T-Beam 3. The CarboShear-L stirrups were placed 12" on center, between the internal 3/8" diameter steel stirrups. More detail of the shear retrofit system is provided in Chapter 5.

CHAPTER 3

3 T-BEAM RECOVERY AND FLEXURAL RETROFIT

3.1 Introduction

The prestressed T-Beam used in this study was salvaged from the Ala Moana Shopping Center Parking Structure. In 2000, when the old parking garage was demolished to make way for a new multilevel parking garage, this T-Beam as well as two nominally identical T-Beams were recovered and transported to the University of Hawaii at Manoa Structural Testing Laboratory (UHM-STL). The top slab forming the flange of the T-Beams was removed, along with the transverse joists, to facilitate shipping of the salvaged beams. This removal was performed using a demolition rig with large hydraulic pincer. Removal of the top slab over the pre-cast beam web occasionally resulted in spalling of concrete at the top of the web. These spalls were repaired with epoxy mortar once the beams were delivered to UHM-STL. In order to replicate the T-Beam behavior of the in-situ beam, a concrete flange was poured onto T-Beam 3 prior to testing.

To ensure shear failure of the T-Beam prior to flexural failure, the beam was tested with a relatively low shear span to depth ratio. In addition, the flexural capacity of T-Beam 3 was increased by the addition of CFRP flexural strengthening. Personnel from Plas-Tech Ltd, Hawaii, installed six pre-cured Carbodur strips on the soffit of the beam as flexural retrofit. They also repaired small surface spalls on the side faces of the beam using a Sika epoxy mortar patching system.

3.2 Epoxy Mortar Spall Repair and Top Slab Replacement

This T-Beam 3, as well as the first two T-Beams tested by Agapay, was repaired using epoxy mortar immediately after the beams were recovered from the field. The procedures for epoxy mortar spall repair are described in detail by Agapay and Robertson (2003).

During the repair, the contact surface was primed using Sika bonding epoxy and formed with plywood (Figure 3.1). A two-part Sika epoxy modified mortar was mixed with clean silica sand and poured into the form (Figure 3.2).

The effective flange width suggested by the ACI 318-02 Building Code for the in-situ condition is 77.5 inches. Because of limitations of the test frame, the flange width was reduced to 66 inches. This slight reduction in flange width was not anticipated to affect the beam flexural or shear performance. The 4.5 inch thick top slab was reinforced according to the original design documents for the parking garage (Figure 3.3 and Figure 3.4).

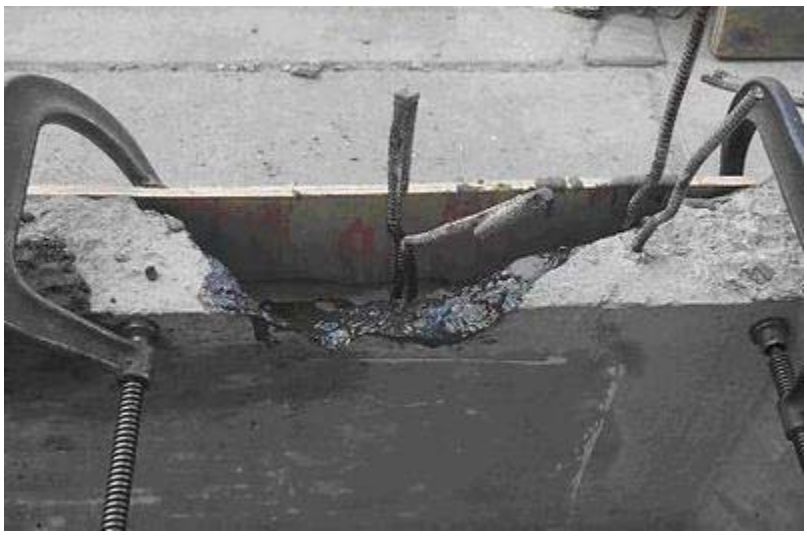

Figure 3.1: Formwork and bonding epoxy for spall repair

Figure 3.2: Pouring epoxy mortar to repair spall

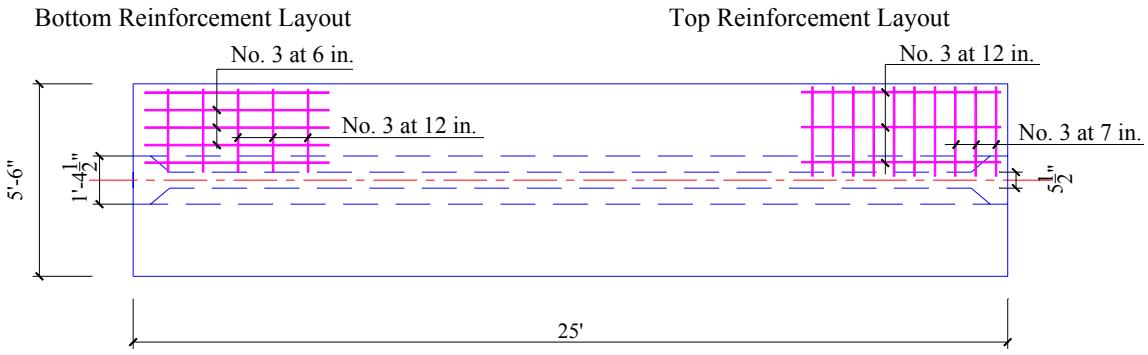

Figure 3.3: Top slab reinforcement layout

Figure 3.4: T-Beam 3 flange reinforcement

The top slab concrete was supplied by a local Ready Mix Concrete company and placed during the summer of 2003 (Figure 3.5).

Figure 3.5: T-Beam 3 top flange concrete placement

3.3 Flexural Retrofit

In order to increase the flexural strength of T-Beam 3, a CFRP flexural retrofit was installed before shear testing. The retrofit was performed by personnel from Plas-Tech Ltd in September, 2003. A pneumatic needle gun was used to roughen the concrete surface to remove the surface cement paste and improve the bond between the CFRP and the concrete (Figure 3.6). Minor spalling damage on the sides of the bottom bulb of the T-Beam was repaired using Sikadur 30 Hi Mod Gel two-part epoxy (Figure 3.7).

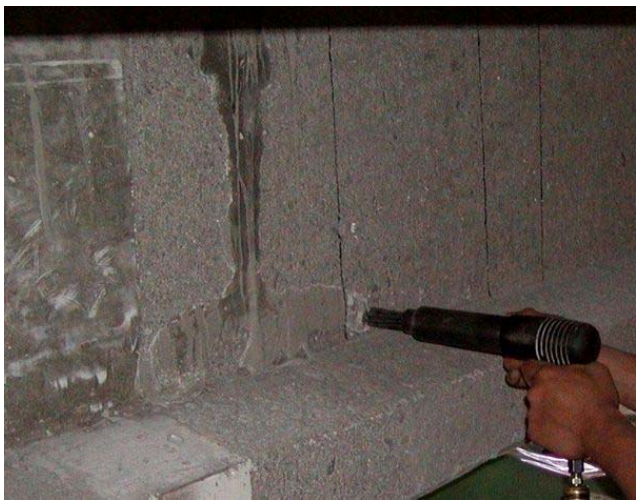

Figure 3.6: Use needle gun to prepare the beam surface

Figure 3.7: Sika 30 Hi Mod Gel Epoxy patch of concrete spall

Pre-cured CFRP Sika Carbodur strips were used for the flexural strengthening. Each strip is 4” wide by 0.047” thick (100 mm by 1.2 mm). Three strips were bonded directly to the concrete surface on the soffit of the T-beam bulb. The second ply of strips was then bonded directly over the first 3 strips. Two 6” wide Sika Wrap Hex 103C uni-direction sheets were applied as anchorage at each end of the flexural reinforcement.

Installation of the flexural strengthening followed standard industry procedures. The Sikadur strips were thoroughly cleaned with solvent until no residue was collected when wiped with a clean cloth. Uniform thin layers of Sika-30 Hi-Mod Gel two-part epoxy were applied to the soffit of the beam, as well as to the surface of the Carbodur strips (Figure 3.8).

Figure 3.8: Trolley used to apply Sika-30 Epoxy to the Carbodur strips

The strips were then pressed firmly onto the epoxy layer (Figure 3.9). Another thin layer of Sika-30 was applied to the bottom of the first ply before installation of the second set of 3 strips. The 6” wide wet lay-up CFRP sheets were saturated in Sikadur

Hex 300 two-part epoxy (Figure 3.10) and applied at each end of the beam to anchor the flexural strips (Figure 3.11).

Figure 3.9: Installation of pre-cured Carbodur strips

Figure 3.10: Saturating CFRP Sheets with Epoxy

Figure 3.11: Apply CFRP anchorage wrap to the end of the Carbodur strips

In addition, in order to prevent delamination of the Carbodur strips in the high flexural moment region, seven 6" wide Sika Wrap Hex 103C uni-direction sheets were applied to the bottom bulb of the T-beam. These wraps did not extend up the web of the beam so as not to affect the beam shear capacity (Figure 3.12).

Figure 3.12: Wet lay-up CFRP wraps in the high flexural moment region

CHAPTER 4

4 TEST SETUP AND INSTRUMENTATION

4.1 Introduction

In this study, a series of tests were performed on the prestressed concrete T-Beam 3. These tests are referred to as the Control Shear Test (T-Beam 3C), Initial Cracking Test (T-Beam 3I), Crack Widening Test (T-Beam 3W), and Shear Retrofit Test (T-Beam 3S).

The testing apparatus was a 300,000 lb capacity hydraulic actuator supported by a four-post frame. Figure 4.1 shows the test frame with T-Beam 3C ready for loading.

Figure 4.1: Four-post Test Frame with T-Beam 3C ready for loading

T-Beam 3 was prestressed with ten 3/8" nominal diameter seven-wire stress relieved strands (6 straight, 4 harped). The existing steel shear reinforcement consisted of double leg #3 stirrups at a nominal spacing of 12" on center along the full length of the beam. Each stirrup consisted of a straight vertical section in the beam web, with no hook or anchorage at the bottom of the beam, and a 90 degrees bend into the top slab at the top of the beam (Figure 4.2).

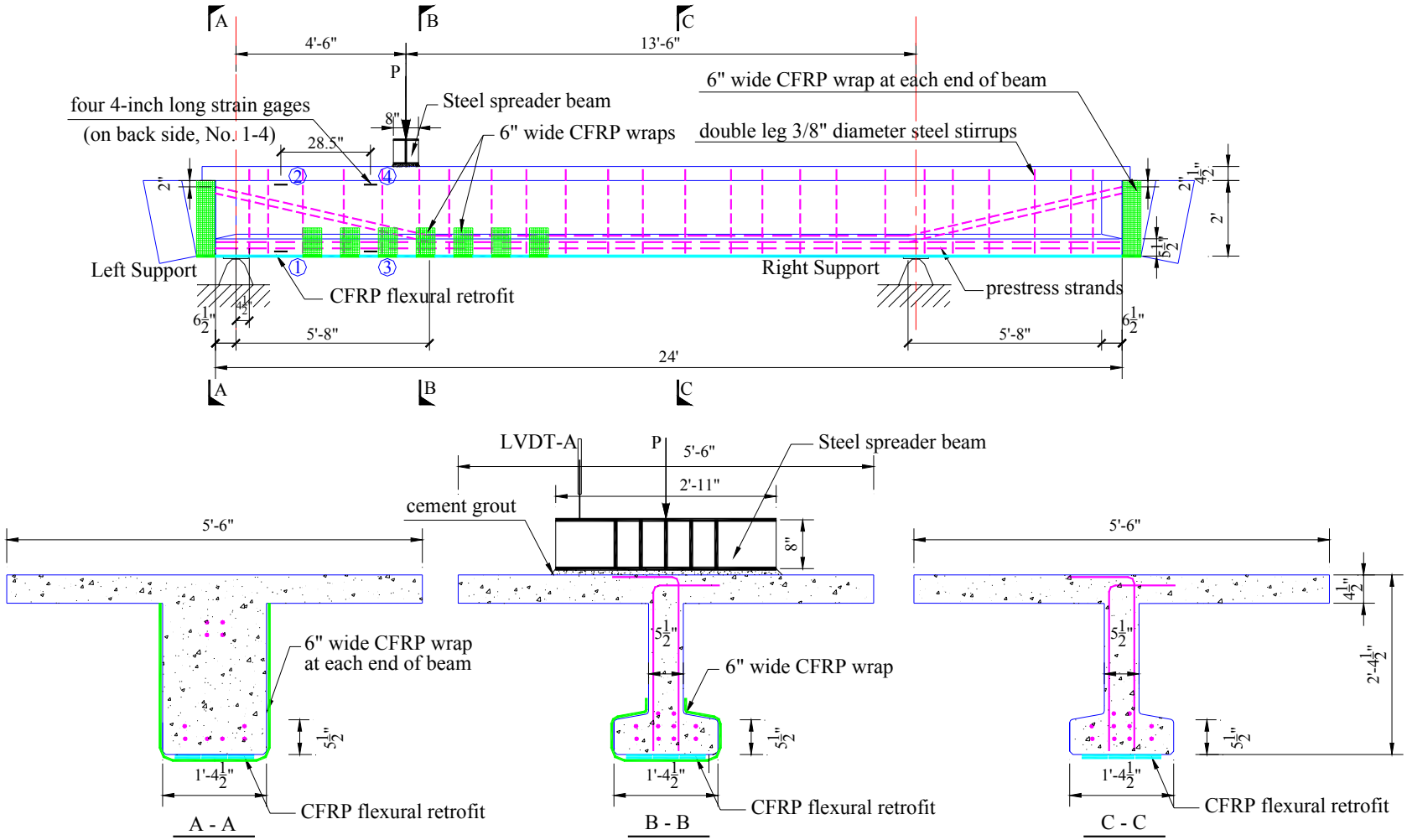

Figure 4.2: T-Beam 3C Layout and Instrumentation

Before testing, instruments such as strain gages, crack gages and LVDTs (Linear Variable Displacement Transducers) were installed according to the requirement of each test. In the sections below, the precise test setup and instrumentation layout for each test is presented in detail. The test procedure and results are described in Chapter 7.

4.2 T-Beam 3 Control Shear Test (T-Beam 3C)

T-Beam 3 Control Shear Test (T-Beam 3C) was performed on the left hand end of the beam. This test served as the control test for the future retrofit test to be performed on the right hand end of the same beam.

The beam was simply supported on an 18 foot span with a single line load applied at 4.5 ft from the left support. Based on the span dimensions, the total load applied to the beam was transferred to the supports in the ratio 3 to 1. The left span (test span) therefore resisted three fourths of the total load applied to the beam. The left end of the beam had a shear span to overall depth ratio of a/h=1.9 and a shear span to effective depth ratio of a/d_p=2.4. These span-to-depth ratios will permit the formation of shear cracks similar to those in the Salt Lake Boulevard Bridge girders.

Figure 4.2 shows the layout and instrumentation for T-Beam 3C. Strain gages 1-4 were installed on the back of the left end shear span near the top and the bottom of the beam to monitor change in bending moment, and subsequently determine applied shear in the shear span. Figure 4.3 shows the location of these gages as well as dashed lines indicating prestressed and shear reinforcement. These 4-inch long gages were Micro-measurement Electrical Resistance Foil strain gages (EA-06-40CBY-120), installed following the manufacturer's instructions. This system of strain measurements is being considered for the field application as a means of monitoring the shear load applied by

traffic on the Salt Lake Boulevard Bridge. LVDT-A was located on the top of the steel spreader beam to monitor the vertical deflection of the beam. The crack sizes were estimated using a visual crack gage (Figure 4.4).

Figure 4.3: 4-inch long strain gages on the back of the beam

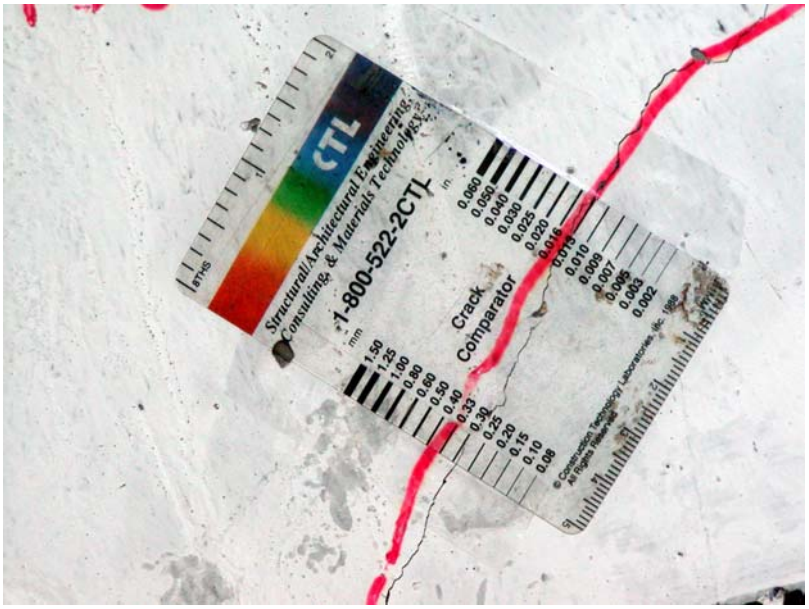

Figure 4.4: Visual crack gage used to estimate crack size

4.3 T-Beam 3 Shear Retrofit Tests

4.3.1 Introduction

After the control shear test (T-Beam 3C) on the left end of the beam, the right end of the same beam was used to perform shear retrofit tests. The sequence of the tests is described below. Before the shear retrofit, the right end of T-Beam 3 was preloaded to induce shear cracks similar to those in the Salt Lake Boulevard Bridge girders. An Initial Cracking Test (T-Beam 3I) was performed under monotonic loading to induce initial shear cracks. After unloading, the crack width extensometers were installed across these cracks. A series of cyclic loading was performed to increase the residual crack size to the same 0.02" (0.5mm) as observed in the Salt Lake Boulevard Bridge girders. This cyclic loading is referred to as the Crack Widening Test (T-Beam 3W). Finally the right hand end of the beam was retrofitted with CarboShear-L stirrups and the Shear Retrofit Test (T-Beam 3S) was performed to evaluate the effect of the retrofit on the crack widths under cyclic loading. The beam was then loaded to failure that resulted from delamination of the flexural Carbodur strips and flexural failure at the load point.

The beam was simply supported on an 18 foot span with a single line load applied at 4.5 ft from the right support, which was exactly symmetrical to the control test performed on the left hand end of the beam. As with T-Beam 3C, the shear span to overall depth ratio was 1.9 and the shear span to effective depth ratio was 2.4. Based on the span dimensions, the total load applied to the beam was transferred to the supports in the ratio 1 to 3. The right span (test span) therefore resisted three fourths of the total load applied to the beam. This beam layout remained the same throughout all three tests, T-Beam 3I, T-Beam 3W and T-Beam 3S. However, the instrumentation of each test was different. Details of the test layout and instrumentation are presented in the following sections.

4.3.2 T-Beam 3 Initial Cracking Test (T-Beam 3I)

T-Beam 3I was performed to induce initial shear cracks in the web of the beam. Figure 4.5 shows T-Beam 3I in the test frame ready for testing. Figure 4.6 shows the layout and instrumentation for T-Beam 3I. As with T-Beam 3C, LVDT-A was located on the top of the steel spreader beam. The crack size was estimated using a visual crack gage.

Figure 4.5: T-Beam 3I in the test frame prior to testing

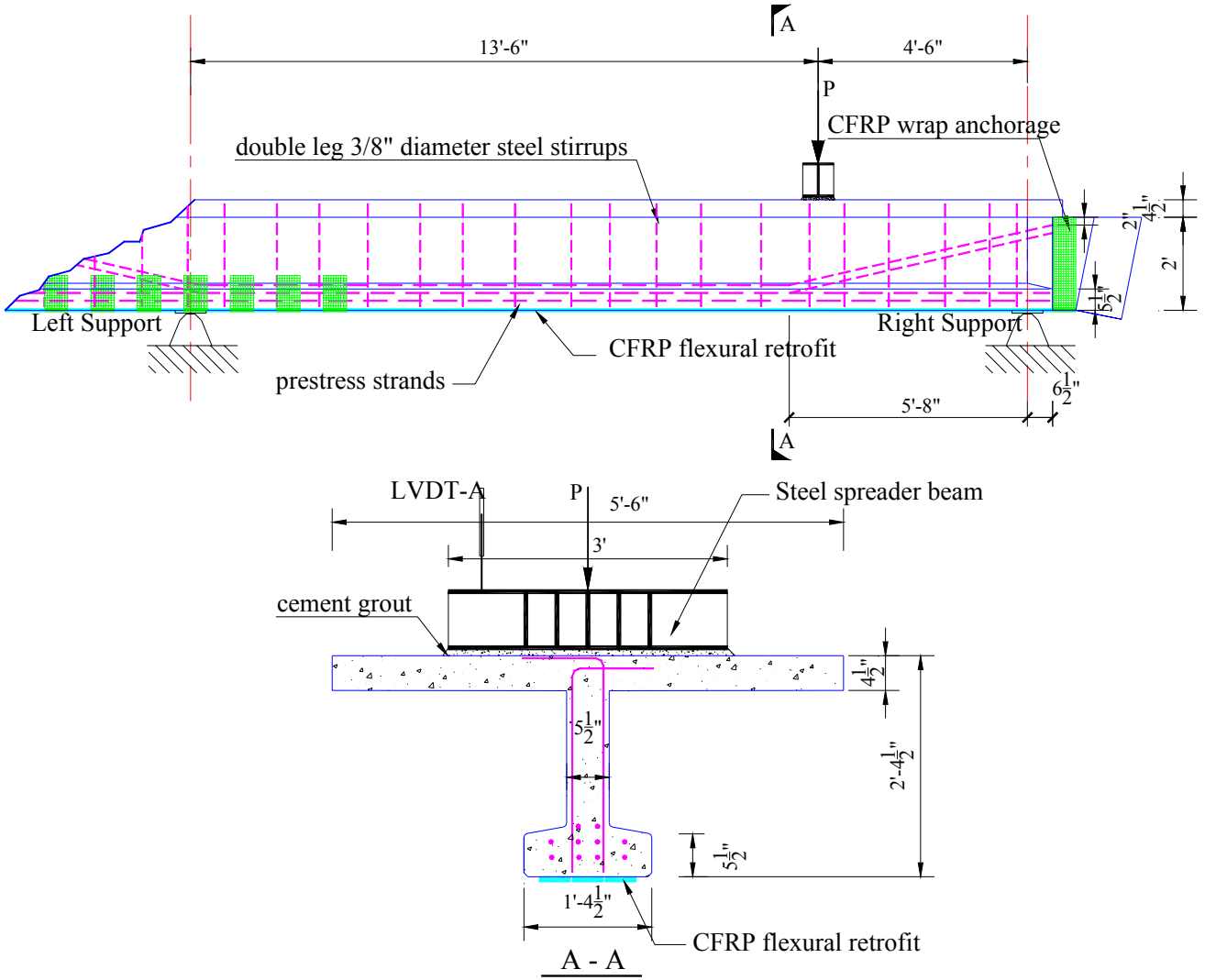

Figure 4.6: T-Beam 3I Layout and Instrumentation

4.3.3 T-Beam 3 Crack Widening Test (T-Beam 3W)

After the initial cracking test (T-Beam 3I), the shear crack in the beam had a residual (unloaded) width of approximately 0.003" (0.08mm) as measured using the visual crack gage. In order to monitor the crack width during subsequent load tests, three electronic crack extensometers were installed across the crack. A Vibrating Wire Crackmeter with a 12.5" gage length was installed on the front of the beam, while crack gages with a 0.5" gage length were installed on either side of the web.

The Geokon Vibrating Wire (VW) Crackmeter (Model 4420-1-25) used in this project was designed to measure movement across joints or tension cracks in soils and joints in rock and concrete. It has a gage length of 12.5" and a range of 1" (25mm). Figure 4.7 shows the installation detail of the VW Crackmeter using epoxy grout anchors. The Crackmeter was installed following the manufacturer's instructions and was monitored using a manual readout box.

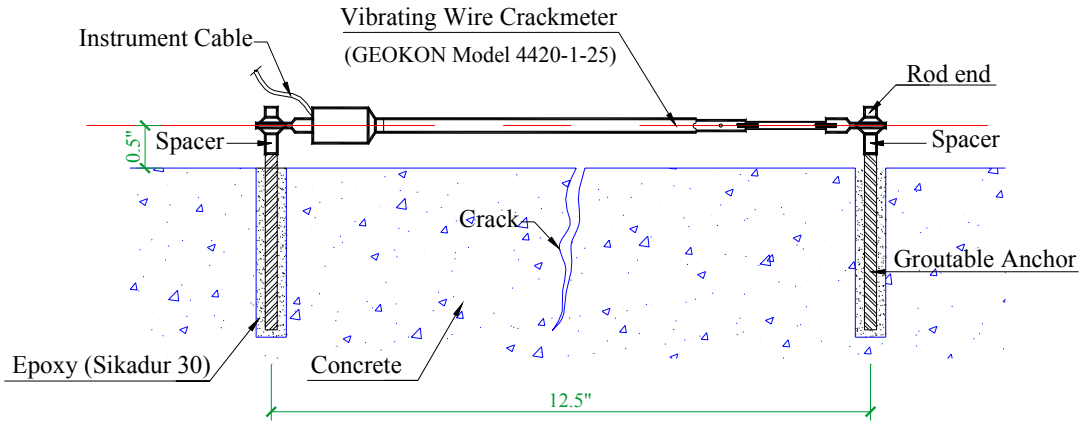

Figure 4.7: Installation detail of Vibrating Wire Crackmeter

Figure 4.8 shows the installation detail of the crack gages (Epsilon Extensometer, Model 3541-003M-040M-ST clip-on gage). Two small steel plates were prepared with one beveled edge as anchors for the crack gage. One plate was attached to each side of

the crack with Sikadur-30 epoxy. Each crack gage was installed such that the notches at the ends of the gage legs engaged the beveled edges of the anchor plates. The movement between the legs of the crack gage is calibrated with the opening of the crack, which made it possible to monitor the relationship between crack sizes and applied load. Figure 4.9 shows a close-up view of a crack gage.

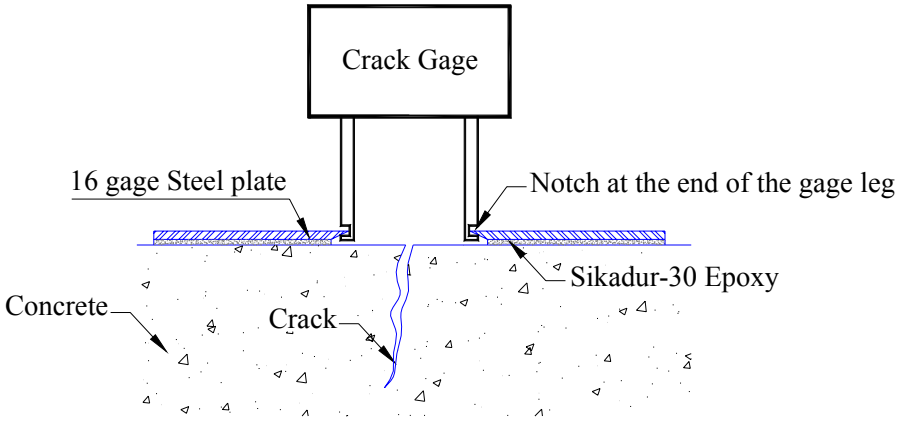

Figure 4.8: Installation detail of crack gage

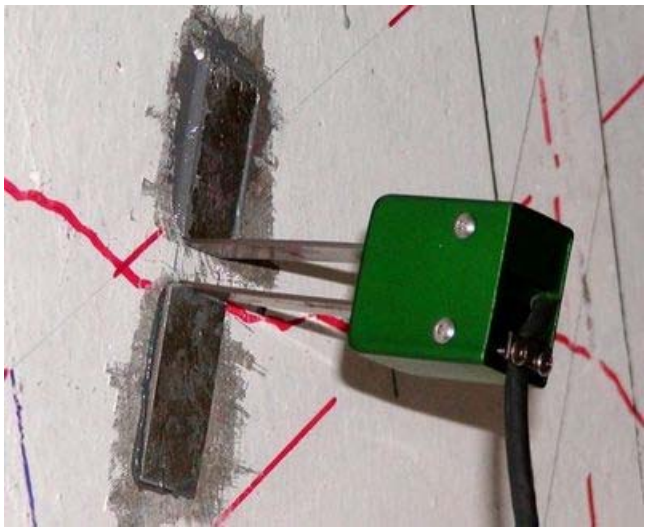

Figure 4.9: Close-up view of crack gage

Figure 4.10 shows the VW Crackmeter and crack gages on the front and the back of the beam after installation. It shows that the extensometers were oriented perpendicular to

the existing major shear crack. In addition, the crack extensometers were placed so as to avoid the future CFRP stirrups (indicated by solid lines in Figure 4.10).

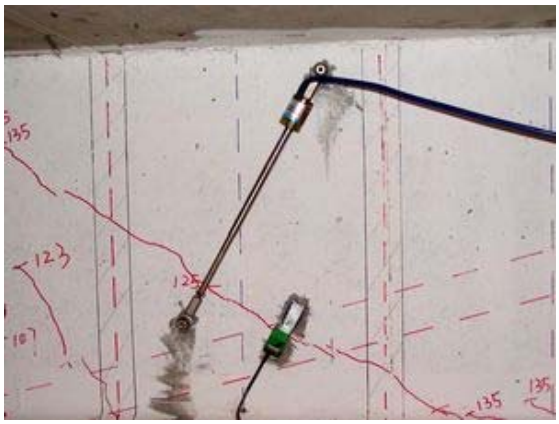

VW Crackmeter and crack gage 1 (front)

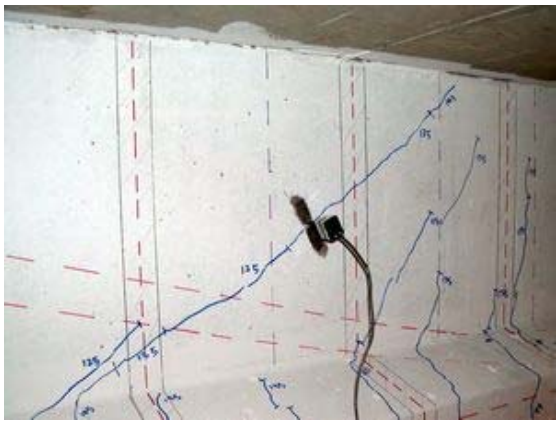

Crack gage 2 (back)

Figure 4.10: VW Crackmeter and crack gages

The test layout and instrumentation setup for Crack Widening Test (T-Beam 3W) is shown in Figure 4.11. The test layout remained the same as T-Beam 3I. LVDT-A was installed on the top of the steel spreader beam to monitor vertical deflection of the beam. Figure 4.12 shows T-Beam 3W in the test frame ready for testing. In addition to the electronic crack width instruments, the visual crack gage was used to measure crack widths at other locations on the beam (Figure 4.13). The visual gage was also used to establish the initial crack size at the crack extensometer locations.

The Crack Widening test consisted of a series of loading cycles at increasing load levels until the maximum residual crack width (no load condition) reached 0.02” (0.5mm), which corresponds to the maximum crack width observed in the Salt Lake Boulevard Bridge girders.

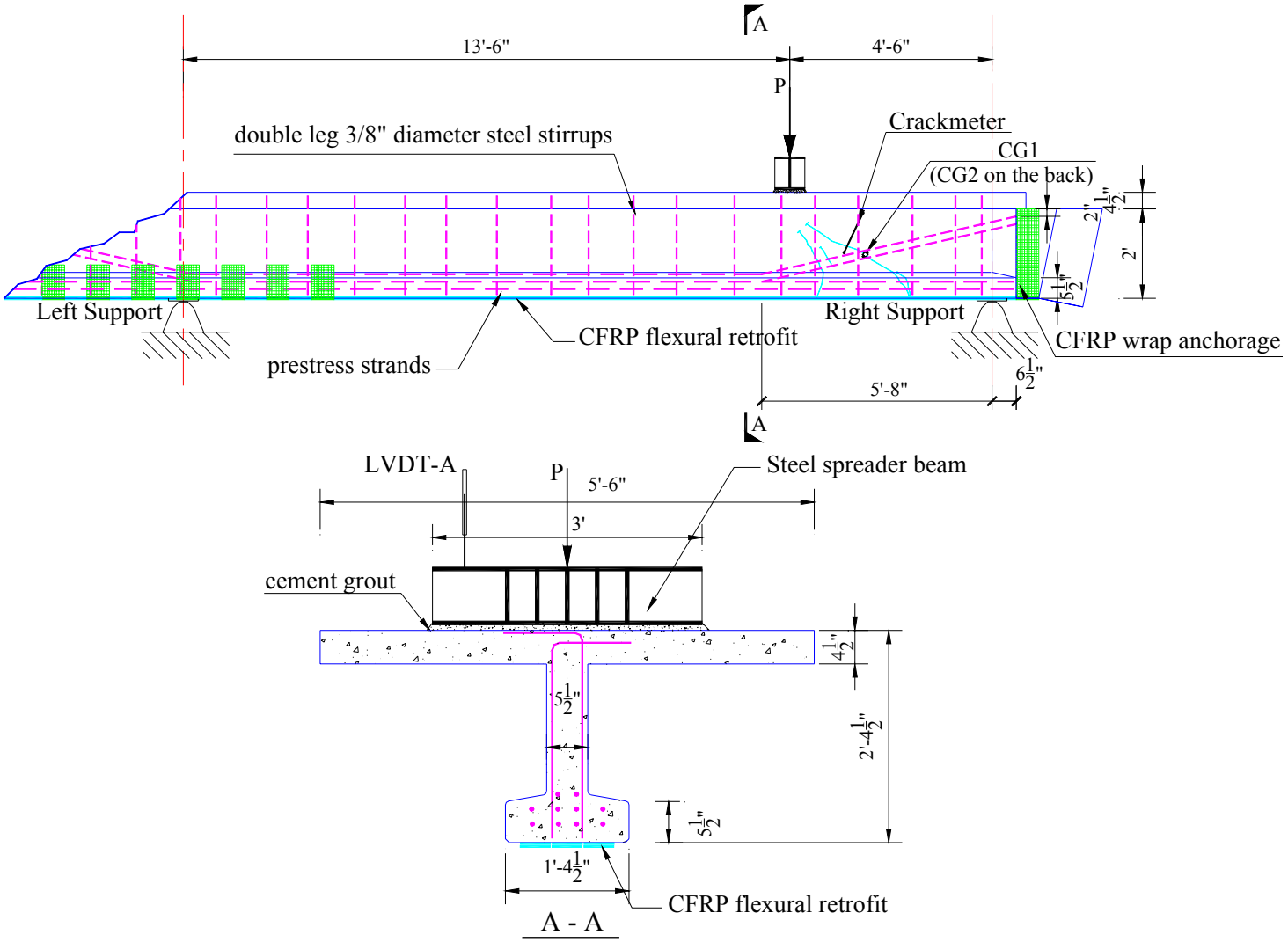

Figure 4.11: T-Beam 3W Layout and Instrumentation

Figure 4.12: T-Beam 3W in the test frame prior to testing

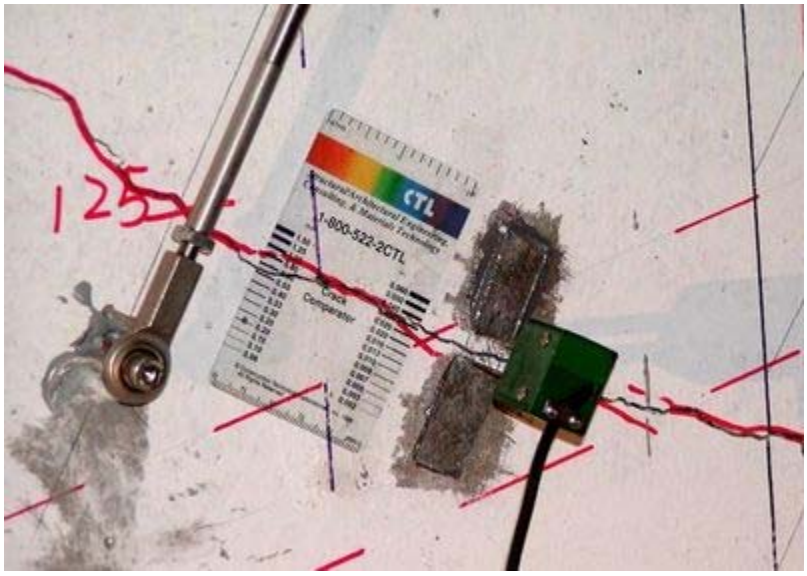

Figure 4.13: Visual Crack Gage and Electronic Crack Extensometers

4.3.4 Shear Retrofit

After the Crack Widening test (T-Beam 3W), the maximum residual shear crack was 0.02" (0.5 mm) wide, and the beam was ready for shear retrofit. In the field application on the Salt Lake Boulevard Bridge, it is likely that the existing cracks will be epoxy injected prior to installation of the CFRP retrofit. If the girders are subjected to the same loading conditions that induced the original cracks, new cracks will likely form close to the epoxy repaired cracks. It will therefore still be important to understand the performance of the CFRP shear retrofit in the presence of shear cracks in the concrete beam. For the current laboratory tests the cracks were not epoxy injected so as to compare their behavior after addition of the CFRP shear retrofit with that observed before retrofit.

The right hand end of the T-Beam 3 was retrofitted with 40 mm (1.6") wide CarboShear-L stirrups with center to center spacing of 12". This spacing represents 0.5d for the T-Beam dimensions. Based on the 4.5 ft shear span dimension, a total of 4 CarboShear-L stirrups were used on each side of the beam. Figure 4.14 shows the shear retrofit for T-Beam 3. In the sections below, the retrofit procedures are described in detail.

Fabrication and Installation of Concrete and FRCC Filler Blocks

In order to provide a continuous bond between the CarboShear-L stirrups and the T-Beam concrete, pre-cast filler blocks were used to fill the recessed web area. The intent was for the filler blocks to transfer the tension in the beam web to the CarboShear-L stirrups. In order to add as little additional weight to the beam as possible, the filler blocks were fabricated only as wide as necessary to provide a bonding surface for the CarboShear-L stirrups.

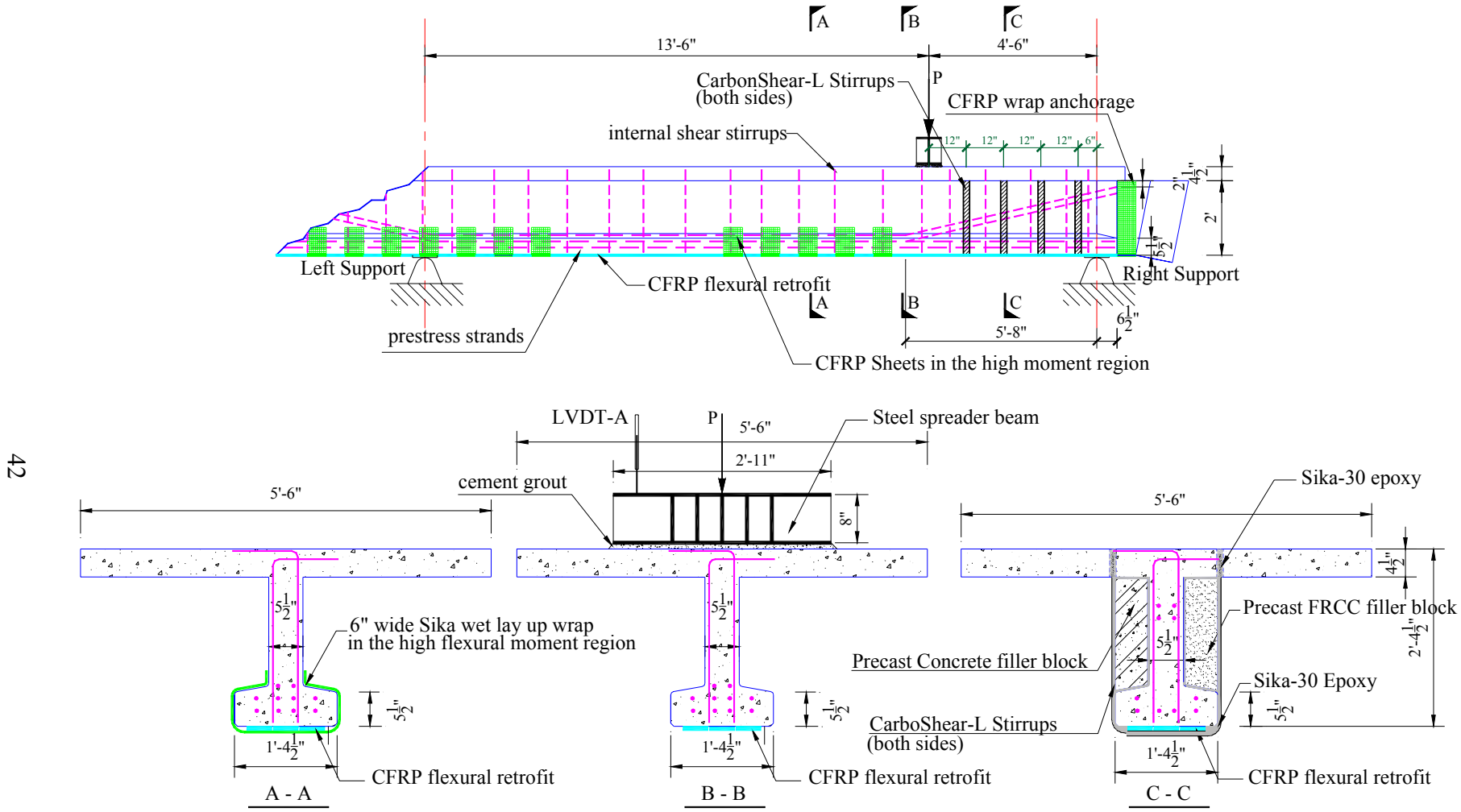

Figure 4.14: T-Beam 3 Shear Retrofit

In this research program, two different cementitious materials were used for the filler blocks to evaluate their ability to transfer tension in the beam web to the CarboShear-L stirrups.

On the back of the beam normal weight concrete filler blocks were used. The concrete mixture was designed to have a similar compressive strength to that of the T-Beam web. These blocks were also reinforced with two 3/8" diameter reinforcing bars, though no dowels were provided between the T-Beam and the filler reinforcing.

On the front of the beam the filler blocks were fabricated using Fiber Reinforced Cementitious Composite (FRCC). FRCC has superior tensile ductility than regular concrete and generally forms numerous closely spaced tensile cracks in place of the larger isolated cracks typical of regular reinforced concrete. It was anticipated that the existing cracks in the T-Beam web would be distributed into smaller cracks in the FRCC filler blocks, which would tend to decrease the localized bond stress on the CarboShear-L stirrups.

The concrete and FRCC filler blocks were pre-cast in wood formwork (Figure 4.15). Each form produced a rectangular concrete panel with dimensions of 40" by 5.5" by 2.5" thick. After moist curing for 7 days, the rectangular panels were cut at mid-length at the correct angle to match the slope on the bottom bulb of the T-Beam. The corners were rounded as necessary for the filler blocks to fit snuggly into the web of the T-Beam. A pneumatic needle gun was used to roughen the contact surface on the side of the beam and on the filler blocks and produce a better epoxy bond (Figure 4.16).

Figure 4.15: Precast Concrete and FRCC panels in the formwork

Figure 4.16: Filler blocks cut to size

The filler blocks were installed using Sika-30 epoxy. A thin layer of epoxy was applied to both contact surfaces before manually pressing the blocks into place (Figure 4.17). Figure 4.18 shows the FRCC filler blocks after installation.

Figure 4.17: Install filler blocks using Sika-30 Epoxy

Figure 4.18: After installation of the filler blocks

For the FRCC blocks, two different types of fiber were used, namely PVA and PP20 (Figure 4.19). The strength and strain capacity of the two types of FRCC are similar, but slightly different performance was anticipated because of the different fiber types. The mix designs and material properties for the concrete and FRCC are present in Chapter 5.

PVA fibers

PP20 fibers

Figure 4.19: Two types of fiber used in FRCC filler blocks

Top Slab Anchorage of CarboShear-L Stirrups

In order to anchor the CarboShear-L stirrups in the compression slab of the T-Beam, slotted holes were created using a concrete coring machine. Three 1" (25 mm) diameter cores were drilled at ½" (12.5 mm) spacing to create a 1" wide by 2" long slot (25 mm by 50 mm) (Figure 4.20).

Figure 4.20: Slot in the top slab for stirrup anchorage

In order to provide the minimum 4" (100 mm) anchorage length recommended by the stirrup manufacturer in the 4.5" (114 mm) thick top slab, a slot was created through the entire slab thickness. A Concrete Coring Machine with 1" diameter core was used to

avoid the concrete pop out that would result from use of a hammer drill. Figure 4.21 shows the coring process while Figure 4.22 shows the bottom of the concrete slab after coring. The coring operation was performed prior to installation of the filler blocks to avoid damage to the filler material.

Figure 4.21: Concrete Coring Machine

Figure 4.22: Anchorage slot cored through top slab

Preparation of CarboShear-L Stirrups

The CFRP stirrups used in this study were Sika CarboShear-L 4/50/100. This designation means the width of the stirrups is 40 mm (1.6”) and the leg lengths are 500 mm (19.7”) and 1000 mm (39.4”), respectively. The stirrup legs were cut to fit the actual dimensions of T-Beam 3.

In order to improve the anchorage at the top end of the CarboShear-L stirrups, the manufacturer recommends pretreatment of the anchorage zone with Sika-30 epoxy. This was performed one day before installation of the CFRP stirrups. The surface of the CarboShear-L stirrup is protected after manufacture by application of a transparent peel-ply. Removal of the peel-ply reveals a clean textured surface ready for epoxy application. This peel-ply was removed over the anchorage length. Sika-30 epoxy was applied to both sides of the stirrup with a serrated towel to form ridges at right angles to the direction of the fibers (Figure 4.23). The anchorage epoxy was allowed to cure for 24 hours before stirrup installation. Figure 4.24 shows the CarboShear-L stirrups after anchorage zone pretreatment.

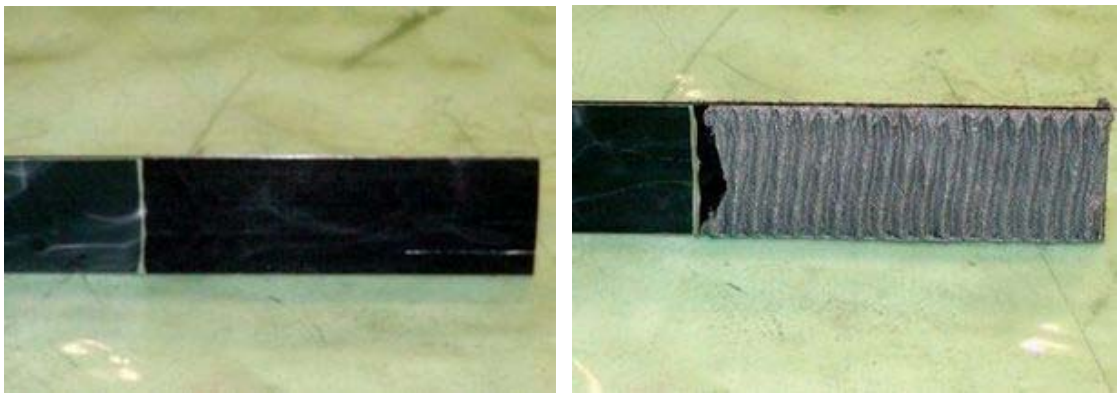

Peel-ply removed in anchorage zone Epoxy applied to anchorage zone

Figure 4.23: Pretreatment of the top end of each CarboShear-L stirrup

Figure 4.24: CarboShear-L stirrups after anchorage zone pretreatment

Installation of CarboShear-L Stirrups

Figure 4.25 shows the installation sequence of CarboShear-L stirrups, following the manufacturer's instruction. The procedure is described in detail below.

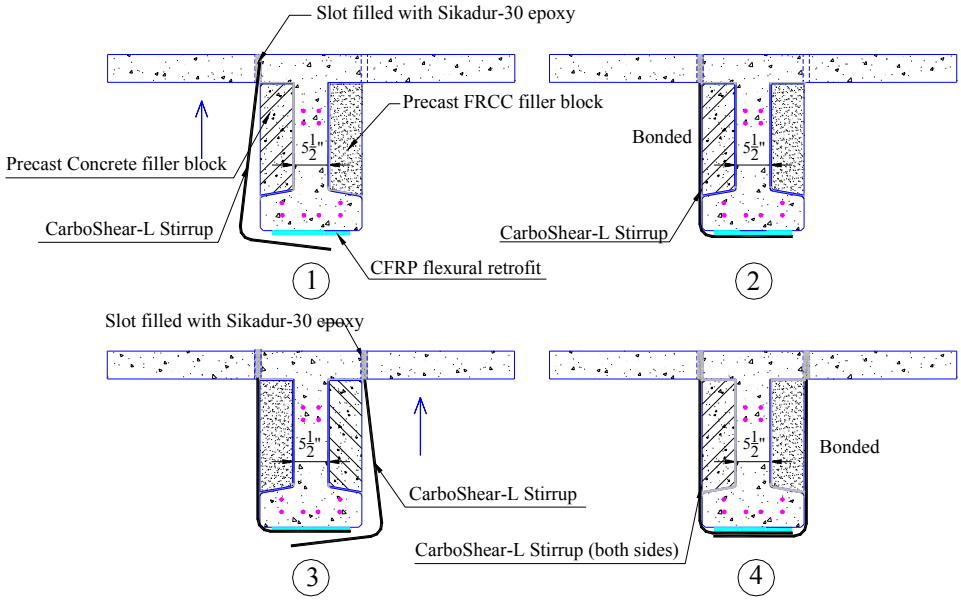

Figure 4.25: Installation sequence of CarboShear-L stirrups

On one side of the web, the slots in the top slab were filled completely with Sika-30 epoxy. A thin layer of Sika-30 epoxy was applied to the roughened surface of the filler block and to the CFRP flexural strips on the soffit of the beam. Additional epoxy was

provided at the stirrup bottom corner to fill the gap between the stirrup radius and the concrete corner bevel. The remaining peel-ply was removed from both faces of the CarboShear-L stirrup. A thin layer of Sika-30 epoxy was applied to the inner face of the stirrup. Holding the stirrup slightly inclined, the vertical leg of the CarboShear-L stirrup was inserted into the epoxy-filled slot in the top slab. The stirrup was then pressed firmly onto the filler block and under the soffit of the beam. The CarboShear-L stirrup on the opposite side of the web was then applied following the same procedure. The exposed surface of the horizontal leg of the first stirrup was primed with Sika-30 epoxy to provide a bond between the overlapping horizontal stirrup legs under the beam soffit. Wood blocks and wedges were used to maintain pressure on the overlapping horizontal legs until the epoxy set. Figure 4.26 shows the CarboShear-L stirrups after installation.

Figure 4.26: CarboShear-L stirrups after installation

Wrap CFRP Sheets Wrap in the High Moment Region

To prevent delamination of the flexural Carbodur strips in the high bending moment region, five 6” wide sheets of Sika Wrap Hex 103C uni-direction fabric were placed

around the soffit of the beam. These wraps were applied to the left of the applied load so as not to interfere with the shear retrofit on the right end of the beam (Figure 4.14)

4.3.5 T-Beam 3 Shear Retrofit Test (T-Beam 3S)

The T-Beam 3 Shear Retrofit Test (T-Beam 3S) was designed to evaluate the performance of the CarboShear-L stirrups installed over existing shear cracks. The beam layout remained the same as for T-Beam 3I and T-Beam 3W, meaning a simply supported span of 18 feet with a single line load applied at 4.5 ft from the right support. LVDT-A was installed on the top of the steel spreader beam to monitor vertical deflection of the beam.

Figure 4.27 shows the layout of the instrumentation for T-Beam 3S. The CarboShear-L stirrups were numbered F1 to F4 on the front of the beam, and B1 to B4 on the back of the beam.

LVDT-1 to LVDT-8 were installed at the top of each stirrup to monitor anchorage slip. LVDT-9 and LVDT-10 were installed at the top of filler blocks on each side of the beam to monitor movement of the filler blocks relative to the beam top slab. Strain gages (SG) 1-52 were installed on the surface of the stirrups following the manufacturer's instructions. Strain gages 7, 14, 21, and 28 were bonded to the surface of the horizontal legs of stirrups F1 to F4 immediately after the bottom radius (i.e. underneath the beam). All strain gages were Micro-measurement electrical resistance gages CEA-06-250UN-350. They were used to monitor strains in the stirrups and to detect delamination of the CarboShear-L stirrups from the concrete substrate. The Vibrating Wire Crackmeter and crack gages 1 and 2 were installed in the same locations as for test T-Beam 3W to monitor the crack width during loading.

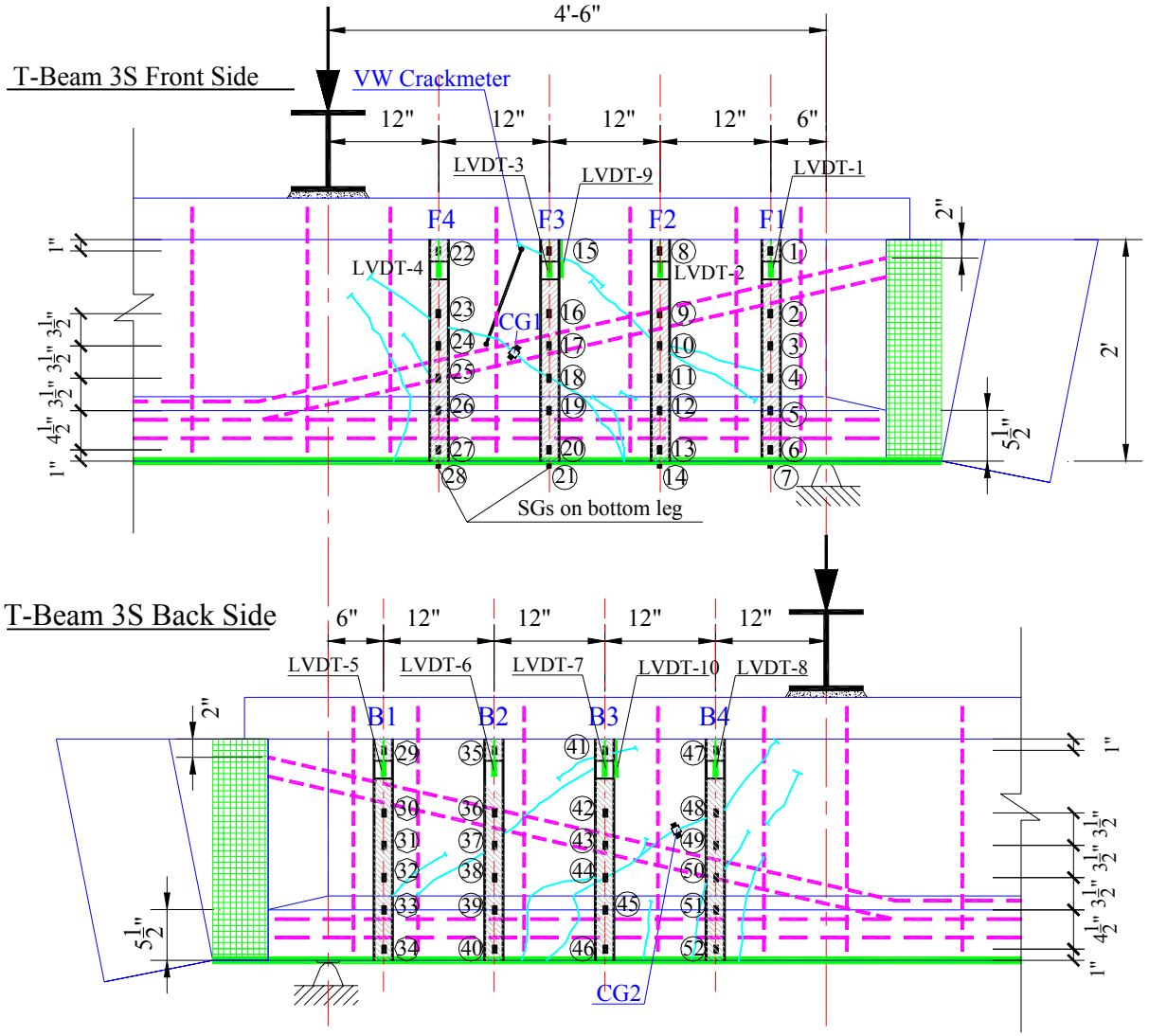

Figure 4.27: Layout of the Instrumentation for T-Beam 3S

Figure 4.28 shows a close-up view of stain gages, LVDTs, VW Crackmeter and crack gage. Figure 4.29 shows T-Beam 3S in the test frame ready for testing.

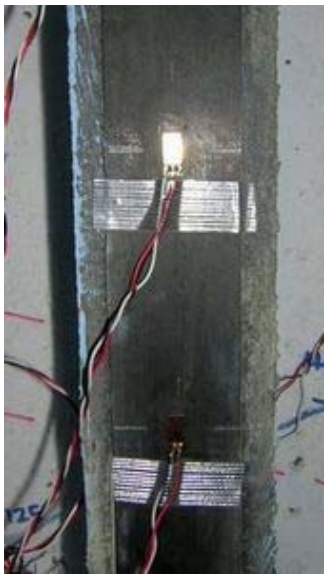

Stain Gages

Crackmeter and Crack Gage 1

Figure 4.28: Close-up view of SGs, LVDTs, VW crackmeter and crack gage

Figure 4.29: T-Beam 3S in the test frame prior to testing

CHAPTER 5

5 MATERIAL PROPERTIES

5.1 Introduction

This chapter presents the material properties of the T-Beam concrete (both pre-cast T-Beam and top slab), reinforcing and prestressing steel, and CarboShear-L stirrups. It also includes the mix design and material properties of the concrete and FRCC filler blocks. These material properties were required for strength calculations in Chapter 6.

5.2 T-Beam 3 Concrete Material Properties

After all testing had been performed on T-Beam 1 and T-Beam 2, a set of 4" diameter by 5.5" long concrete cores were drilled from un-cracked sections of the pre-cast beam web and anchorage blocks using a Concrete Coring Machine. The cores were tested in compression and the resulting strengths adjusted according to ASTM C42-99 due to their non-standard cylinder size. From these compressive strengths, the modulus of elasticity of the concrete was estimated using the expression, $E = 40\sqrt{f_c} + 1000\,(\text{ksi})$ (ACI 1984). Details of the core testing are described in Chapter 6 of Agapay and Robertson (2003).

The material properties of T-Beam 3 were nominally the same as T-Beam 1 and T-Beam 2. Therefore, the compressive strength of the pre-cast concrete of T-Beam 3 and the corresponding modulus of elasticity values were determined from the average result of the tests performed on T-Beams 1 and 2. Table 5-1 shows the average and standard deviation for concrete compressive strengths and corresponding modulus of elasticity values determined from the tests performed on T-Beam 1 and T-Beam 2.

Table 5-1: T-Beam 1 and T-Beam 2 Concrete Properties

	Precast Beam, 4" x 5.5" cores			
	No. of samples	**Avg. f_c (psi)**	**Std. Dev. (psi)**	**E (ksi)**
T-Beam 1	6	8413	329	4669
T-Beam 2	4	8397	555	4665

The compressive strength and modulus of elasticity of the concrete used in the top slab of T-Beam 3 was determined using 6" diameter by 12" long cylinders cast when the top slab was placed. Table 5-2 shows the T-Beam 3 concrete material properties.

Table 5-2: T-Beam 3 Concrete Compressive Strength and Modulus of Elasticity

	Precast Beam				**Top Slab**			
	f_c		**E**		**f_c**		**E**	
	(psi)	(Mpa)	(ksi)	(Gpa)	(psi)	(Mpa)	(ksi)	(Gpa)
T-Beam 3	8405	58.0	4667	32.2	5114	35.3	3104	21.4

5.3 Steel Reinforcement Tensile Strengths

Internal shear stirrups and prestressing strands were recovered from T-Beam 1 and 2 after all beam tests were complete. The shear stirrups were two-legged #3 deformed reinforcing bars. The prestressing stands were 3/8" nominal diameter seven-wire stress-relieved strands with a design nominal tensile strength of 250 ksi. Coupons of these materials were prepared and tested in tension to determine their yield and ultimate strengths. The material properties of T-Beam 3 were nominally the same as T-Beam 1 and 2. The steel reinforcement strengths determined from T-Beam 1 and 2 were therefore also used for T-Beam 3. Table 5-3 lists the yield and ultimate strengths of the shear stirrups and prestressing strands determined from the tests performed on T-Beam 1 and 2.

Table 5-3: Steel Reinforcement Properties

Description	No. of samples	Yield Stress				Ultimate Stress			
		Avg. f_y		Std. Dev.		Avg. f_u		Std. Dev.	
		(ksi)	(Mpa)	(ksi)	(Mpa)	(ksi)	(Mpa)	(ksi)	(Mpa)
Shear stirrups	9	50.9	350.9	1.27	8.8	73.1	504.0	3.31	22.8
Prestress strands	2	/	/	/	/	272	1875.4	/	/

5.4 CFRP Material Properties

The CarboShear-L stirrups used in this study were Sika type 4/50/100 (1.2mm thickness). The stirrup width is 40 mm (1.6") and the leg lengths are 500 mm (19.7") and 1000 mm (39.4"). The stirrup legs were cut to fit the actual dimensions of T-Beam 3. The remnants were tested to determine the tensile strength and modulus of elasticity of the CarboShear-L stirrups. Table 5-4 lists the material properties determined from the tests performed on the CarboShear-L stirrups, as well as the technical data provided by the manufacturer.

Table 5-4: CarboShear-L Stirrup Material Properties

CarboShear-L Stirrups	No. of Spec.	Tensile Strength				ε_{ult}	No. of Spec.	Modulus of Elasticity			
		Avg. f_{CSL}		Std. Dev.				Avg. E_{CSL}		Std. Dev.	
		ksi	Mpa	ksi	Mpa			ksi	Gpa	ksi	Gpa
Coupons Tests	6	373	2570	16	110	0.016	4	22924	158	576	3971
Data from Manufacturer	/	381	2624	/	/	0.017	/	22475	155	/	/

Agapay and Robertson (2003) list the material properties of the 4" wide pre-cured Carbodur strips (used for flexural retrofit) and the Sika Wrap Hex 103C uni-direction wet lay-up sheets (used for anchorage). These properties are repeated in Table 5-5.

Table 5-5: Flexural CFRP Material Properties

CFRP Material	Tensile Strength, f_{CFRP}		Modulus of Elasticity, E_{CFRP}	
	ksi	Mpa	ksi	Gpa
Carbodur strips	406	2799.3	23900	164.8
Sika Wrap Hex 103C	139	958.4	10600	73.1

5.5 Mix Design and Material Properties for the Concrete and FRCC Filler Blocks

In order to install the CarboShear-L stirrups around the T-Beam section, concrete and FRCC filler blocks were pre-cast in the laboratory and installed in the web area of the beam as described in Chapter 4. Table 5-6 and Table 5-7 list the mix design for the concrete and FRCC used in the filler blocks.

Table 5-6: Mix Design for the pre-cast filler blocks (US Customary)

Concrete			FRCC 1 (with PVA fiber)			FRCC 2 (with PP20 fiber)		
Material	1.5 ft^3	1 yd^3	Material (lb)	0.35 ft^3	1 yd^3	Material (lb)	0.35 ft^3	1 yd^3
w/c	0.35	0.35	Cement	14.84	1144.8	Cement	14.84	1144.8
#3 Fine (lb)	87.68	1578.2	Fly ash	11.87	915.68	Fly ash	11.87	915.68
Dune Sand (lb)	23.61	424.98	Sand	11.87	915.68	Sand	11.87	915.68
Concrete Sand (lb)	44.02	792.36	Water	6.53	503.74	Water	6.53	503.74
Cement (lb)	43.68	786.24	2 % PVA fiber	0.57	43.97	2 % PP20 fiber	0.40	30.86
Water (lb)	18.34	330.12	SP***	0.22	16.97	SP***	0.22	16.97
Daratard * (fl oz)	1.40	25.2	* Retarding Admixture ** Air entraining Admixture *** Super Plasticizer					
Darex ** (fl oz)	1.27	22.86						

Table 5-7: Mix Design for the pre-cast filler blocks (SI Units)

Concrete			FRCC 1 (with PVA fiber)			FRCC 2 (with PP20 fiber)		
Material	42.5 L	1 m^3	Material (kg)	10 L	1 m^3	Material (kg)	10 L	1 m^3
w/c	0.35	0.35	Cement	6.732	673.2	Cement	6.732	673.2
#3 Fine (kg)	39.77	935.76	Fly ash	5.386	538.6	Fly ash	5.386	538.6
Dune Sand (kg)	10.71	252.0	Sand	5.386	538.6	Sand	5.386	538.6
Concrete Sand (kg)	19.97	469.88	Water	2.962	296.2	Water	2.962	296.2
Cement (kg)	19.81	466.12	2 % PVA fiber	0.260	26.0	2 % PP20 fiber	0.180	18.0
Water (kg)	8.32	195.76	SP***	0.101	10.1	SP***	0.101	10.1
Daratard * (ml)	41.22	969.88	* Retarding Admixture ** Air entraining Admixture *** Super Plasticizer					
Darex ** (ml)	37.48	881.88						

The compressive strength of the concrete was determined using 6" diameter by 12" long cylinders cast when the concrete filler blocks were poured. Compressive strength of FRCC 1 and 2 were determined from 4" diameter by 8" long cylinders. Table 5-8 lists the compressive strength and modulus of elasticity of the pre-cast concrete, FRCC 1 and 2.

Table 5-8: Material Properties of the Filler Blocks

	No. of Spec.	Compressive Strength, f_c		Modulus of Elasticity, E	
		psi	Mpa	ksi	Gpa
Concrete	2	7101	49.0	4371	30.1
FRCC 1 (PVA)	1	12251	84.5	/	/
FRCC 2 (PP20)	1	9865	68.0	/	/

CHAPTER 6

6 THEORETICAL BEAM SHEAR STRENGTHS

This chapter presents shear strength predictions for the control T-Beam 3 without shear retrofit and for the retrofitted T-Beam 3. It also includes a prediction for the short-term (instantaneous) load-deflection relationship for the beam.

In 1994, the American Association of State Highway and Transportation Officials (AASHTO) adopted the Load-Resistance Factor Design (LRFD) specifications for the design of bridge structures (AASHTO, 1999). Based on the AASHTO LRFD bridge design specifications, analysis shows that the Salt Lake Boulevard Bridge girders are under-designed for shear (KAI Hawaii, 2003)

In this research program, the original shear capacity of the control beam (left end of T-Beam 3) is predicted using the AASHTO, "LRFD Bridge Design Specifications", as well as the ACI 318-02, "Building Code Requirements for Structural Concrete". For the shear retrofitted right end of T-Beam 3, the ACI 440.2R-02 approach and the recommendations from the manufacturer (Sika Corporation, 2002) are used to predict the contribution of the CarboShear-L stirrups. The short-term deflection of the T-Beam is calculated based on the ACI code recommendation. Details of these calculations are presented in Appendix A.

The predicted shear strengths and the short-term load-deflection relationship are compared with the observed test results in Chapter 8.

6.1 Shear Strength of T-Beam 3 (without shear retrofit)

The original shear capacity of the T-Beam (left end of T-Beam 3) is predicted by using the AASHTO "LRFD Bridge Design Specifications" (AASHTO, 1999), as well as by using the ACI 318-02 "Building Code Requirement for Structural Concrete" (ACI318, 2002).

The T-Beam was simply supported on an 18 feet span with a single line load applied at 4.5 ft from the left support. Based on the span dimensions, the total load applied to the beam was transferred to the supports in the ratio 3 to 1. The left span (test span) therefore resisted three fourths of the total load applied to the beam.

The T-Beam was prestressed with ten 3/8" diameter seven-wire stress relieved strands. The existing internal steel stirrups were 2-leg #3 stirrups at approximately 12" spacing. Figure 6.1 shows the T-Beam layout and geometrical dimensions for the original shear capacity calculation. The shear strength analysis and shear profile along the length of the beam are developed in this section. Detailed calculations are presented in Appendix A along with a list of notation used in the computations.

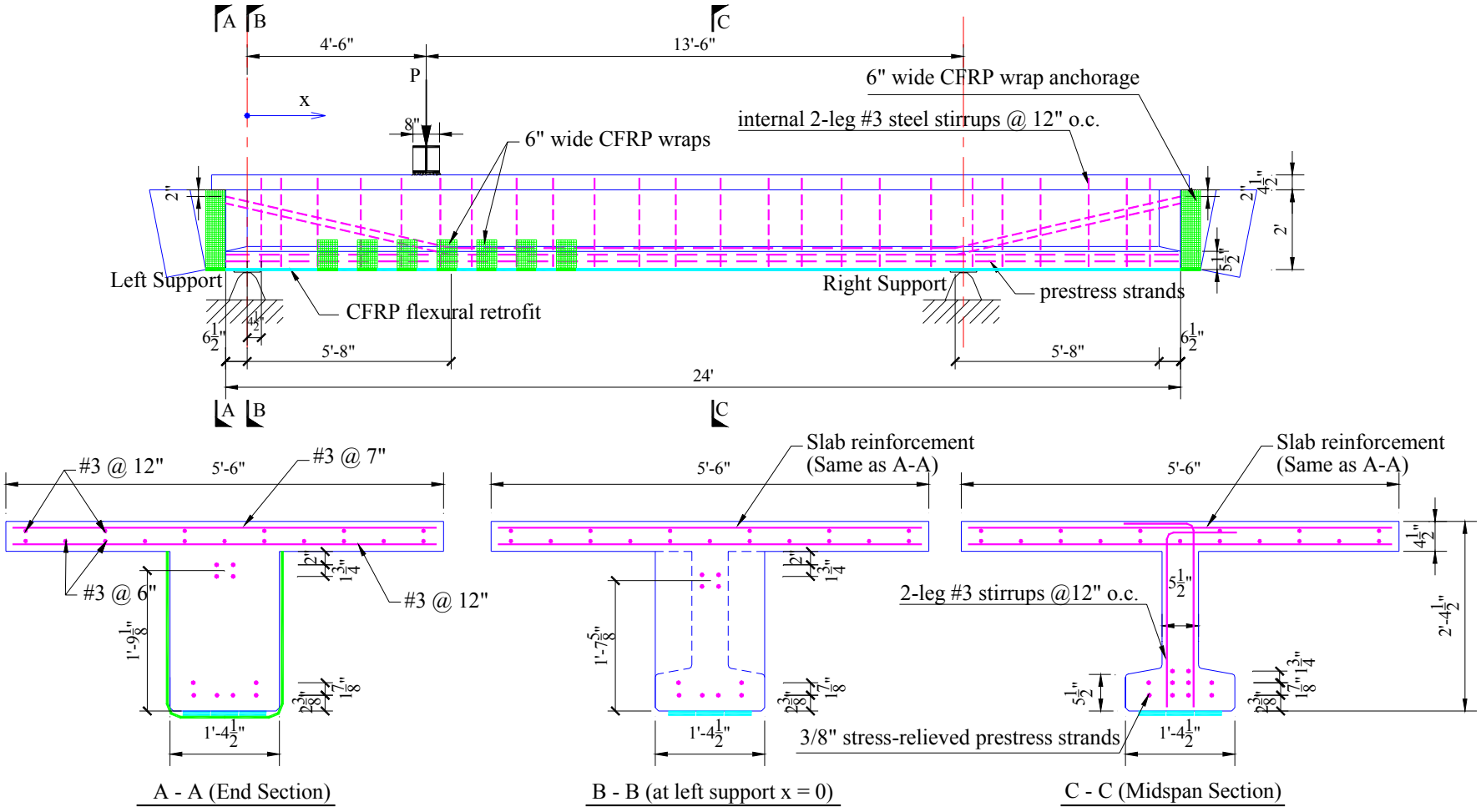

Figure 6.1: T-Beam 3 layout for the control shear strength calculation

6.2.1 *Using the AASHTO "LRFD Bridge Design Specifications" to Calculate V_n*

Based on the AASHTO "LRFD bridge design specifications", V_n, the nominal shear resistance of the prestressed beam, is given as:

$$V_{n\_AASHTO}(x) = V_p(x) + V_c(x) + V_s(x)$$

where: x = distance from the left hand end of the beam, as shown in Figure 6.2

V_p = nominal shear strength provided by vertical component of the harped longitudinal tendons

$$V_p = P_e \cdot \sin\psi$$

V_c = nominal shear strength provided by the tensile stresses in the concrete, and

$$V_c(x) = 0.0316\beta(x)\cdot\sqrt{f_c'\cdot 10^{-3}}\cdot b_v \cdot d_v(x)$$

V_s = nominal shear strength provided by the tensile stresses in the web reinforcement, and

$$V_s(x) = \frac{A_v \cdot f_y \cdot d_v(x)\cdot Cot\,\theta(x)}{s}$$

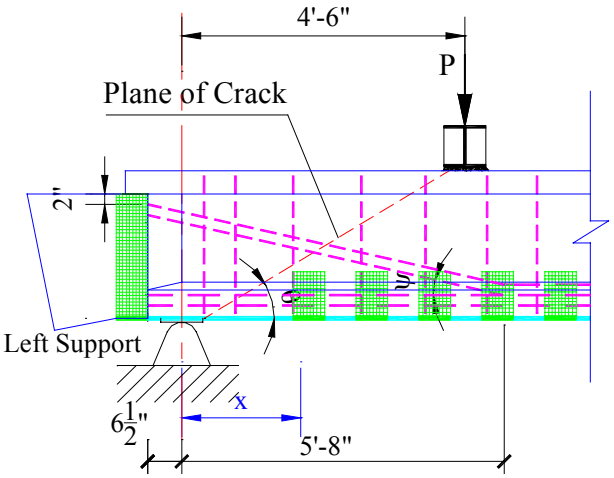

Figure 6.2: T-Beam Parameters for AASHTO

In order to determine the nominal shear resistance of the prestressed T-Beam, the values β and θ are needed to compute V_c and V_s. For prestressed concrete sections, AASHTO assumes a shear crack with inclination θ to the horizontal. The crack inclination θ will change along the beam span. With the assumed θ, the strain in the tensile reinforcement, ε_x, can be obtained using

$$\varepsilon_x(x) = \frac{\frac{M_u(x)}{d_v(x)} + 0.5 \cdot N_u + 0.5 \cdot V_u(x) \cdot Cot\theta(x) - A_{ps} \cdot f_{po}}{2 \cdot \left(E_s \cdot A_s + E_{ps} \cdot A_{ps} + E_f \cdot A_f\right)}$$

With the value of ε_x, AASHTO Table 15.9 is used to check whether the angle θ is close to the one assumed in the first trial. If so, then the β value obtained from AASHTO Table 15.9 is used to compute V_c and V_s; if not, the procedure is repeated until the predicted θ is very close to the value obtained from Table 15.9. The procedure to calculate V_n using AASHTO "LRFD Bridge Design Specifications" for T-Beam 3 is presented in Appendix A.

6.2.2 Using ACI 318-02 to Calculate V_n

Compared with the AASHTO code, the ACI approach to calculate the shear capacity for beams is simpler and more straightforward, without requiring a trial and adjustment procedure. Based on the ACI 318-02, "Building Code Requirements for Structural Concrete", V_n, the nominal shear resistance of the prestressed beam, is given as:

$$V_{n\_ACI}(x) = V_c(x) + V_s(x)$$

Where: x = distance from the left hand end of the beam, as shown in Figure 6.2

V_c = nominal shear strength provided by concrete section, including the effect of harped tendons, given by:

$$V_{c\_ACI}(x) = min\left(V_{cw}(x), V_{ci}(x)\right)$$

V_s = nominal shear strength provided by steel stirrups

$$V_{s\_ACI}(x) = \frac{A_s \cdot f_y \cdot d_p(x)}{s}$$

The concrete contribution, V_c, is the lesser of V_{ci} and V_{cw}. For V_{ci}, the flexure-shear strength, the ACI code gives

$$V_{ci}(x) = 0.6 \cdot \lambda \cdot \sqrt{f_c'} \cdot b_w \cdot d_p(x) + V_d(x) + \frac{V_i(x) \cdot M_{cr}(x)}{M_{max}(x)}$$

For V_{cw}, the web-shear strength, the ACI code gives

$$V_{cw}(x) = \left(3.5\lambda \cdot \sqrt{f_c'} + 0.3 f_{pc}(x)\right) \cdot b_w \cdot d_p(x) + V_p(x)$$

The ACI 318-02, "Building Code Requirements for Structural Concrete" procedure to calculate V_n for T-Beam 3 is presented in Appendix A. The notation used in these formulas is explained in Appendix A.

6.2.3 Plot of Shear Capacity Profile for T-Beam 3

Figure 6.3 shows the profile of V_c, the nominal shear strength provided by concrete. Compared to the ACI code, the AASHTO approach gives a much lower estimate of shear capacity, especially in the test shear span between the left support and the load point.

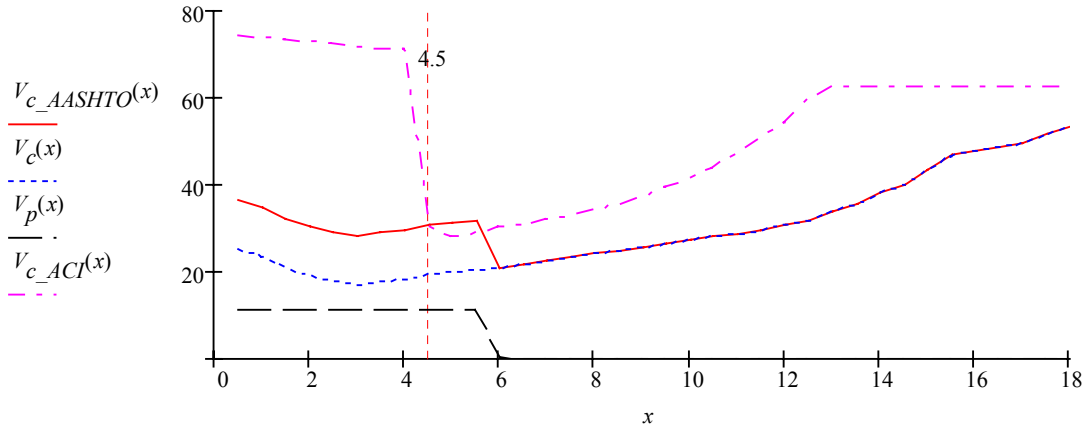

Where: $V_{c\_AASHTO}(x) := V_c(x) + V_p(x)$

Figure 6.3: Shear capacity of concrete, V_c

Figure 6.4 shows the profile of V_s, the nominal shear strength provided by shear reinforcement. The difference between the AASHTO and the ACI approach is that the AASHTO Code considers the crack inclination, θ, while the ACI Code assumes a constant 45° crack inclination. This results in a higher contribution of the steel stirrups in the AASHTO approach.

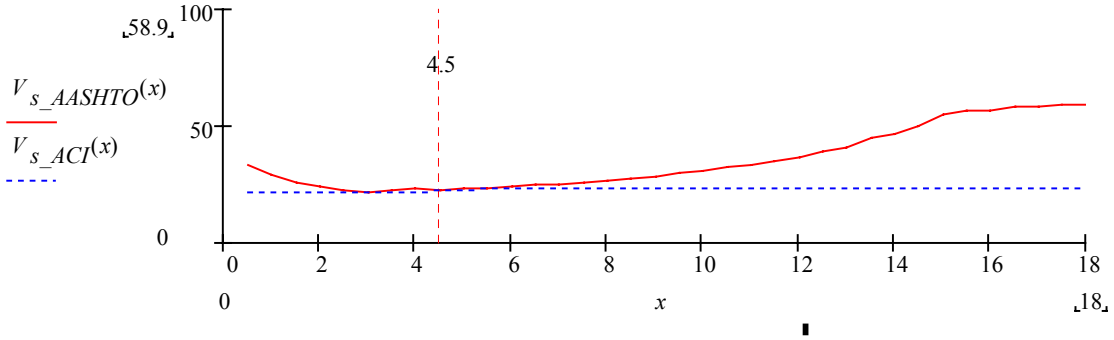

Figure 6.4: Shear capacity of steel stirrups, V_s

Figure 6.5 shows the applied shear diagram for T-Beam 3C at maximum load, and the shear capacity predicted by the AASHTO and ACI codes for the beam without CFRP shear retrofit.

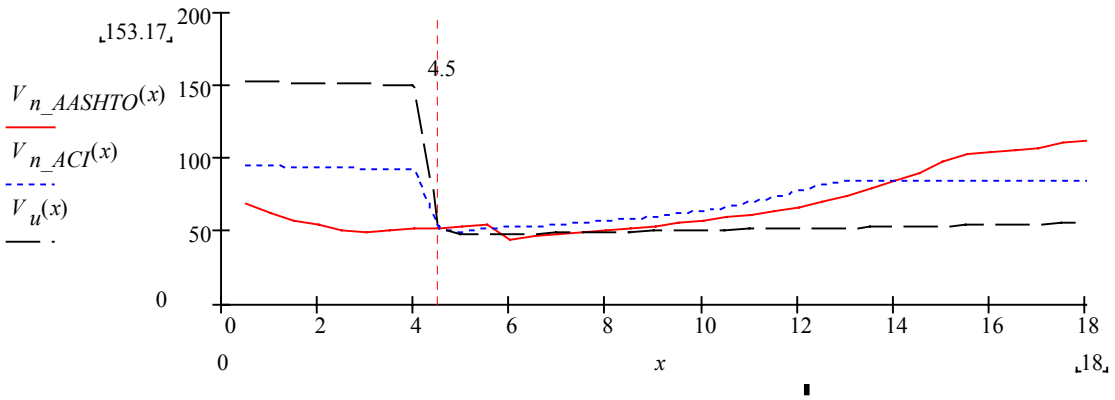

Figure 6.5: Shear capacity and shear diagram of T-Beam 3C

The minimum shear capacity predicted by AASHTO code for the test span (left span) is, V_n = 49.77 kips at 3' from the left support, while the ACI code prediction is V_n = 92.24 kips at 4' from the left support. The maximum shear supported by the left shear span was 153 kips.

Both codes are conservative in predicting shear capacity of the T-Beam, with more conservatism in the AASHTO prediction. These values are compared with the observed strengths in Chapter 8.

6.3 Shear Strength of the T-Beam 3 with CarboShear-L Stirrups

6.3.1 Introduction

The concrete and existing steel stirrup contributions to the total shear strength were computed based on the AASHTO and ACI 318-02 code as described above. The additional shear strength provided by the CarboShear-L stirrups was computed according to the ACI 440.2R-02 report (ACI 440, 2002) and the recommendations from the manufacturer (Sika Corporation, 2002). ACI 440.2R-02 assumes that these strengths are cumulative so that the total shear strength of T-Beam 3 with shear retrofit is the sum of shear strengths contributed by the concrete, internal steel stirrups and FRP stirrups.

Figure 6.6 shows the beam layout for the calculation of the shear capacity of the beam with shear retrofit. The geometrical dimensions were exactly the same as the left hand end of T-Beam 3C (Figure 6.1).

The shear strength analysis and the minimum shear capacity along the test span (right span) are developed in the next section.

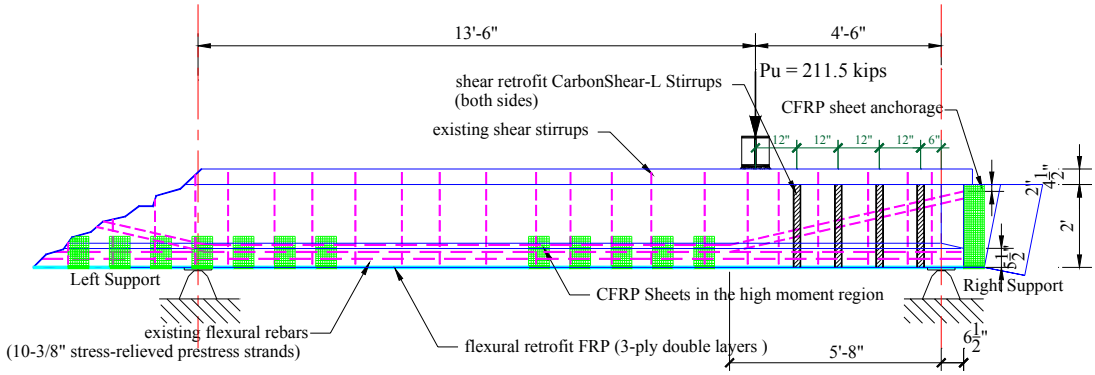

Figure 6.6: Layout of the T-Beam 3 with shear retrofit

6.3.2 Contribution of Concrete and Existing Steel Stirrups (V_c and V_s)

The concrete and existing steel stirrups contributions to the total shear strength were computed at 0.5 ft intervals from the right support to the load point following the same procedure as described in Section 6.1.

Based on the AASHTO code, the minimum contribution of concrete and existing steel stirrups to the overall shear strength was 48.59 kips at 2.5' from the right support.

Based on ACI code, the minimum contribution of concrete and existing steel stirrups to the overall shear strength was 92.24 kips at 4' from the right support.

6.3.3 Contribution of CarboShear-L Stirrup Shear Retrofit (V_f)

The beam was retrofitted in shear using 40mm (1.57") wide CarboShear-L stirrups at 12" spacing. The ACI 440.2R-02 report, "Guide for the design and Construction of

Externally Bonded FRP Systems for Strengthening Concrete Structures", (ACI 440, 2002) does not include guidelines for the CarboShear-L stirrup retrofit system. However, this retrofit system is similar to the full-wrap FRP system presented in Chapter 10 of ACI 440.2R-02. The additional shear strength provided by the CarboShear-L stirrups was computed based on these provisions. The additional shear strength provided by the CarboShear-L stirrups was also predicted using the manufacturer's recommendations (Sika Corporation, 2002).

ACI440.2R-02 Prediction

In this section, the additional shear strength provided by the CarboShear-L stirrup was computed based on the guidelines from the ACI 440.2R-02. This retrofit system was considered similar to the full-wrap FRP system.

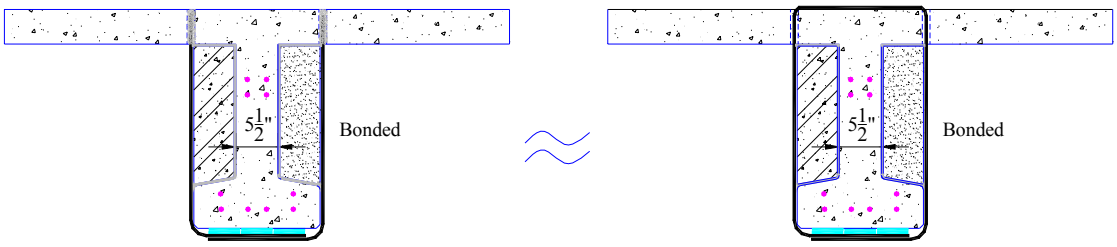

CarboShear-L Stirrup System Full-Wrap FRP System

CarboShear-L Properties:

$\psi_f := 0.95$ (ACI 440R-02, Table10.1 for full-wrap member)

$d_p := 22.8 \quad in$ (Based on the ACI code)

$d_f := d_p \qquad d_f = 22.8 \quad in$

$n := 1$ ply $\quad s_f := 12$ in $\quad w_f := 1.57$ in $\quad f_{c'} = 8405$ psi

$E_f := 22924$ ksi $\quad t_f := 0.05$ in $\quad f_{fu} := 372.7$ ksi $\quad C_E := 1$ (no environmental influence)

Calculation of V_f:

$A_{fv} := 2 \cdot n \cdot t_f \cdot w_f$ $\quad A_{fv} = 0.16$ in^2 $\quad \varepsilon_{fu} := \frac{C_E \cdot f_{fu}}{E_f}$ $\quad \varepsilon_{fu} = 0.02$

$\varepsilon_{fe} := 0.004$ $\quad \varepsilon_{fe} = 0.004 \le 0.75 \cdot \varepsilon_{fu} = 0.008$ So : $\quad \varepsilon_{fe} := 0.004$

$f_{fe} := E_f \cdot \varepsilon_{fe}$ $\quad f_{fe} = 91.7$ ksi $\quad V_f := \frac{A_{fv} \cdot f_{fe} \cdot d_f}{s_f}$ $\quad V_f = 27.35$ $kips$

Contribution of CFRP sheets to shear strength is: $\psi_f V_f = 26$ $kips$

Based on Recommendation from the Manufacturer, Sika Corporation

In this section, the additional shear strength provided by the CarboShear-L stirrup was computed based on the recommendation Sika Corporation. The main difference is the assumed maximum strain, ε_{fe}. Sika recommends a maximum 0.7% strain, while ACI 440.2R-02 limits the strain to 0.4%.

CarboShear-L Properties:

$\psi_f := 0.95$ (ACI 440R-02, Table10.1 for full-wrap member)

$d_p := 22.8$ in (Based on the ACI code)

$d_f := d_p$ $\quad d_f = 22.8$ in

$n := 1$ ply $\quad s_f := 12$ in $\quad w_f := 1.57$ in $\quad f_{c'} = 8405$ psi

$E_f := 22924$ ksi $\quad t_f := 0.05$ in $\quad f_{fu} := 372.7$ ksi

Then , calculate V_f:

$A_{fv} := 2 \cdot n \cdot t_f \cdot w_f$ $\quad A_{fv} = 0.16$ in^2 (ACI 440R-02, Eq.10-4)

$\varepsilon_{fe} := 0.007$ (from EMPA Tests, provided by Sika manufacturer's instructions)

$f_{fe} := E_f \cdot \varepsilon_{fe}$ $\quad f_{fe} = 160.47$ ksi (ACI 440R-02, Eq.10-5)

$V_f := \frac{A_{fv} \cdot f_{fe} \cdot d_f}{s_f}$ $\quad V_f = 47.87$ $kips$

Contribution of CFRP sheets to shear strength is: $\psi_f \cdot V_f = 45.47$ $kips$

The recommendation from the manufacturer gives greater credit to the retrofit system.

6.3.4 Nominal Shear Capacity of the T-Beam with Shear Retrofit

For the purposes of this report, the nominal shear capacity of the beam with shear retrofit will be based on the ACI 440 procedure. Therefore, the nominal shear capacity of the right hand end of T-Beam 3 with shear retrofit is: $V_n = V_c + V_s + V_p + V_f$ = 16.23 + 20.07 + 11.29 + 26 = 74.52 kips, based on the AASHTO procedure, and $V_n = V_c + V_s + V_f$ = 70.89 + 21.35 + 26 = 118.24 kips, based on the ACI 318-02 procedure. These values are compared with the observed strengths in Chapter 8.

6.4 Prediction of the Short-Term Load-Deflection Relationship

In this section, the short-term load-deflection relationship of the T-Beam without retrofit is predicted based on the ACI code provisions. The calculations include 2 stages, precracking and postcracking. In the precracking stage, the uncracked member is assumed to have linear elastic behavior and ends at the initiation of the first flexural crack. In the postcracking stage the structural member develops acceptable controlled cracking in both distribution and width. Most beams lie in this region at service load.

Because of uncertainty regarding the effective prestress in the beam, and the concrete cracking strength, upper and lower bound estimates were included. The effective prestress was assumed to be between 0.7 and 0.8 f_{pi}, and the modulus of rupture was assumed to be between 6 and 7.5 $\sqrt{f_c}$. These ranges produce upper and lower bound estimates of the cracked moment of inertia.

The calculation procedure is presented in Appendix A. The prediction is compared with the observed result in Chapter 8.

Figure 6.7 shows the prediction for the short-term load-deflection relationship of the T-Beam 3C without retrofit based on the ACI code.

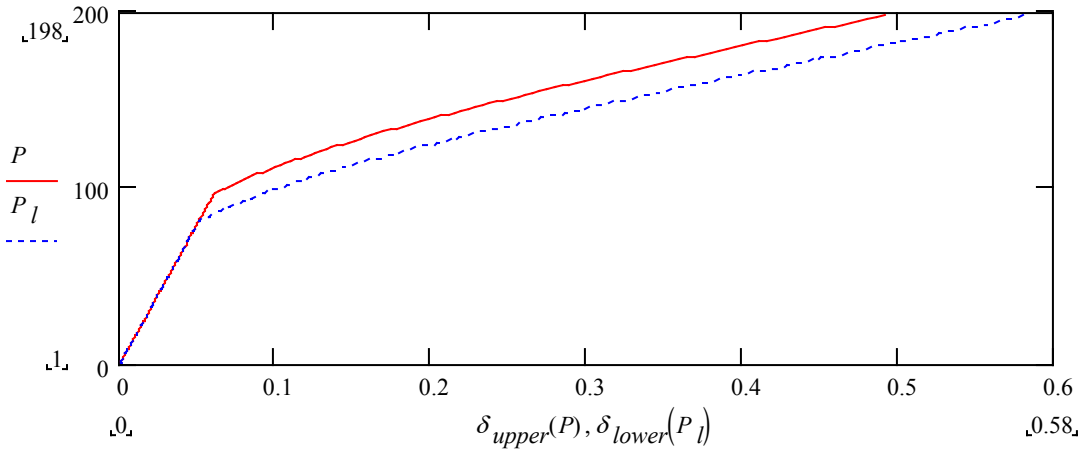

Figure 6.7: Short-term load-deflection relationship prediction

CHAPTER 7

7 TEST PROCEDURES AND RESULTS

This chapter presents the test procedures and results of all the tests performed in this study. In the first section of this chapter, the test system is introduced. In the rest of the chapter, the loading procedures, beam response and test results of T-Beam 3C, T-Beam 3I, T-Beam 3W and T-Beam 3S are presented in sequence. In addition, the beam failure modes of T-Beam 3C and T-Beam 3S are described in detail.

7.1 Test systems

All the loading in this study was performed in displacement control. The majority of each test was performed under the control of the MTS TestStar II controller. In order to cycle the applied load at selected points during the tests, control was transferred from the MTS TestStar II to manual control. All unloading cycles and some of the reloading cycles were performed manually.

Throughout the test, including all loading and unloading operations, instrument output was recorded by a National Instrument Data Acquisition system running Labview. These recordings included applied load, actuator displacement, load point LVDT displacement, as well as any other sensors installed on the specimen, such as strain gages, crack gages and LVDTs.

US Customary units are used in this chapter when referring to the beam loads. The conversion from US Customary system to SI system is: 1 kip equals 4.45 kN.

7.2 T-Beam 3 Control Shear Test (T-Beam 3C)

Figure 7.1 shows the initial setup for T-Beam 3C. The beam was simply supported on an 18 feet span with a single line load applied at 4.5 ft from the left support. A detailed description of the test setup and instrumentation is provided in Chapter 4.

Figure 7.1: T-Beam 3C ready for testing

7.2.1 Loading Procedure and Beam Response

The initial loading of the beam was performed in displacement increments of 0.01" as measured by the actuator displacement sensor. This displacement did not correspond directly to the true beam displacement at the load point because of the flexibility in the test frame and swivel head loading platen. Final load-displacement relationships were based on the beam deflections measured by the LVDT-A located at the load point.

At a total load of 85 kips, the first visible flexural cracks were detected in the bottom of the beam under the load point. These cracks extended through the bulb at the bottom of the beam, but not into the web of the beam.

At a total load of 94 kips, the flexural cracks extended slightly into the web of the beam. The maximum crack size was still less than 0.003" (0.08mm). At 103 kips, new

flexural cracks had formed on both front and back faces of the beam with the largest crack width approximately 0.005" (0.15mm). Loading was increased to 113 kips without significant increase in the crack sizes.

At a total load of 121 kips, which represents a shear in the left span of 91 kips, the first web shear cracks formed. The cracks projected through the web and were evident on both sides of the beam. These hairline shear cracks were approximately 0.004" (0.1mm) wide. The crack width estimates were made with a visual crack gage. The crack orientations were between 28 and 34 degrees from the horizontal on both front and back of the web. The inclination decreased slightly to between 24 and 28 degrees close to the support (Figure 7.2). These crack inclinations are somewhat lower than the values of θ predicted by AASHTO, which vary from 27^o at the support to 43.9^o at the load point (section 6.2.1). Note that in all figures of beam cracking, markers have been used to highlight the cracks (Red on the front of the beam and blue on the back). The cracks therefore appear much wider than their actual size.

Front of the beam Back of the beam

Figure 7.2: First web shear cracks formed at 121 kips total load

The MTS controller was switched to manual control and the load was slowly released to zero. Reloading to 124 kips was performed under displacement control by the MTS

controller. During reloading, both flexural and shear cracks extended slightly and the shear crack width increased to approximately 0.005” (0.15mm).

The beam was again unloaded and reloaded to 124 kips. The maximum shear crack width now measured 0.007” (0.2mm). A third cycle to zero load and return to 120 kips resulted in slight extensions at the ends of the shear crack but no measurable increase in crack width. A final cycle was performed to zero and back to 123 kips with no noticeable change in the crack length or width.

The load was then increased to 129 kips. The shear crack width was measured at 0.016” (0.4mm). The load was further increased to 134 kips, by which point the maximum shear crack width under load had increased to 0.02” (0.5mm).

The beam was again subjected to a series of unloading and reloading cycles at the 134 kip level. The visual crack gage was used to estimate crack width during unloading and reloading cycles.

During the first unloading cycle, the residual crack width at zero load was approximately 0.013” (0.3mm). On reloading to 134 Kips, the crack width opened to 0.025” (0.6mm). The load was again reduced to zero, with the crack closing to between 0.013 and 0.016” (0.3 to 0.4mm). The beam was reloaded to 133Kips, opening the crack to 0.025 to 0.03” (0.6 to 0.75mm). The beam was again unloaded to zero load, with the residual crack size now 0.016” (0.4mm).

The beam was subjected to another three loading and unloading cycles from zero to 130 kips. The residual crack under no load was now relatively constant at 0.02” (0.5mm). Under a total load of 130 kips, the crack opened to 0.04” (1 mm).

The total load was increased to 138 kips at which point the shear crack width had increased to 0.04 to 0.05" (1 to 1.25mm). At 148 kips the crack size was between 0.05 and 0.06" (1.25 to 1.5 mm). The load was cycled to zero and back to 148 kips for two cycles. The residual crack width at zero load was 0.03" (0.75mm). Figure 7.3 shows the cracks on the front and back of the T-Beam at a total load of 148 kips.

Front of the beam Back of the beam

Figure 7.3: Shear cracks on both sides of the T-Beam at 148 kips

The load was now increased monotonically from 148 kips to failure (Figure 7.4). The T-Beam failed in shear at a maximum load of 198 kips, which represents a shear in the left span of 150 kips. The details of the failure are presented in Section 7.2.4.

Figure 7.4: Failure of T-Beam 3C

7.2.2 Shear-Displacement Relationship

The vertical deflection of T-Beam 3C was recorded by the LVDT-A installed on the top of the steel spreader beam as described in Chapter 4. Based on the span dimensions, the total load applied to the beam was transferred to the supports in the ratio 3 to 1. Therefore, the shear in the test shear span (left end of beam) resisted three fourths of the total load applied to the beam. Figure 7.5 shows the shear-displacement relationship recorded during the test. The shear-displacement curves of T-Beam 3C, T-Beam 3I, T-Beam 3W and T-Beam 3S are compared and discussed in Chapter 8.

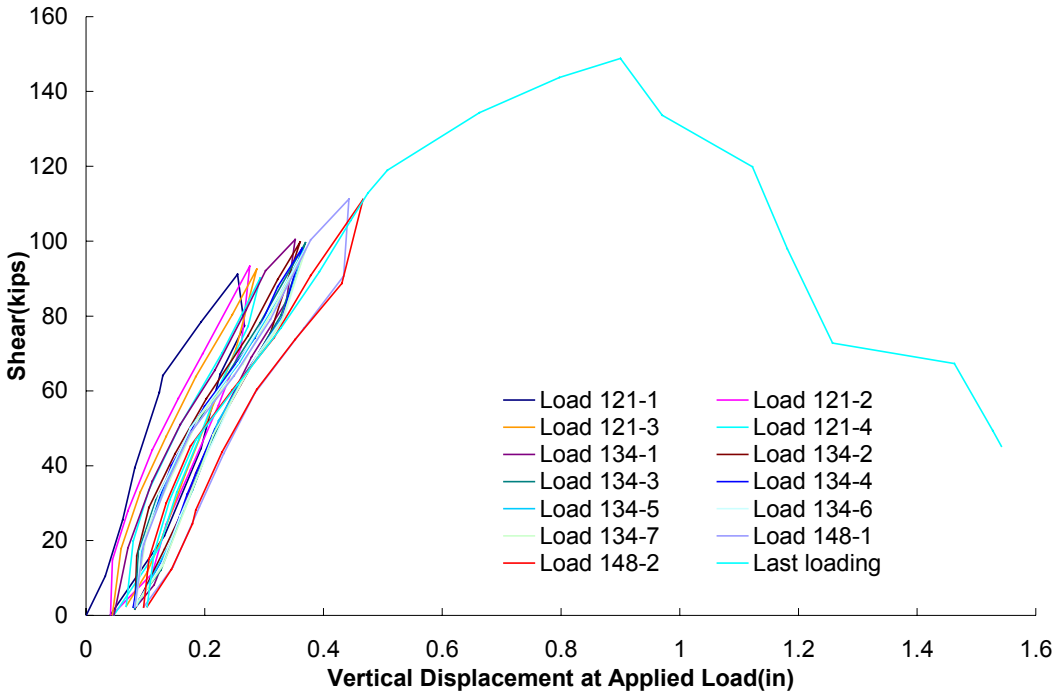

Figure 7.5: T-Beam 3C shear-displacement relationship

7.2.3 Strain Gage Readings on the Web of the T-Beam

Four 4-inch long strain gages were installed on the shear span near the top and the bottom of the beam to monitor change in bending moment, and subsequently to determine applied shear in the left shear span. The gage locations are described in Chapter 4 and shown in Figure 4.2. This system of strain measurements is being

considered for the field application as a means of monitoring the shear load applied by traffic on the Salt Lake Boulevard Bridge girders. Figure 7.6 shows the beam section stress-strain relationship, where:

$$\sigma_T = \frac{M \cdot y_t}{I_g}, \quad \sigma_B = \frac{M \cdot y_b}{I_g} \quad \Rightarrow \quad M = \frac{(\sigma_T + \sigma_B) \cdot I_g}{h}$$

where: $h = y_t + y_b$

Using the strain recorded by the strain gages:

$$M_1 = \frac{(straingage_2 + straingage_1) \cdot E_p \cdot I_g}{h}, \quad M_2 = \frac{(straingage_4 + straingage_3) \cdot E_p \cdot I_g}{h}$$

The shear force can then be obtained from,

$$V = \frac{(M_2 - M_1)}{\Delta x}$$

This expression ignores the dead load that was in place when the strain gages were installed and zeroed. The strain recorded by the gages is the result of the applied point load only. In the field application the strain gages would again record only the change in strain caused by wheel loads. It was anticipated that this system would only provide useful data while the concrete beam was uncracked. Once flexural or shear cracking occurs, the strain gage readings no longer represent the true beam bending strain.

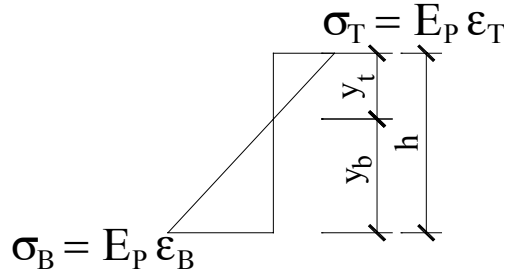

Figure 7.6: Beam section stress-strain relationship

The shear forces derived from the strain gage readings are compared with the applied shear in Figure 7.7. There is a relatively linear correlation between the strain gage system results and the actual shear force.

However, the strain gage system overestimated the applied shear by about 4.7%. This is likely the result of errors in the moment of inertia of the section and the modulus of elasticity of the beam material. This can be corrected by calibrating the strain gage system with known loads. It would appear that with proper calibration, this strain gage system could be used in the field as a means of monitoring the shear load applied by traffic on the Salt Lake Boulevard Bridge.

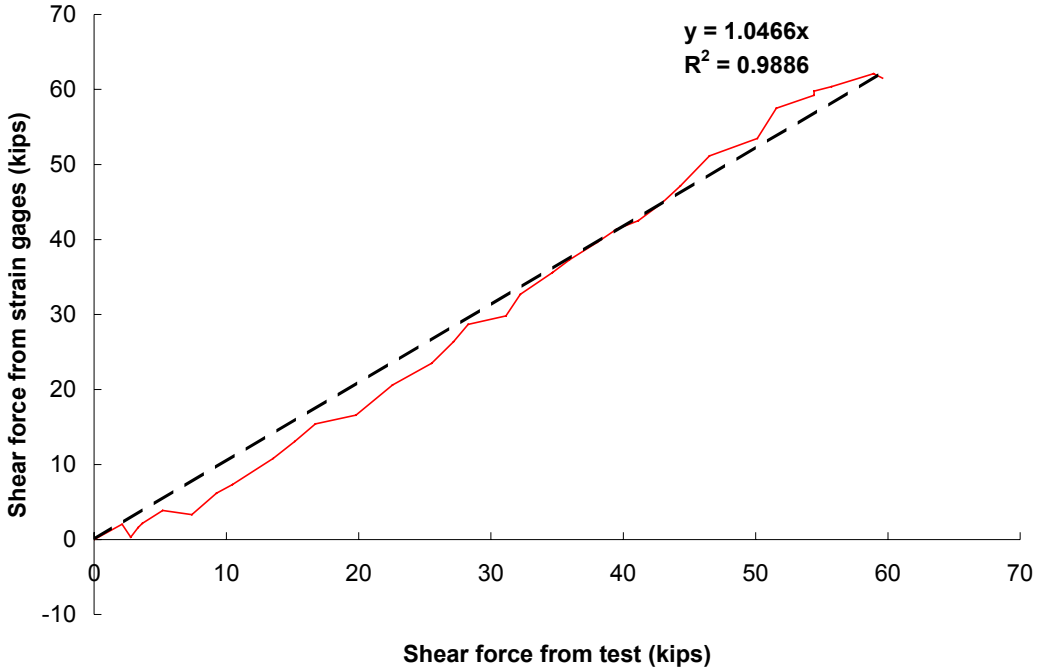

Figure 7.7: Comparison of shear forces from strain gages and test data

7.2.4 Failure of T-Beam 3C

T-Beam 3C failed in shear at a maximum load of 198 kips (shear force of 150 kips). Figure 7.8 shows both sides of the T-Beam after failure.

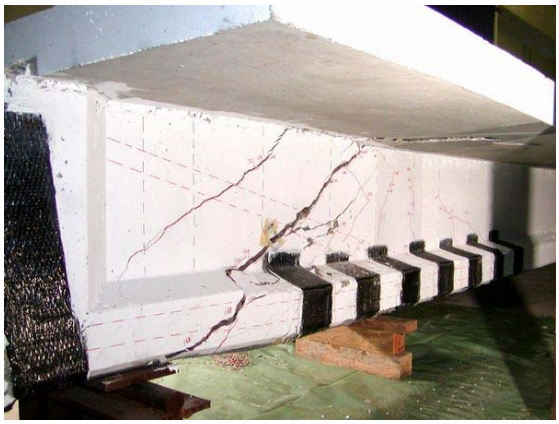

Front of the beam

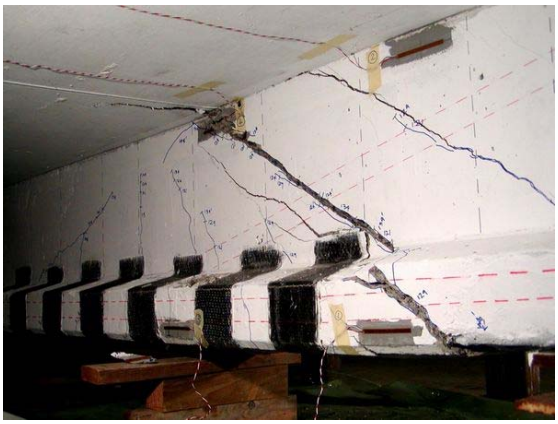

Back of the beam

Figure 7.8: T-Beam 3C after failure

After failure of T-Beam 3C, the following observations were made:

1. The primary shear crack opened significantly prior to failure.
2. Two of the internal steel stirrups crossing the shear crack failed in tension, while another two stirrups pulled out of the bottom bulb due to the lack of anchorage at the ends of the straight bars (Figure 7.9).
3. The harped prestressing tendons and the catenary action of the carbodur flexural FRP prevented complete collapse, but the load capacity reduced dramatically after shear stirrup failure.
4. The tensile CFRP Carbodur strips delaminated from the base of the shear crack to the support and from the crack to the first CFRP wrap around the soffit of the beam bulb (Figure 7.10). This first CFRP wrap was compromised by the cracking in the concrete substrate.
5. There was no visible damage to the second CFRP wrap or to the Carbodur strip bond beyond the second CFRP wrap (Figure 7.11).

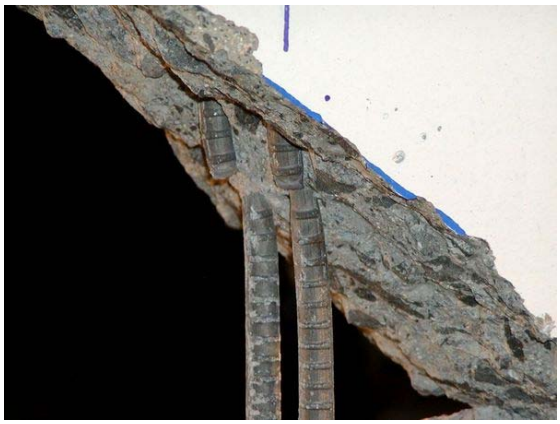

Stirrups failed in tension

Stirrups pulled out of bottom bulb

Figure 7.9: Failure of internal steel stirrups

Figure 7.10: Delamination of the flexural Carbodur strips

Figure 7.11: No visible Carbodur delamination beyond the second CFRP wrap

7.3 T-Beam 3 Initial Cracking Test (T-Beam 3I)

T-Beam 3I was the first test performed on the right hand end of T-Beam 3. This test was performed to create initial shear cracks in the web of the beam. Figure 7.12 shows the test setup for T-Beam 3I. More detailed information on the test setup and instrumentation is provided in Chapter 4.

Figure 7.12: T-Beam 3I ready for testing

7.3.1 Test Procedure and Beam Response

Loading of T-Beam 3I was performed in displacement increments of 0.01". At a total load of 83 kips the first visible flexural cracks were detected in the bottom of the beam under the load point.

At a total load of 89 kips, the flexural cracks extended slightly into the web of the beam. At 99 kips, new flexural cracks formed and at 107 and 115 kips, the flexural cracks extended upwards in the web.

At a total load of 125 kips, the first shear crack formed in the web of the beam. The crack orientation was 34 degrees from the horizontal on the front of the web, and 35

degrees on the back. Closer to the support, the crack inclination on the front decreased to 28 degrees, and to 27 degrees on the back.

At a total load of 145 kips, the maximum shear crack width under load had increased to 0.02” (0.5mm) and the cracks extended slightly towards the top slab near the load and towards to bottom bulb near the support. The MTS controller was switched to manual control and the load was slowly released to zero and the test stopped.

Figure 7.13 shows the resulting shear cracks formed in the web of the T-Beam. The residual crack width under no load for the main shear crack was between 0.003 and 0.005” (0.08 to 0.13 mm).

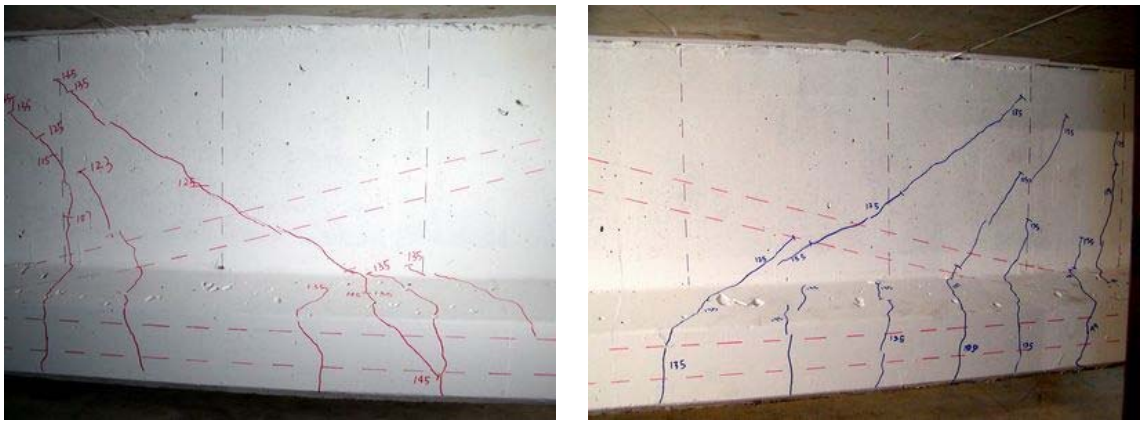

Front of the beam Back of the beam

Figure 7.13: Shear cracks formed in the web of the beam

7.3.2 Shear-Displacement Relationship

The vertical deflection of T-Beam 3I was recorded by LVDT-A installed on the top of the steel spreader beam. As for T-Beam 3C, the shear in the test span (right span) is three fourths of the total load. Figure 7.14 shows the shear-displacement relationship during the T-Beam 3I test. The shear-displacement curves of T-Beam 3C, T-Beam 3I, T-Beam 3W and T-Beam 3S are compared and discussed in Chapter 8.

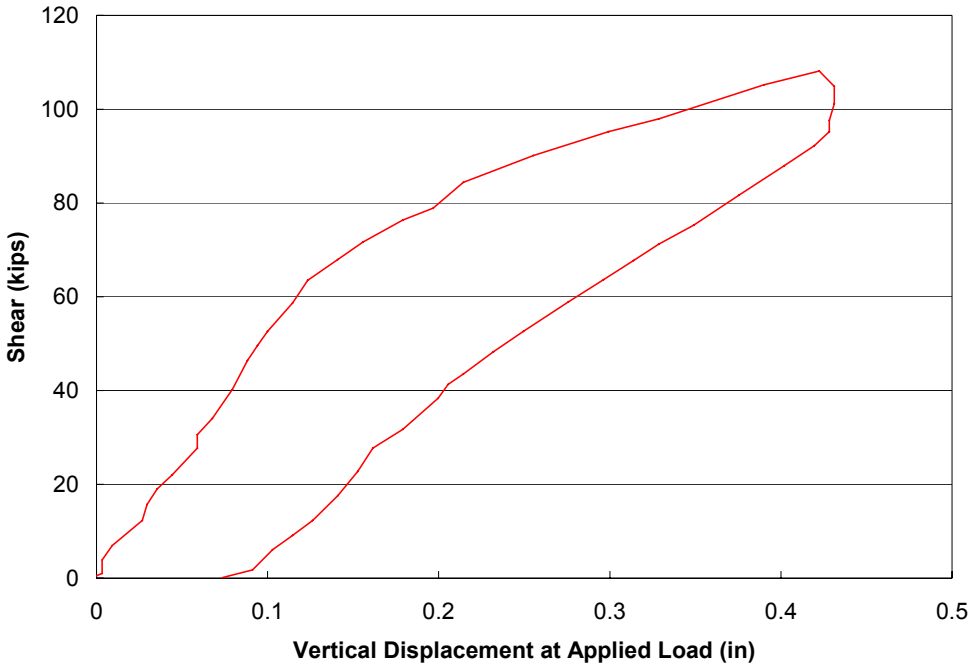

Figure 7.14: T-Beam 3I shear-displacement relationship

7.4 T-Beam 3 Crack Widening Test (T-Beam 3W)

After installation of the VW Crackmeter and two crack gages, the Crack Widening test was performed to increase the residual crack width to that observed in the Salt Lake Boulevard Bridge girders (0.02", 0.5mm). Figure 7.15 shows the test setup for T-Beam 3W. A detailed description of the test setup and instrumentation is provided in Chapter 4.

Figure 7.15: T-Beam 3W ready for testing

7.4.1 Test Procedure and Beam Response

Before loading, the residual cracks at the locations of the Crackmeter and crack gages were measured using the visual crack gage. The crack widths were all about 0.003" (0.08mm).

The initial loading of T-Beam 3W was performed in displacement increments of 0.01" to a total load of 125 kips, corresponding to the initiation of shear cracking in T-Beam 3I. Under this load the crack widths were about 0.01 to 0.03" (0.25mm to 0.76mm). The MTS controller was switched to manual control and the load slowly released to zero. The residual crack width had increased to 0.005" (0.125mm).

Reloading to 122 kips was performed under displacement control by the MTS controller. This load cycling was repeated for another 3 cycles, with no significant change in residual crack width. The total load was then increased to 145 kips. The shear cracks under load were now about 0.02" (0.50mm) wide. The beam was subjected to 5 unloading and loading cycles at this load level. The third loading cycle was inadvertently taken to 150 kip load, but subsequent cycles were again at the 145 kip level. During each cycle, the residual crack size increased slightly. The cycling was stopped when the maximum residual shear crack width reached 0.02" (0.50mm). The T-Beam was now ready for shear retrofit.

7.4.2 Shear-Displacement Relationship

The vertical deflection of T-Beam 3W was recorded by LVDT-A installed on the top of the steel spreader beam. Figure 7.16 shows the shear-displacement relationship for T-Beam 3W. The shear-displacement curves for T-Beam 3C, T-Beam 3I, T-Beam 3W and T-Beam 3S are compared and discussed in Chapter 8.

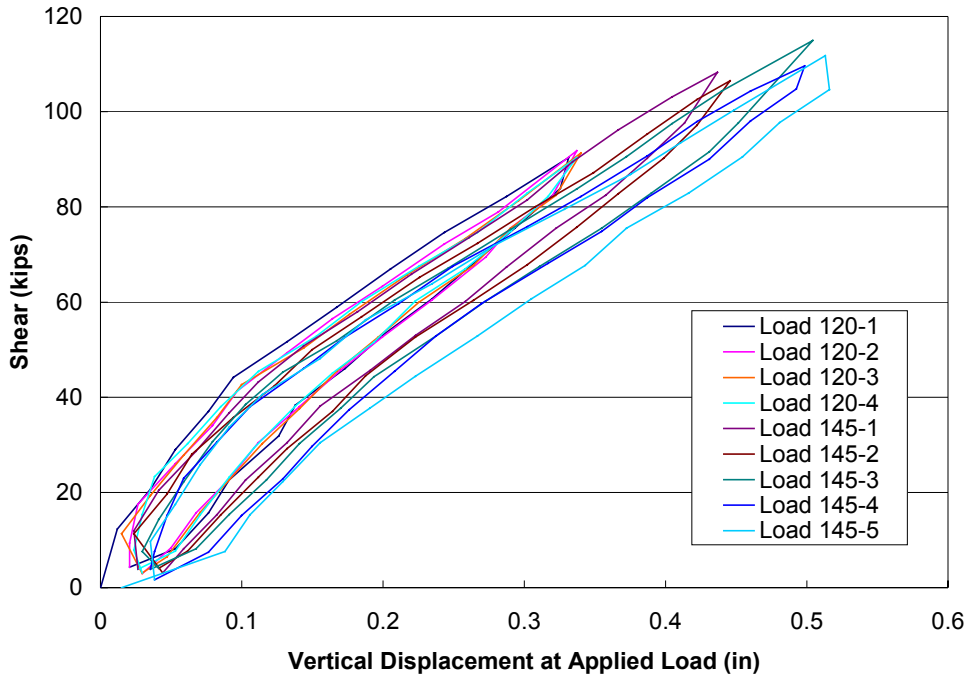

Figure 7.16: T-Beam 3W shear-displacement relationship

7.4.3 Crack Widths Recorded by VW Crackmeter and Crack Gages

In order to monitor the crack widths during loading, a Vibrating Wire (VW) Crackmeter and two crack gages were installed across the main shear crack on the web of the beam. The installation is described in Chapter 4 and the locations are shown in Figure 4.10. The NI Labview system recorded the crack gage output. The VW Crackmeter readings were recorded using a manual readout unit.

Figure 7.17 shows the applied shear vs. crack width relationship from crack gage 1.

During load cycling to the 120 kip level, the maximum crack width increased only very slightly and the residual crack width remained constant at around 0.005" (0.125mm).

When the load was increased to 145 kips, the maximum shear crack size under load increased dramatically from 0.018" to 0.026" (0.46mm to 0.66mm). The residual crack

width increased to 0.008” (0.20mm) after load cycle 145-1. With each additional cycle at the 145 kips load level, the shear crack width continued to increase. This is likely the result of yielding of the internal steel shear reinforcement and bond degradation between the stirrups and the web concrete.

After 5 cycles to the 145 kip load level (with one loaded inadvertently to 150 kips), the maximum crack width under load was 0.047” (1.2mm) and the residual crack width at the crack gages was 0.016” (0.41mm). Towards the bottom of the web, the residual crack width increased to 0.02” (0.51mm) as measured using the visual crack gage. The test was therefore terminated.

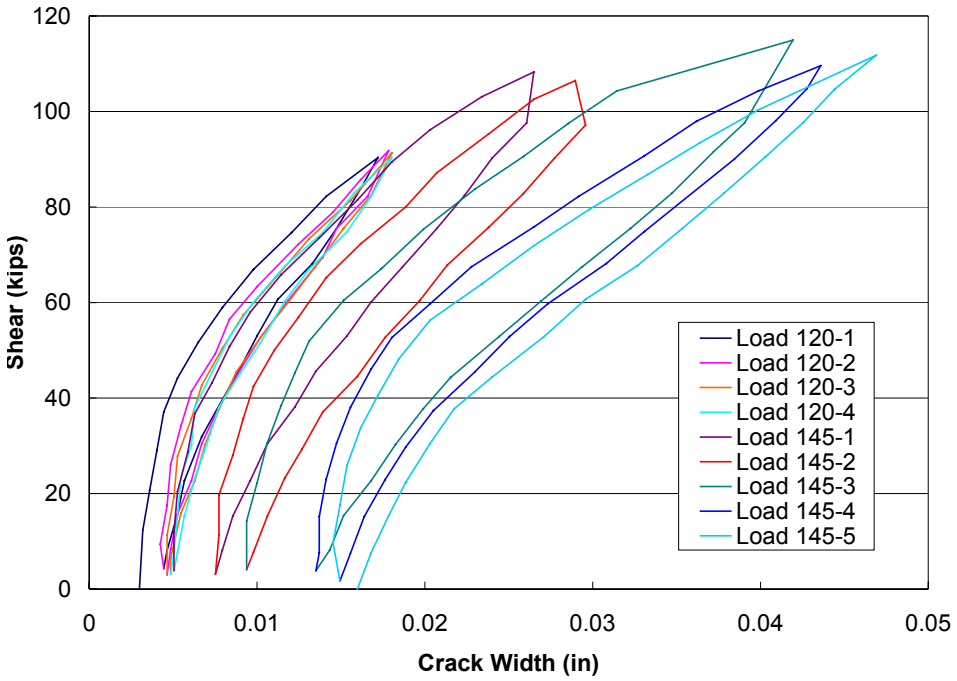

Figure 7.17: T-Beam 3W shear versus crack width from crack gage 1

Figure 7.18 and Figure 7.19 show the applied shear versus crack width relationship for crack gage 2 and the VW Crackmeter, respectively. The crack widening followed the same pattern as described above for crack gage 1.

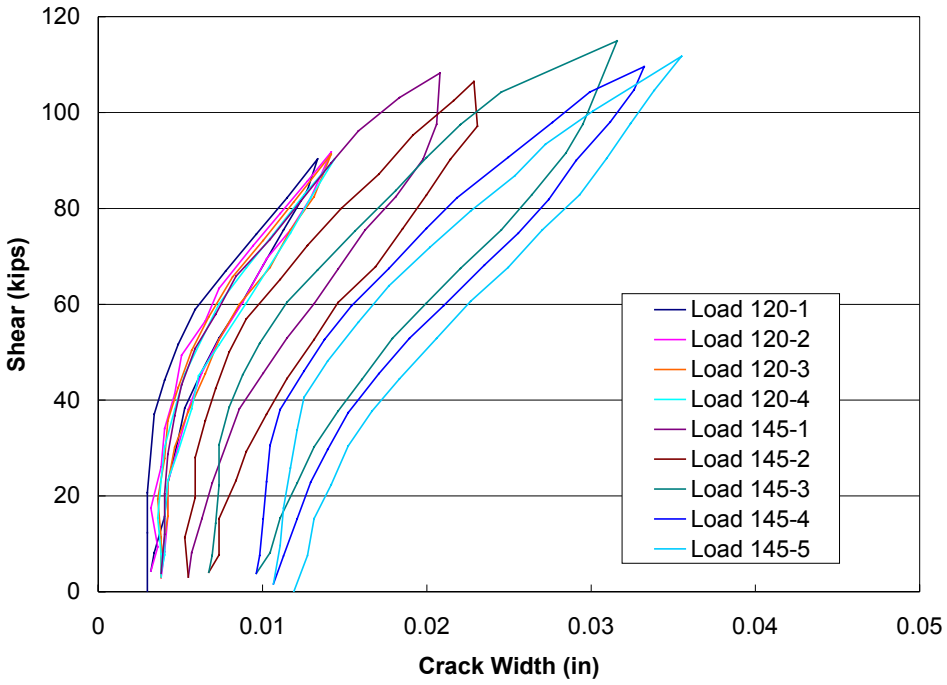

Figure 7.18: T-Beam 3W shear versus crack width from crack gage 2

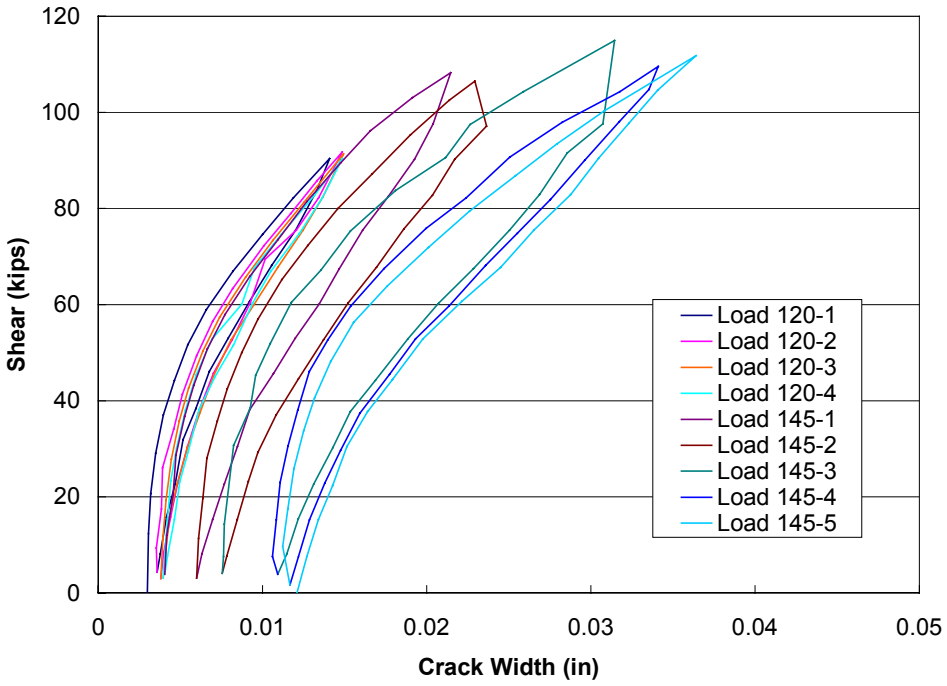

Figure 7.19: T-Beam 3W shear versus crack width from the VW Crackmeter

The crack width measurements from crack gage 2 and the VW Crackmeter are very similar. These gages were at the same location on the crack but on opposite sides of the

web. During the final load cycle, the maximum crack width under load was 0.036" (0.91mm) and the residual crack width after unloading was 0.012" (0.30mm) for both of these sensors.

These crack widening measurements from T-Beam 3W are compared with those from T-Beam 3S in Chapter 8.

7.5 T-Beam 3 Shear Retrofit Test (T-Beam 3S)

As described in section 4.3.4, the right end shear span of T-Beam 3 was now retrofitted for shear using CarboShear-L stirrups over the existing shear cracks. T-Beam 3S testing was performed to evaluate the performance of this shear retrofit system. The beam layout remained the same as for T-Beam 3I and T-Beam 3W. Figure 7.20 shows T-Beam 3S ready for testing. More detailed information on the test setup and instrumentation is provided in Chapter 4.

Figure 7.20: T-Beam 3S ready for testing

7.5.1 Test Procedure and Beam Response

Before testing, the residual crack widths at the locations of the VW Crackmeter and crack gages were measured using the visual gage. All cracks had closed slightly since the end of test T-Beam 3W, with all crack widths now about 0.01" (0.25mm). In order to monitor the effect of the retrofit on the crack widths during cyclic loading, the beam was subjected to the same loading routine used for T-Beam 3W. This would allow for comparison of T-Beam 3W and T-Beam 3S crack widths, change in crack sizes during each cycle, and change in residual crack size after each cycle.

Therefore, following the same loading procedure as for T-Beam 3W, the initial loading of T-Beam 3S was performed in displacement increments of 0.01" to 120 kips. The MTS controller was switched to manual control and the load was slowly released to zero. After the first cycle (Load 120-1), cracks had formed in both concrete and FRCC filler blocks. Reloading to 122 kips was performed by the MTS controller and unloading again by manual control. After the second cycle (Load 120-2), cracks appeared between the beam bottom bulb and the concrete filler blocks. It was noted that more cracks formed in the FRCC filler blocks than in the concrete filler blocks (Figure 7.21).

Concrete filler blocks FRCC filler blocks

Figure 7.21: Cracks in the concrete and FRCC filler blocks

During the next two load cycles to 120 kips, no significant changes were observed. The load was then increased to 145 kips and the beam was subjected to unloading and loading for 4 cycles at this load level.

During the test, output from the VW Crackmeter and crack gages was compared with that recorded during testing of T-Beam 3W. The effect of the CarboShear-L stirrups could therefore be evaluated during the test. It was observed that the crack widths under load were smaller than those from T-Beam 3W after load cycle 145-2. The change in crack width during each cycle was also reduced. The change in residual crack width after each cycle was smaller than those from T-Beam 3W after load cycle 120-2. It appeared that the CarboShear-L stirrups were able to control the opening of the existing shear cracks and prevented growth in the width of the residual cracks after unloading. More details of the crack width comparisons are presented in Chapter 8.

After repeating the same cyclic loading as performed on T-Beam 3W, the load was increased to induce delamination of CarboShear-L stirrups and failure of the beam.

Delamination of portion of the CarboShear-L stirrups was noted at a total load of 175 kips. Wide cracks formed at this load point due to the separation between the filler blocks and the beam bottom bulb, which initiated delamination of the stirrups. Figure 7.22 shows a close-up view of the delamination of the third CarboShear-L stirrup from the right support (F3) on front of the beam.

At a total load of 210 kips, the flexural retrofit Carbodur strips began to delaminate from the beam soffit in the right shear span. The existing flexural cracks under the load point increased in width and the bottom legs of the CarboShear-L stirrups were pulled

laterally by the delamination of the bottom Carbodur strips. Eventually the T-Beam failed in flexure with rupture of all 10 prestressing strands (Figure 7.23).

Figure 7.22: Delamination of Carboshear-L F3 on front of beam

Figure 7.23: T-Beam 3S flexural failure

7.5.2 Shear-Displacement Relationship

The vertical deflection of T-Beam 3S was recorded by LVDT-A installed on top of the steel spreader beam. Figure 7.24 shows the shear-displacement relationship for T-Beam 3S. The shear-displacement curves of T-Beam 3C, T-Beam 3I, T-Beam 3W and T-Beam 3S are compared and discussed in Chapter 8.

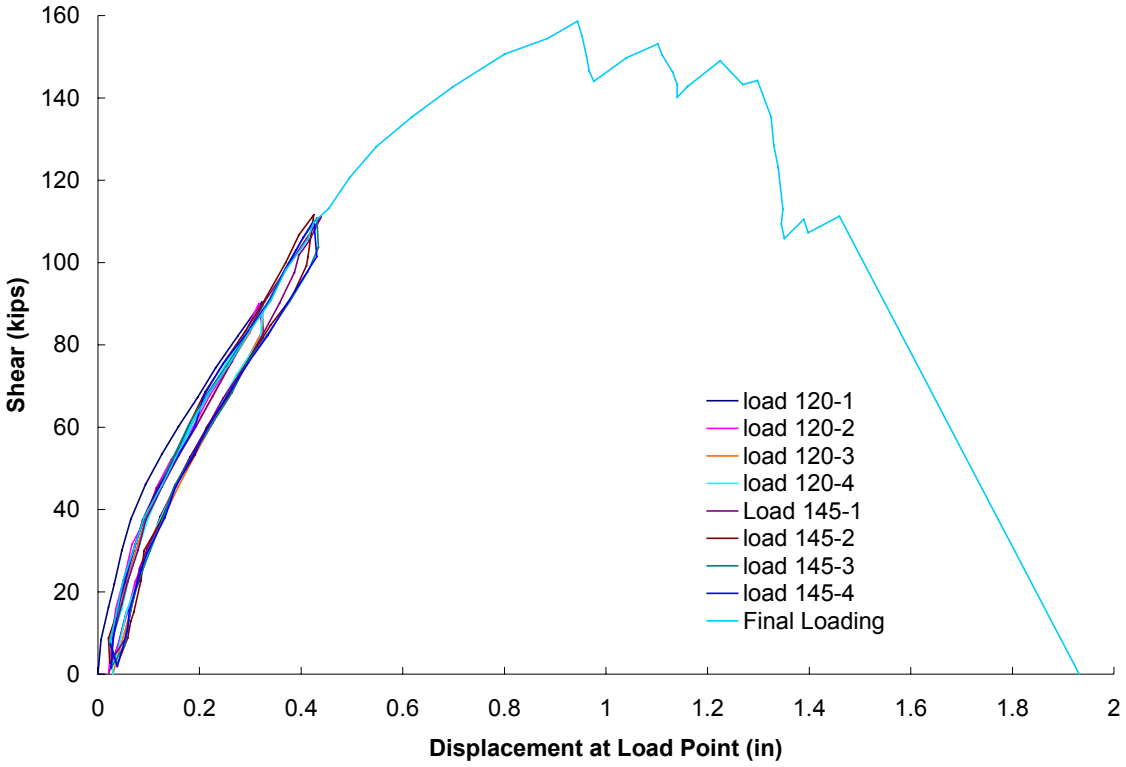

Figure 7.24: T-Beam 3S shear-displacement relationship

7.5.3 Crack Widths Recorded by VW Crackmeter and Crack Gages

The VW crackmeter and crack gages 1 and 2 were used to monitor the crack widths under applied load in the test of T-Beam 3S. The extensometer locations were identical to those used for T-Beam 3W. The installation is described in Chapter 4 and the locations are shown in Figure 4.10. The NI Labview system recorded the crack gage output. The VW Crackmeter readings were recorded using a manual readout unit.

Figure 7.25 shows the applied shear versus crack width relationship recorded by crack gage 1. During the first load cycle to 120 kips, the residual crack width increased from 0.01" to 0.012" (0.25 to 0.30mm). During subsequent cycles at the 120 kip load level, the residual crack width remained constant. When the load was increased to 145 kips, the maximum shear crack width under load increased from 0.027 to 0.035" (0.69 to 0.89mm), while the residual crack width increased to about 0.013" (0.33mm) after the first unloading (Load 145-1). During subsequent cycles to the 145 kip load level, no change was noted in the residual crack width. During load cycle 145-4, the maximum crack width under load was 0.037" (0.94mm) and the residual crack width was 0.013" (0.33mm). The CarboShear-L stirrups appear to control both the opening of the cracks during loading and prevent growth of the residual crack width.

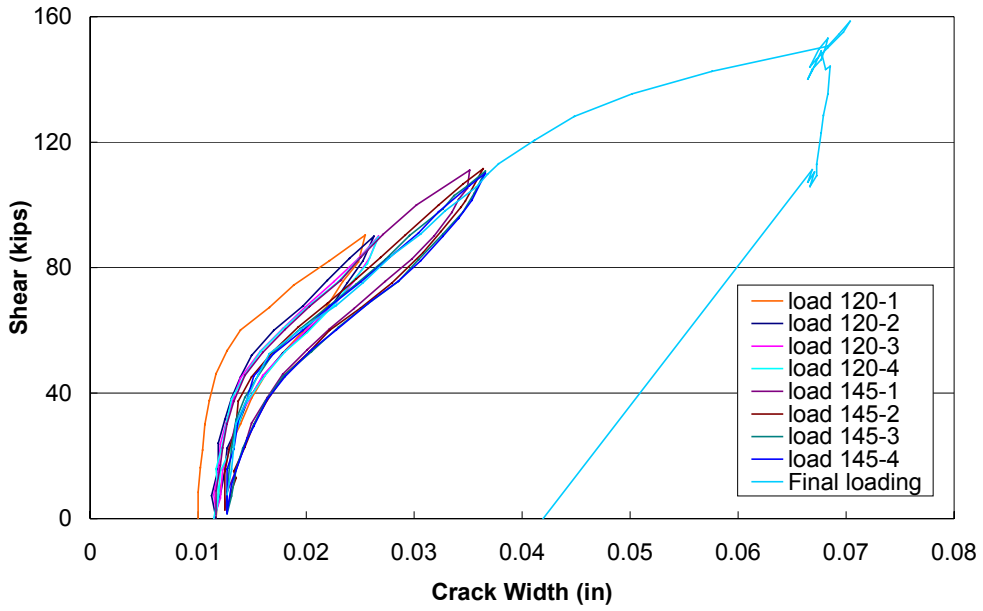

Figure 7.25: T-Beam 3S shear versus crack width from crack gage 1

Figure 7.26 and Figure 7.27 show the applied shear versus crack width relationships from crack gage 2 and the VW Crackmeter. During load cycle 145-4, the maximum crack width measured by crack gage 2 under load was 0.028" (0.71mm), while the residual

crack width was 0.012” (0.30mm) after unloading. The corresponding values for the VW Crackmeter were 0.031” (0.78mm) and 0.012” (0.30mm). Again it is apparent that the CarboShear-L stirrups have contributed to controlling the crack widths. More detailed discussion and comparison of the crack widths during tests of T-Beam 3W and T-Beam 3S are presented in Chapter 8.

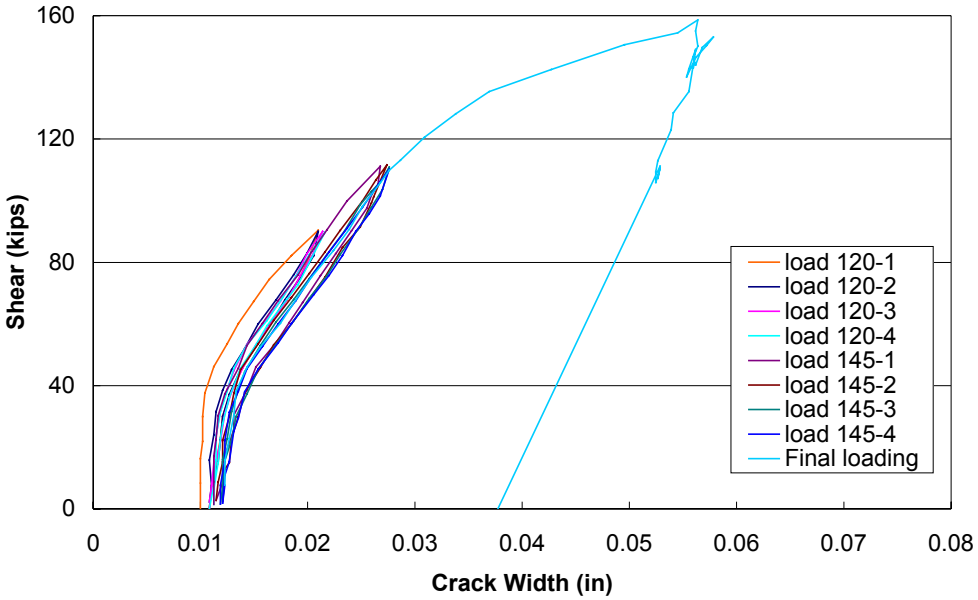

Figure 7.26: T-Beam 3S shear versus crack width from crack gage 2

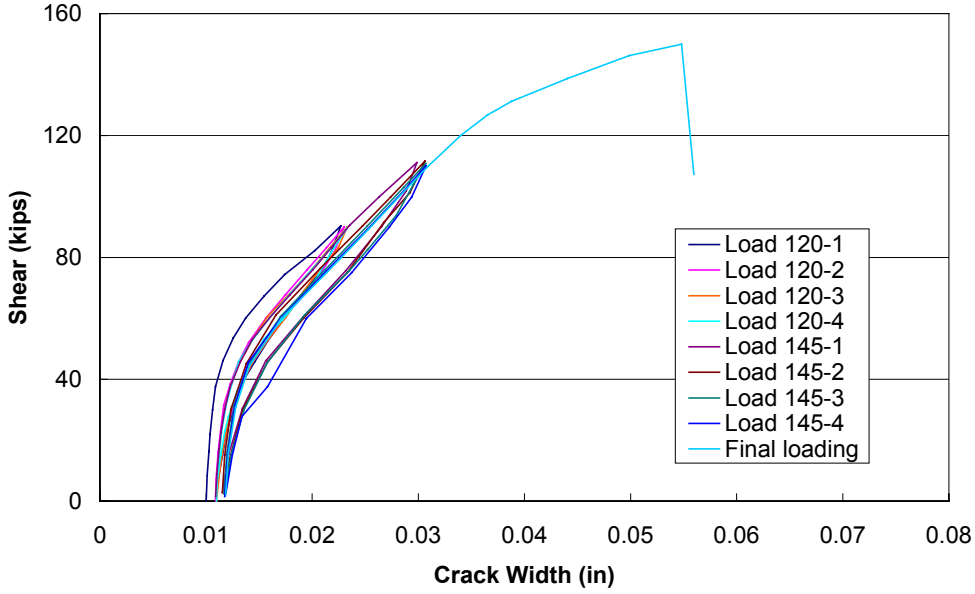

Figure 7.27: T-Beam 3S Shear versus crack width from the VW crackmeter

7.5.4 LVDT Measurements

In order to monitor the CarboShear-L stirrup anchorage at the top slab, an LVDT was installed at the top of each CarboShear-L stirrup. LVDTs were also installed at the top of one filler block on each side of the web to monitor movement between the filler block and the top slab during testing. The installation is described in Chapter 4 and the locations are shown in Figure 4.27. The readings from all of these LVDTs remained around zero throughout the test, which indicated that there was no anchorage slip at the top of the stirrups or separation between the filler blocks and top slab during testing of T-Beam 3S.

7.5.5 Strain Gage Measurements

In order to monitor strains in the CarboShear-L stirrups, 52 strain gages (SG) were bonded to the surface of the stirrups. Strain gage locations are shown in Figure 4.27. A detailed description of gage installation is presented in Chapter 4.

The results from all SGs on an individual stirrup were plotted together to evaluate the strain distribution in the stirrup. The final loading cycle was also plotted separately to identify potential delamination during loading to failure. The strains at the start of this final loading cycle were zeroed for easier comparison.

Figure 7.28 to Figure 7.35 show the SG readings for each stirrup on T-Beam 3S. Figure 7.36 to Figure 7.43 show the SG readings for each stirrup for the final loading cycle only. Discussion of these strain results is presented in detail in Chapter 8.

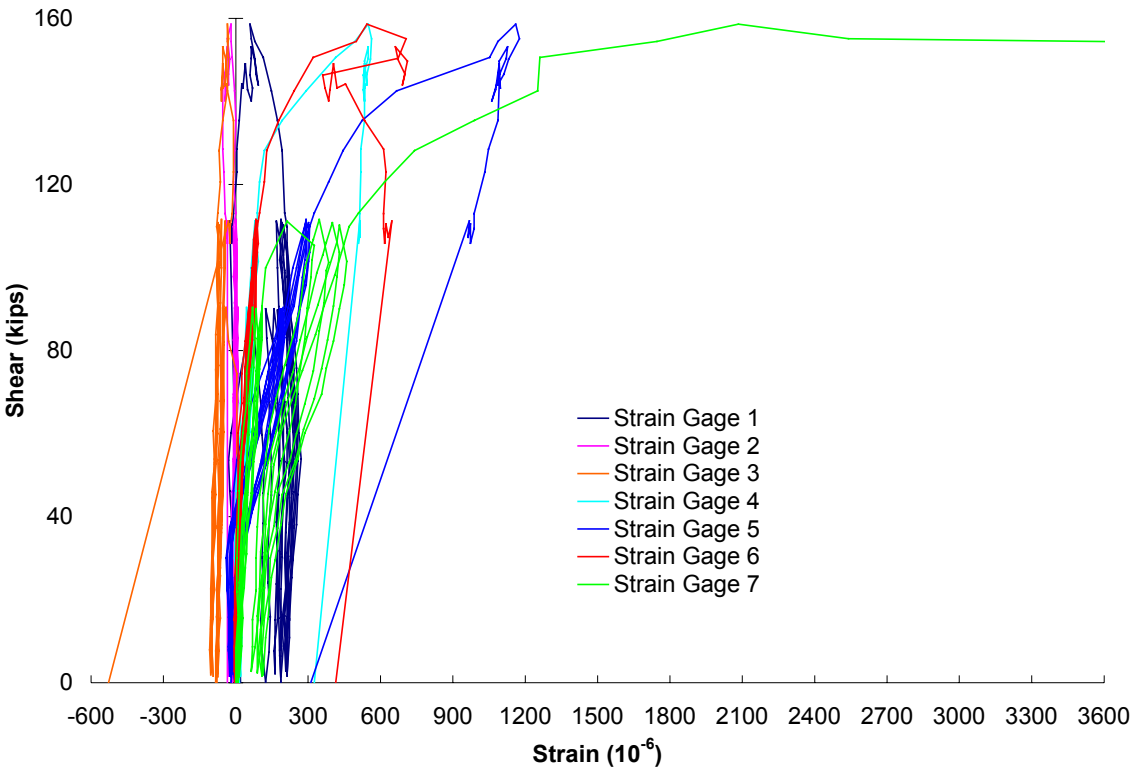

Figure 7.28: Strain gages 1-7; CarboShear-L F1 on front of beam (near support)

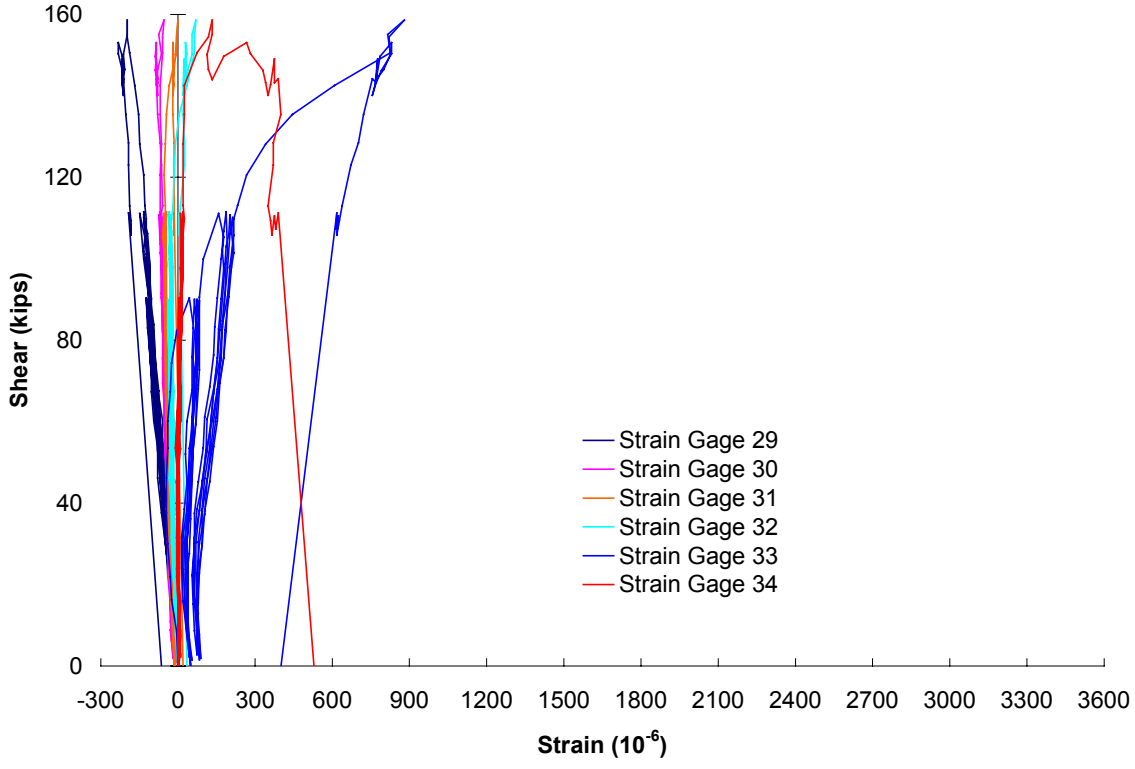

Figure 7.29: Strain gages 29-34; CarboShear-L B1 on back of beam (near support)

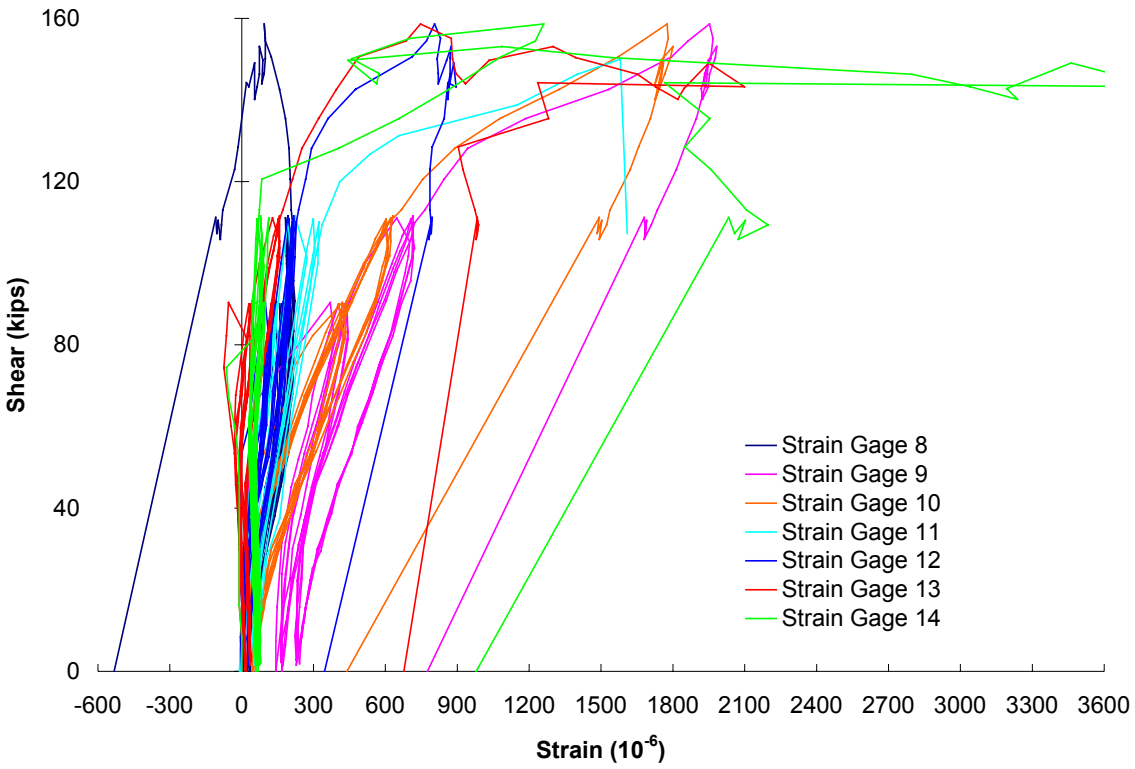

Figure 7.30: Strain gages 8-14; CarboShear-L F2 on front of beam

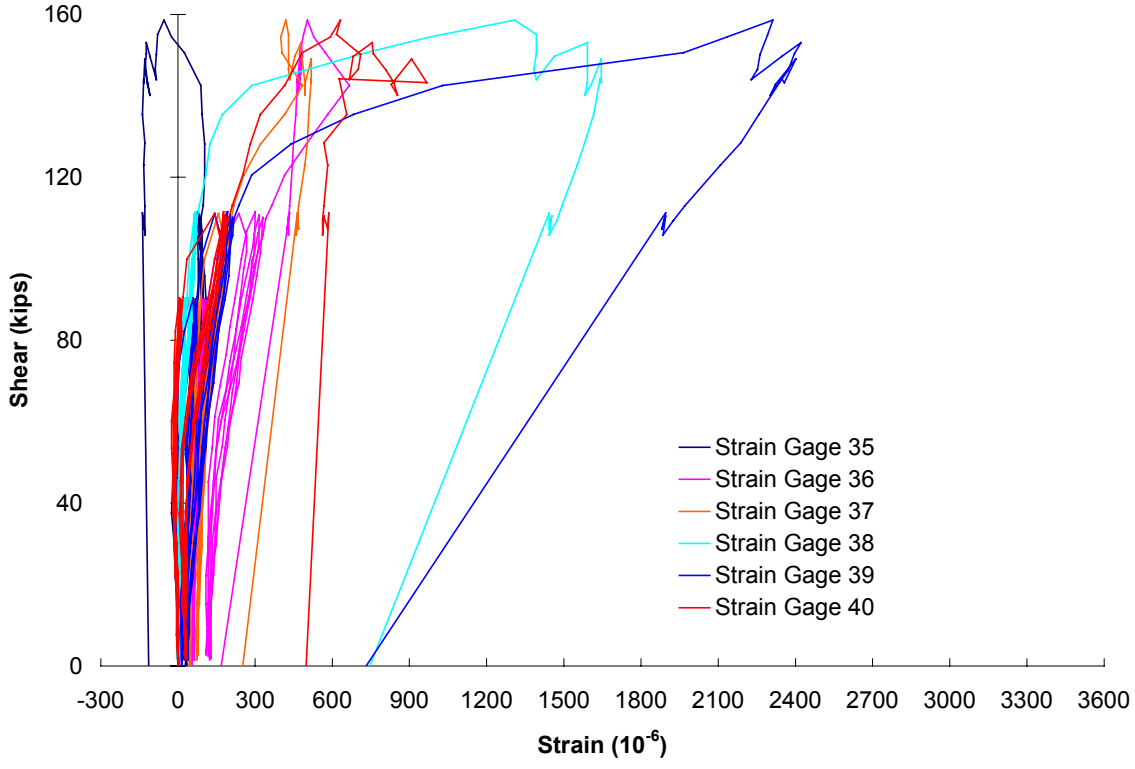

Figure 7.31: Strain gages 35-40; CarboShear-L B2 on back of beam

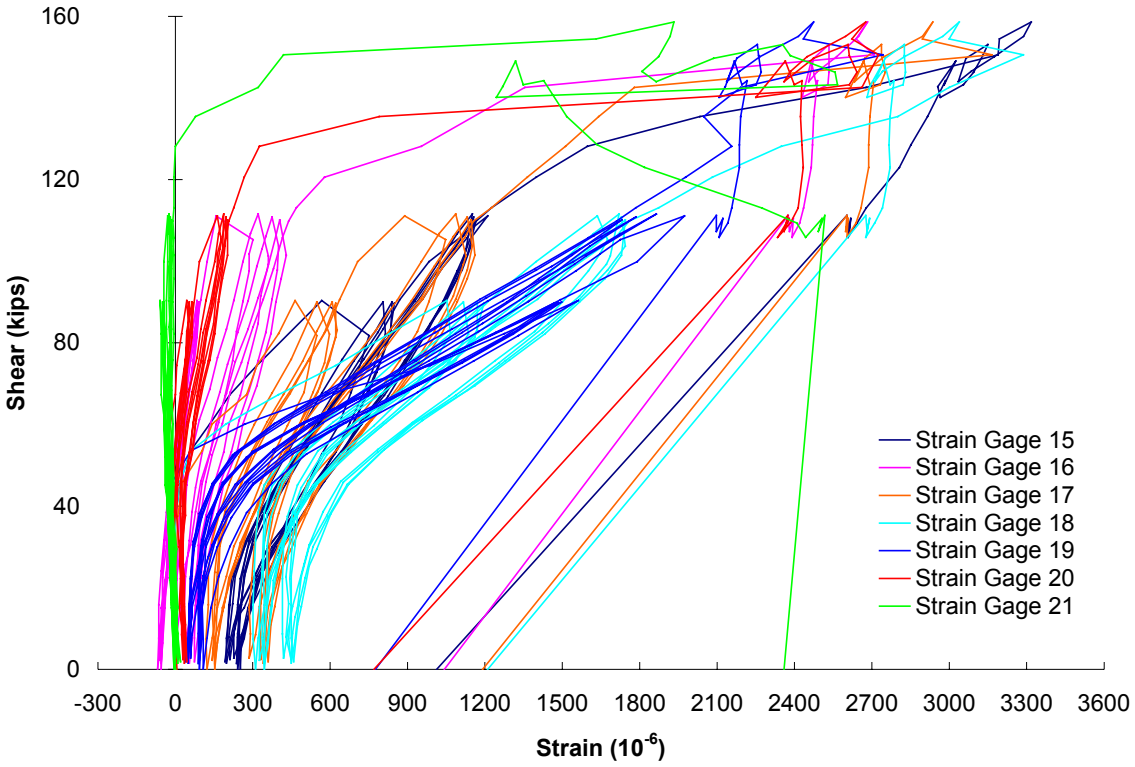

Figure 7.32: Strain gage 15-21; CarboShear-L F3 on front of beam

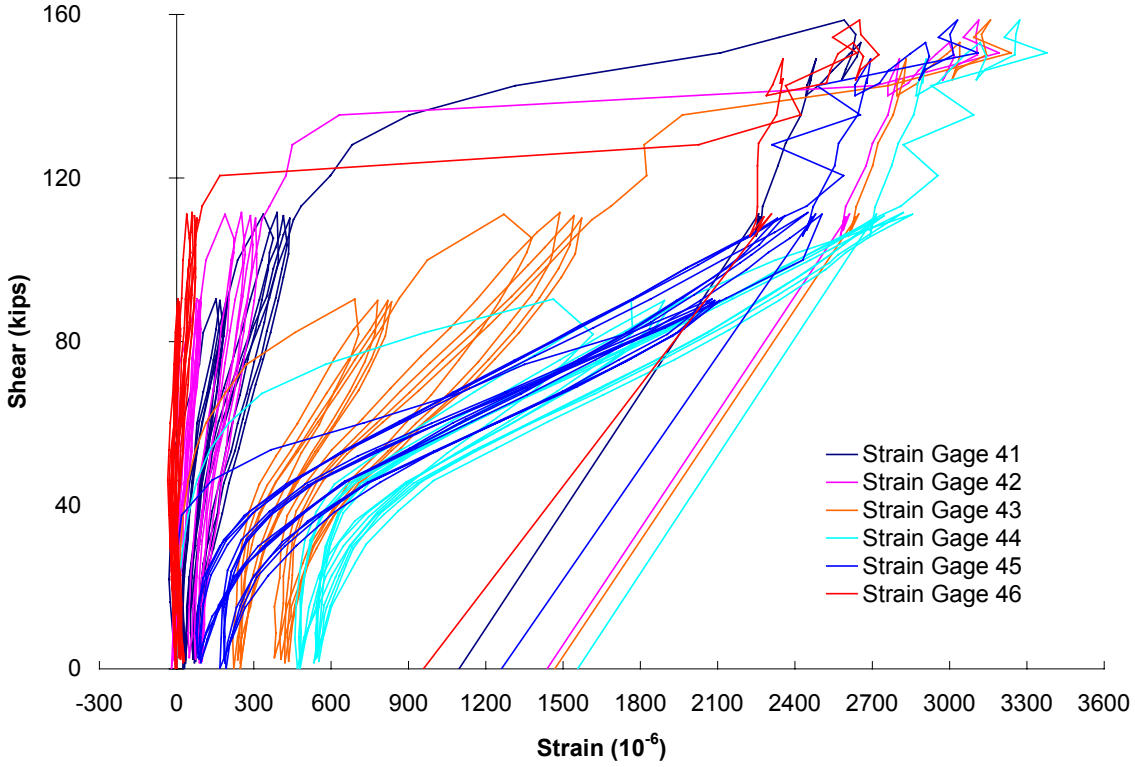

Figure 7.33: Strain gage 41-46; CarboShear-L B3 on back of beam

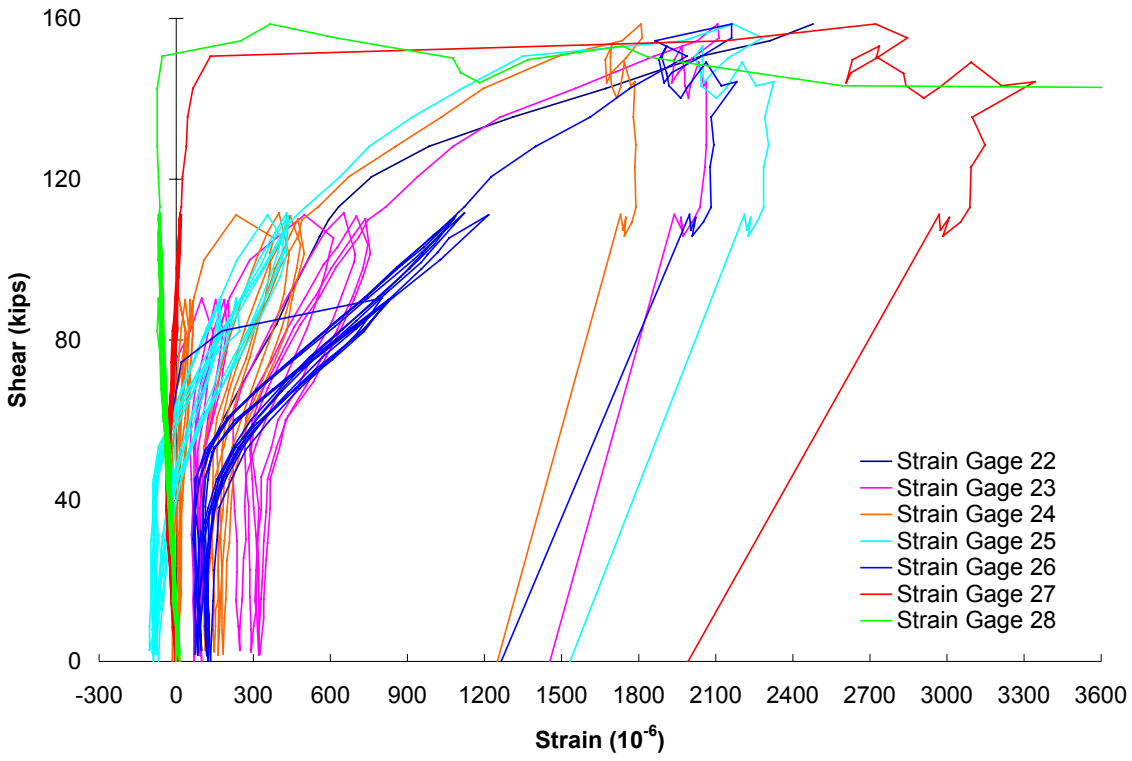

Figure 7.34: Strain gages 22-28; CarboShear-L F4 on front of beam (near load)

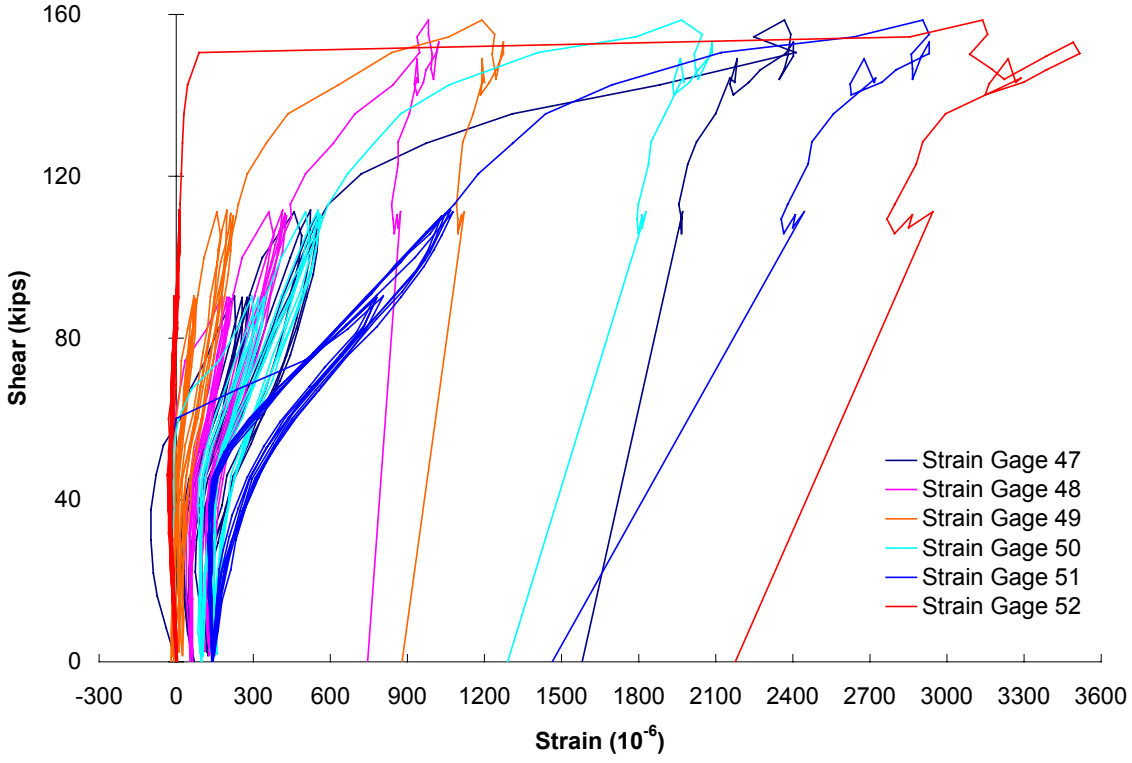

Figure 7.35: Strain gage 47-52; CarboShear-L B4 on front of beam (near load)

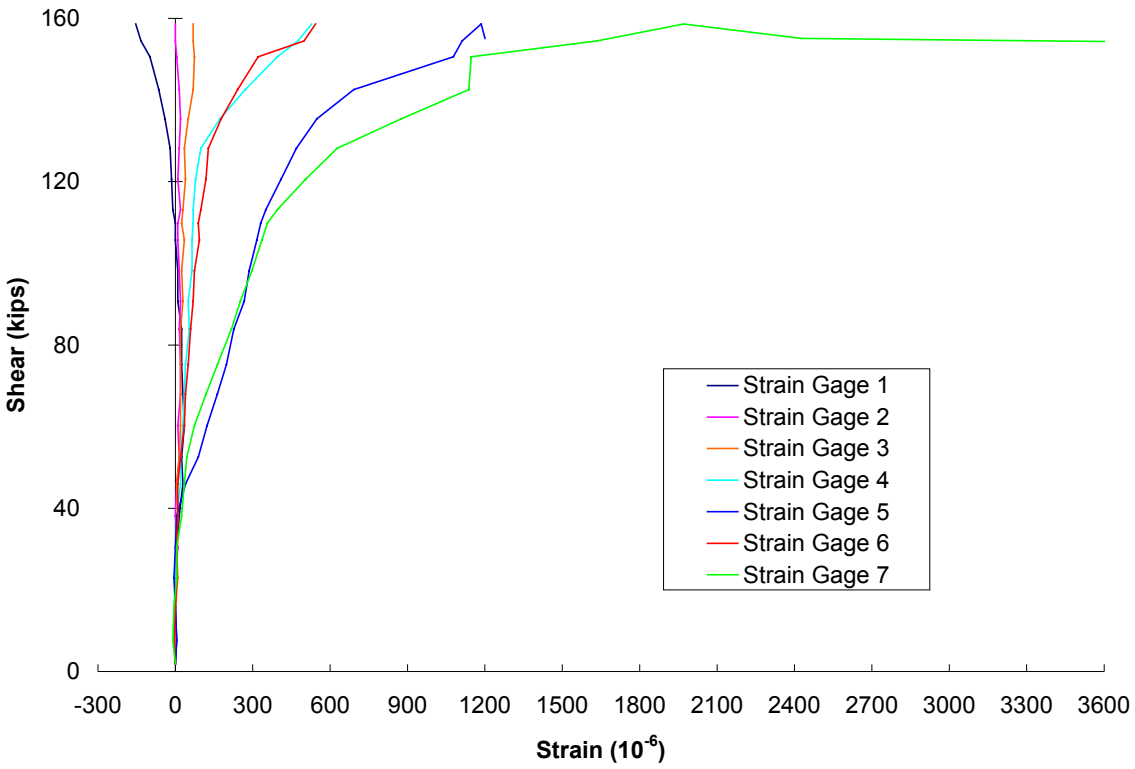

Figure 7.36: Strain Gages 1-7 on CarboShear-L F1 - final loading

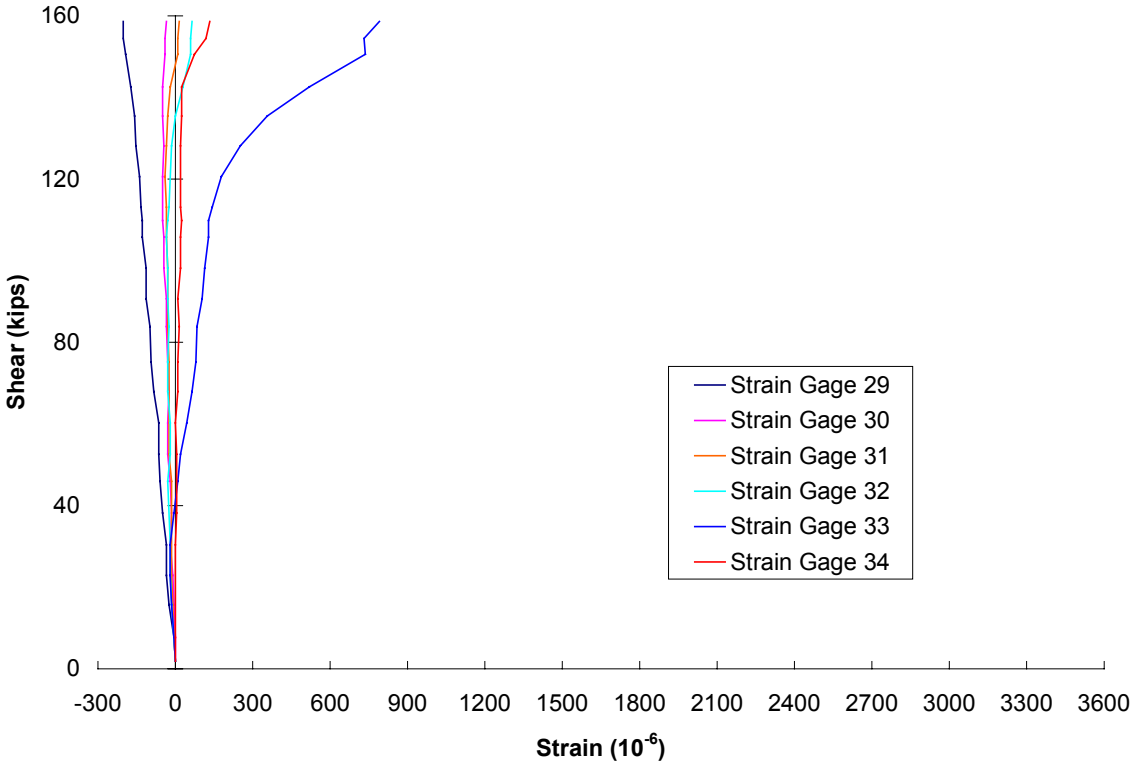

Figure 7.37: Strain Gages 29-34 on CarboShear-L B1 - final loading

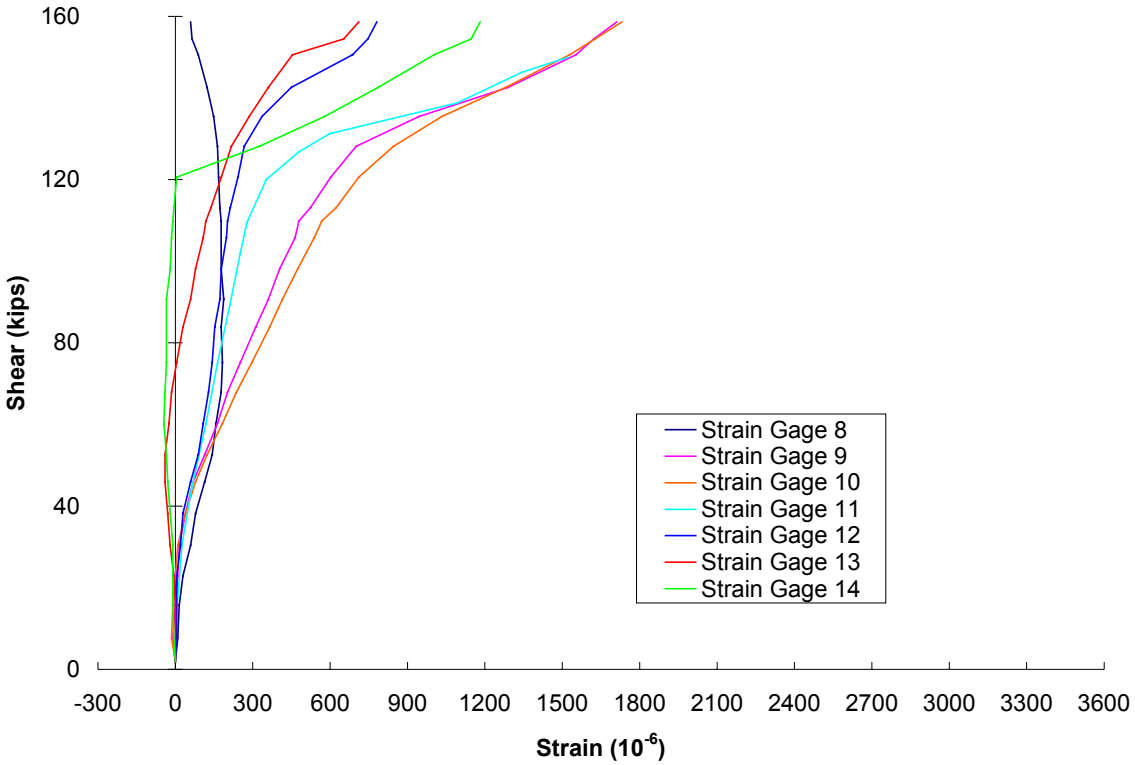

Figure 7.38: Strain Gages 8-14 on CarboShear-L F2 - final loading

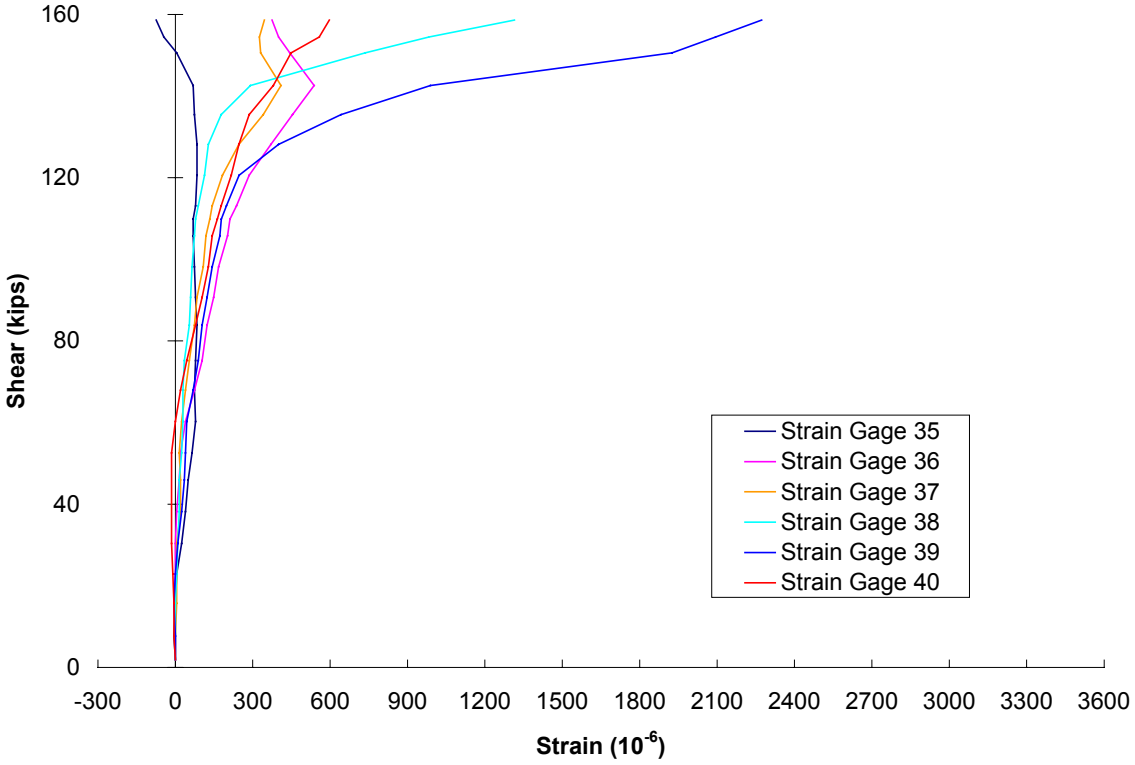

Figure 7.39: Strain Gages 35-40 on CarboShear-L B2 - final loading

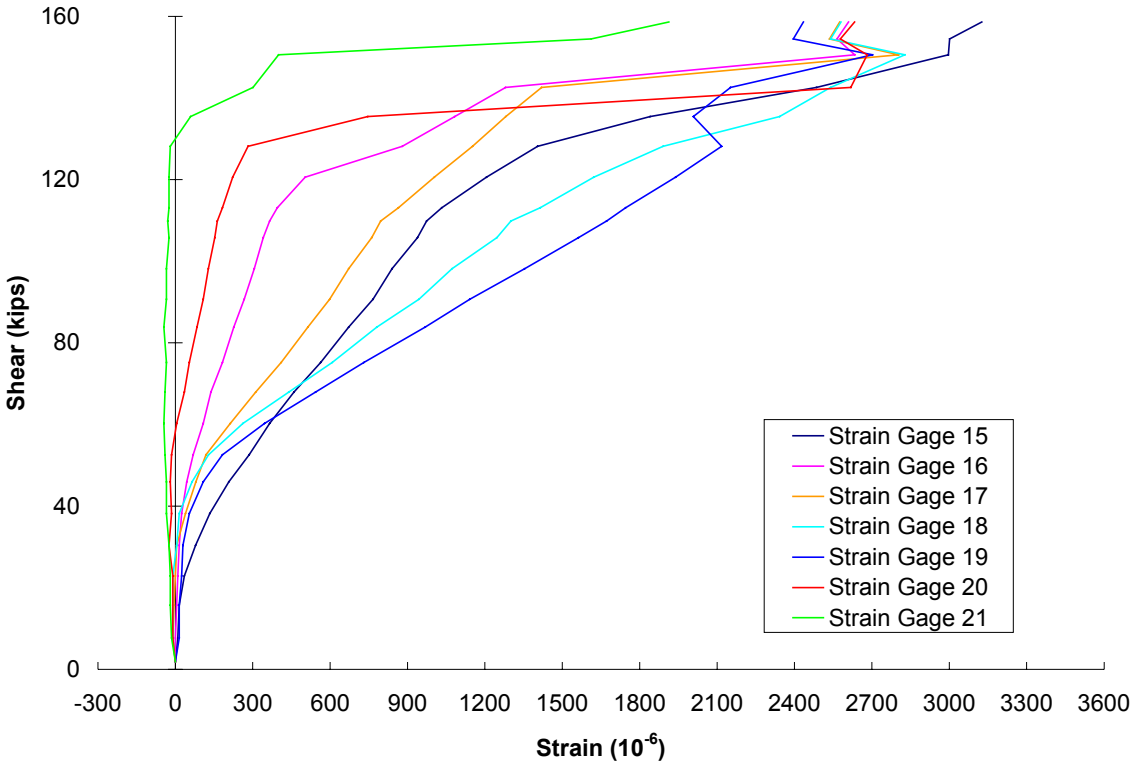

Figure 7.40: Strain Gages 15-21 on CarboShear-L F3 - final loading

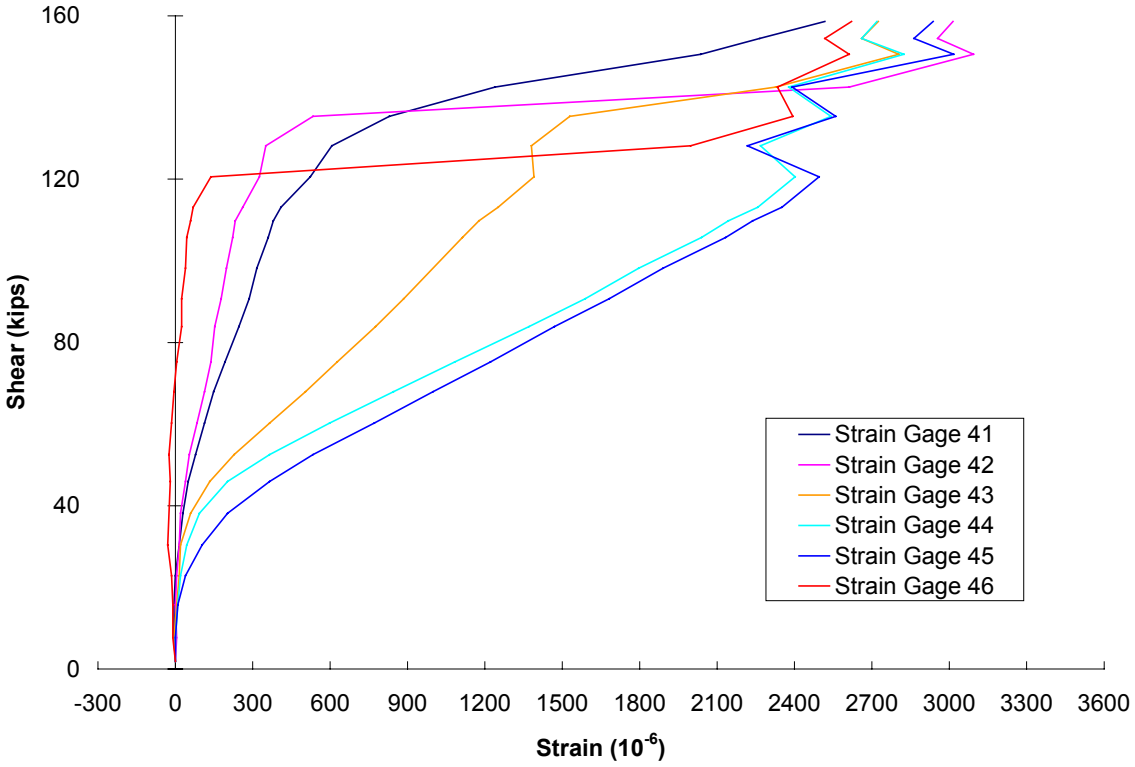

Figure 7.41: Strain Gages 41-46 on CarboShear-L B3 - final loading

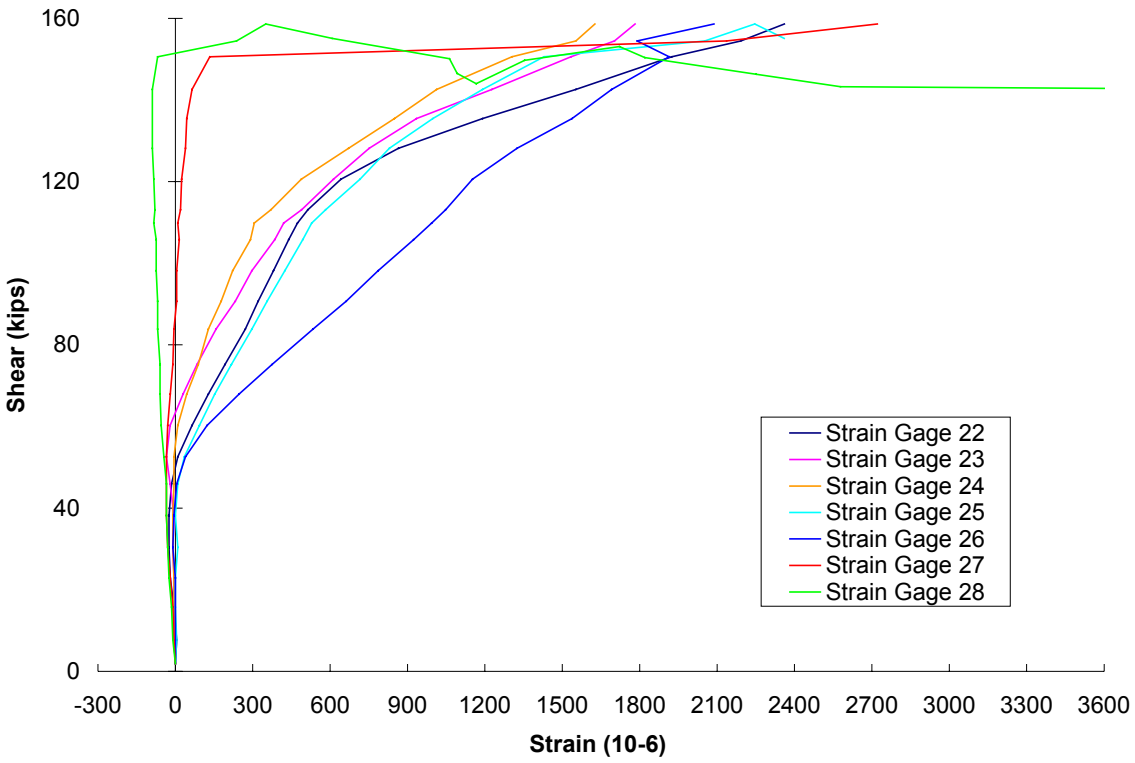

Figure 7.42: Strain Gages 22-28 on CarboShear-L F4 - final loading

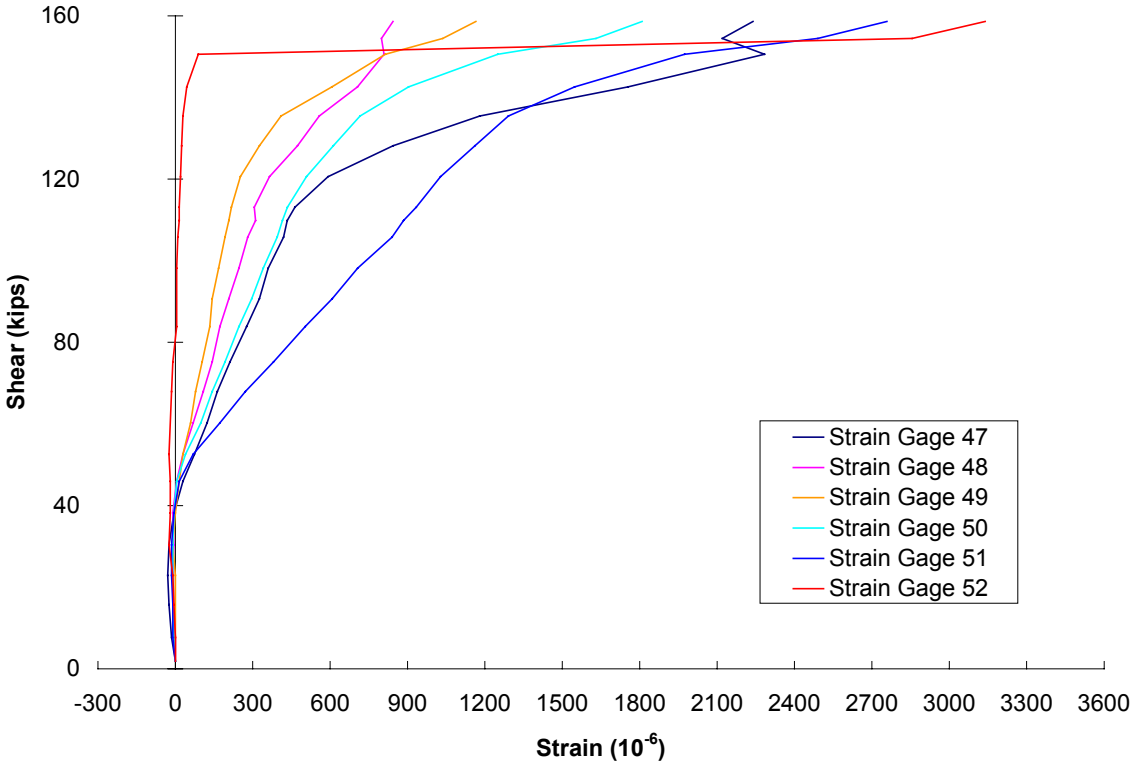

Figure 7.43: Strain Gages 47-52 on CarboShear-L B4 - final loading

CHAPTER 8

8 DISCUSSION

Results from the tests performed in this study are compared and discussed in detail in this chapter. In section 8.1, the shear-displacement relationships from T-Beam 3C, T-Beam 3I, T-Beam 3W and T-Beam 3S tests are compared and discussed. The results are compared with the predicted strengths computed in Chapter 6. In addition, the load-displacement relationship determined from the T-Beam 3C test is compared with the short-term load-displacement prediction, presented in Chapter 6.

In section 8.2, crack width from T-Beam 3W and T-Beam 3S tests are compared and discussed to evaluate the performance of the CarboShear-L stirrups.

In section 8.3, the strain gage readings from each CarboShear-L stirrup on T-Beam 3S are discussed as a means to monitor delamination of the stirrups.

US Customary units are used in this chapter when referring to the beam loads. The conversion from US Customary system to SI system is: 1 kip equals 4.45 kN.

8.1 Comparison of the Shear-Displacement Relationships

The vertical deflections at the load point for T-Beam 3C, T-Beam 3I, T-Beam 3W and T-Beam 3S were measured by LVDT-A located on the top of the steel spreader beam. The shear-displacement curve for each test was shown separately in Chapter 7.

In order to compare the performance of all the tests, the shear-displacement relationships are plotted in pairs. Figure 8.1 to Figure 8.4 show comparisons of T-Beam 3C and T-Beam 3I, T-Beam 3C and T-Beam 3W, T-Beam 3W and T-Beam 3S, and T-

Beam 3C and T-Beam 3S, respectively. The predicted shear capacities covered in Chapter 6 are also shown in these figures. V_n (AASHTO) represents the theoretical prediction for the original beam shear capacity calculated based on the AASHTO code. V_n (ACI 318-02) is the theoretical prediction from the ACI code.

From Figure 8.1 to Figure 8.4, the following observations are made:

1. The left and right ends of T-Beam 3 are virtually identical and comparable, because:
    a. The backbones of the initial loading of T-Beam 3C and T-Beam 3I are almost exactly the same (Figure 8.1).
    b. The loading and unloading cycles for T-Beam 3C and T-Beam 3W at the same load level are similar (Figure 8.2).
2. The CarboShear-L stirrup retrofit system increased the beam stiffness and reduced beam deflection.
    a. The slopes of the shear-deflection curves for T-Beam 3S are slightly greater than those for T-Beam 3W at the same load level. This indicates that application of CarboShear-L stirrups has increased the beam stiffness (Figure 8.3).
    b. Under cyclic loading to the same load level, the deflections of T-Beam 3S are smaller than those of T-Beam 3W (Figure 8.3).
    c. Figure 8.4 indicates the CarboShear-L stirrup retrofit system increased stiffness and strength under final loading.

3. Both AASHTO and ACI 318 estimates of the unstrengthened shear capacity of the beam are conservative, especially the AASHTO prediction.

The shear failure observed in the control test of T-Beam 3C was prevented by the addition of the CarboShear-L stirrups. Instead, T-Beam 3S failed in bending when the Carbodur flexural retrofit delaminated from the beam soffit (Figure 8.5)

The maximum load supported by the shear retrofit beam T-Beam 3S was 7% greater than the control beam. If flexural failure had not occurred, it is likely that a larger load could have been supported. Two additional beams are planned to evaluate the ultimate shear strength improvement with CarboShear-L stirrup shear retrofit.

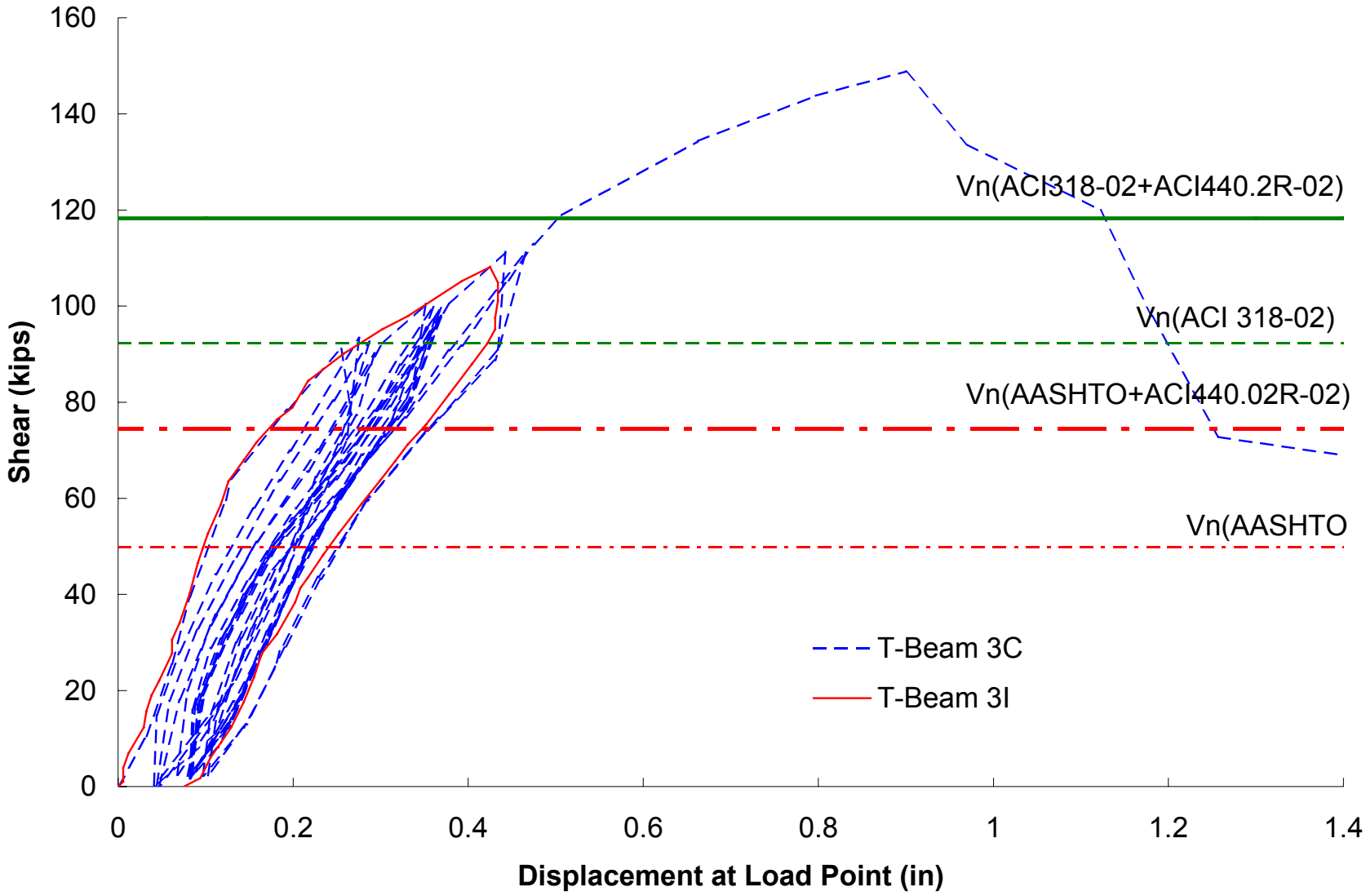

Figure 8.1: Shear-displacement relationships for T-Beam 3C and T-Beam 3I

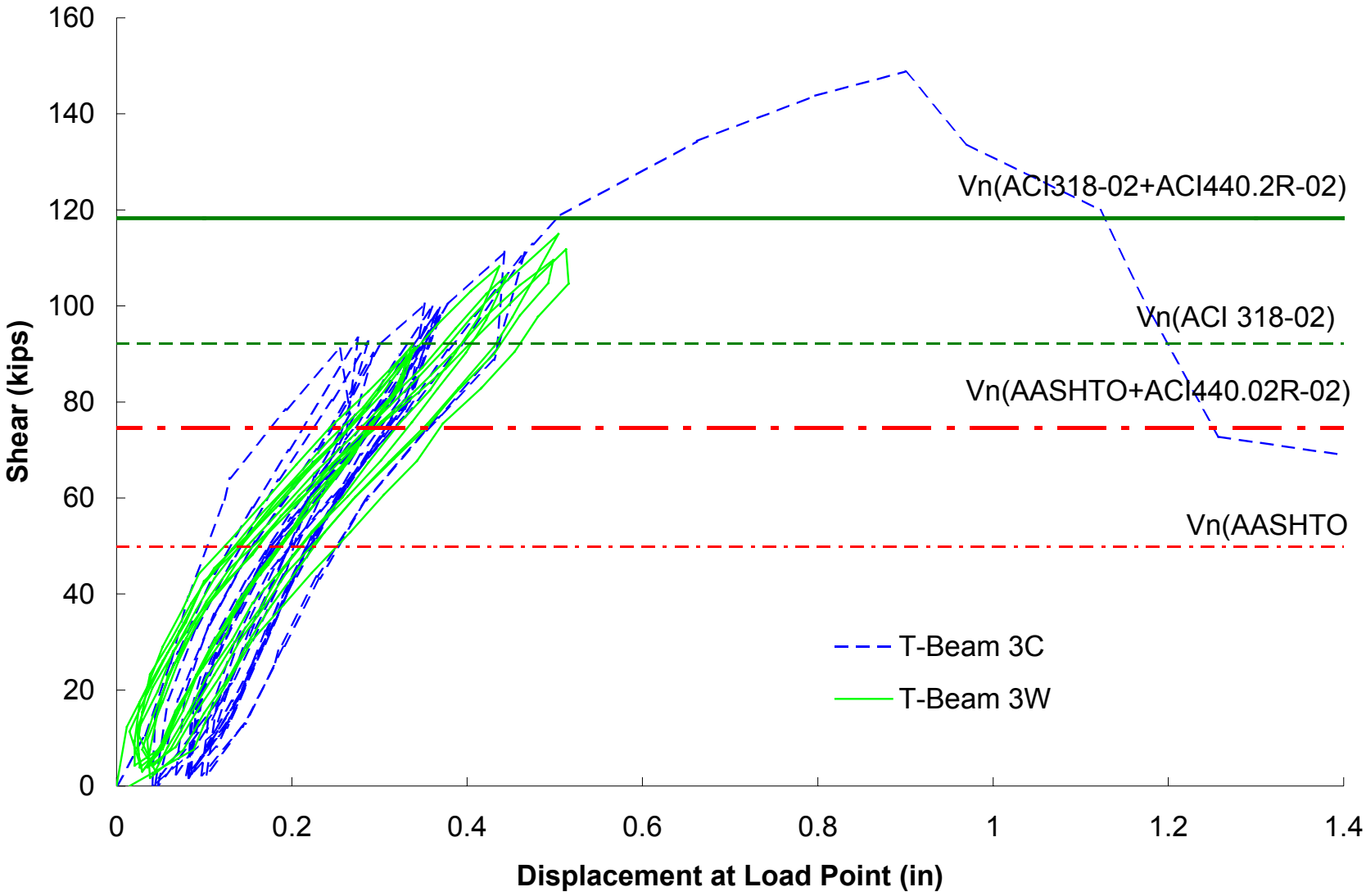

Figure 8.2: Shear-displacement relationship for T-Beam 3C and T-Beam 3W

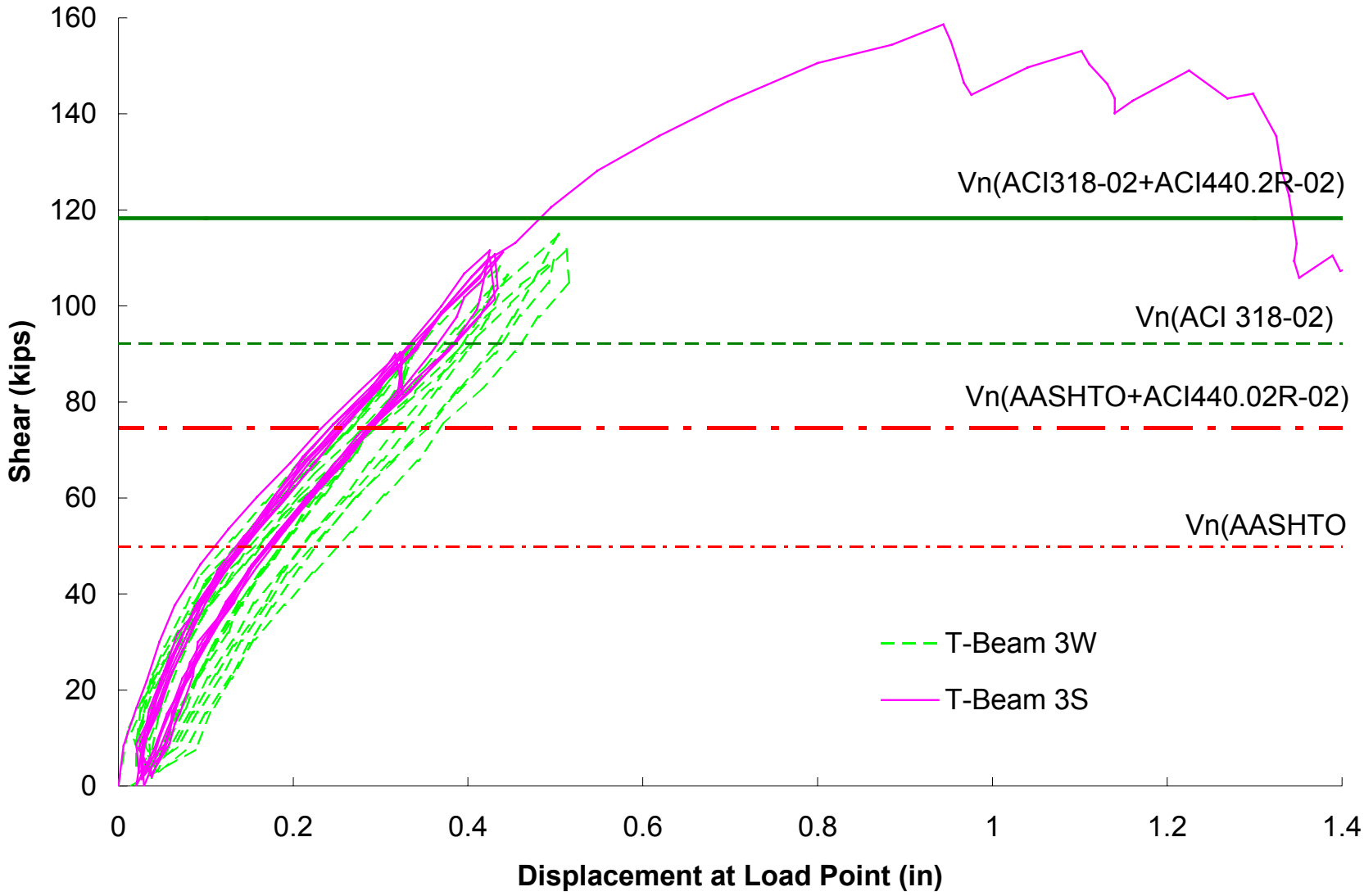

Figure 8.3: Shear-displacement relationship for T-Beam 3W and T-Beam 3S

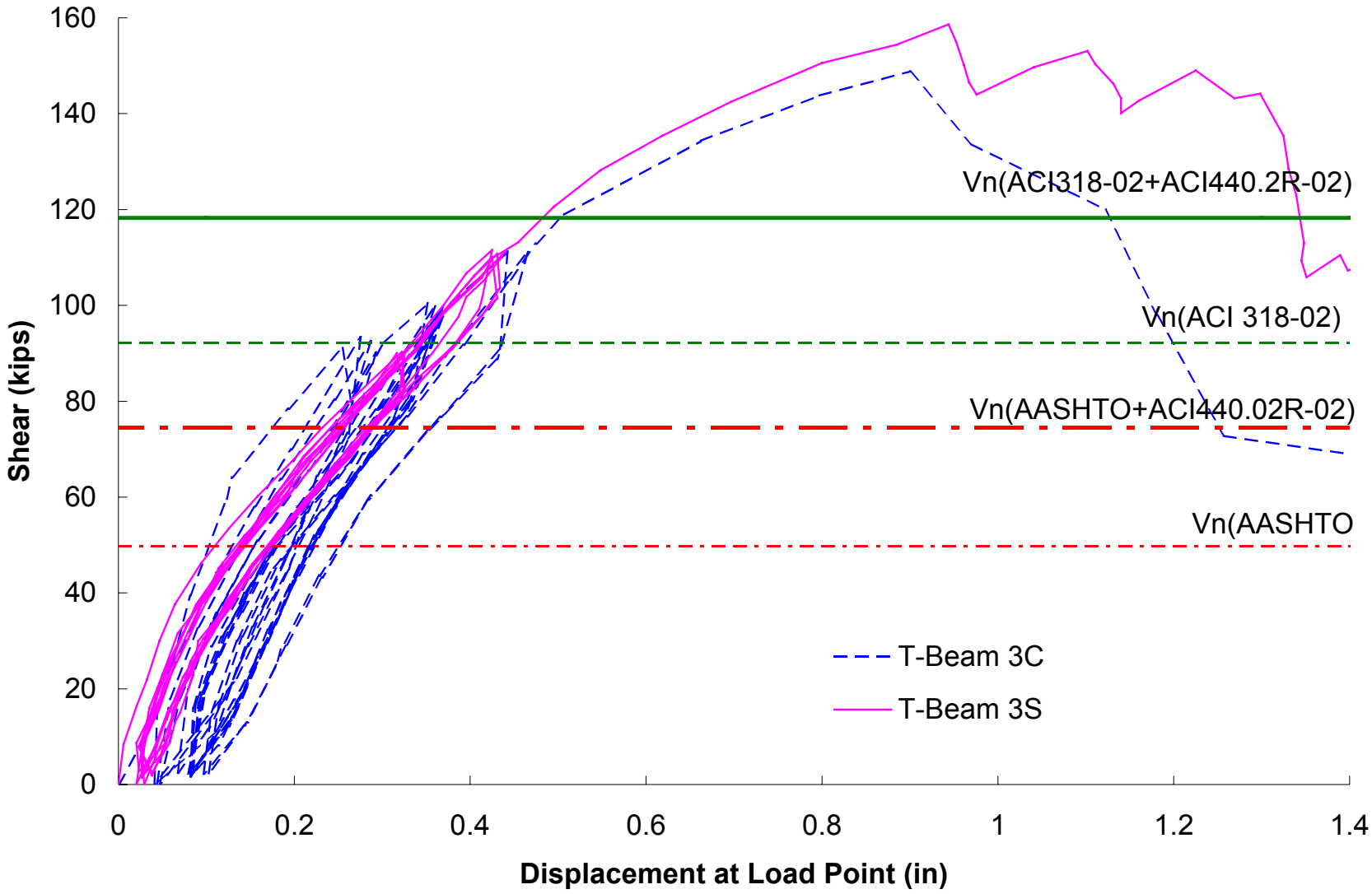

Figure 8.4: Shear-displacement relationship for T-Beam 3C and T-Beam 3S

Figure 8.5: Carbodur flexural retrofit delamination from the beam soffit

In Figure 8.6, the load-displacement relationship from T-Beam 3C is compared with the short-term load-displacement predictions presented in Chapter 6.

In the precracking stage, the beam stiffness is significantly lower than the prediction based on gross uncracked section properties. This is probably caused by pre-existing cracking in T-Beam 3. The T-Beam was recovered from the Ala Moana parking structure, which had been in service for over twenty years. It is likely that thermal, shrinkage and service loading effects might have resulted in flexural cracks in the beam. It is also possible that flexural cracks may have been caused during beam removal and transport to the testing laboratory. Because of the prestress in the beam, these cracks would remain closed until the beam is loaded. These cracks would reduce the initial beam stiffness.

In the postcracking stage, there is good agreement between the slope of the prediction and the test result. During testing of T-Beam 3C the first flexure crack was observed at a load level of 85 kips, which coincides with the theoretical prediction of between 82 and 97 kips.

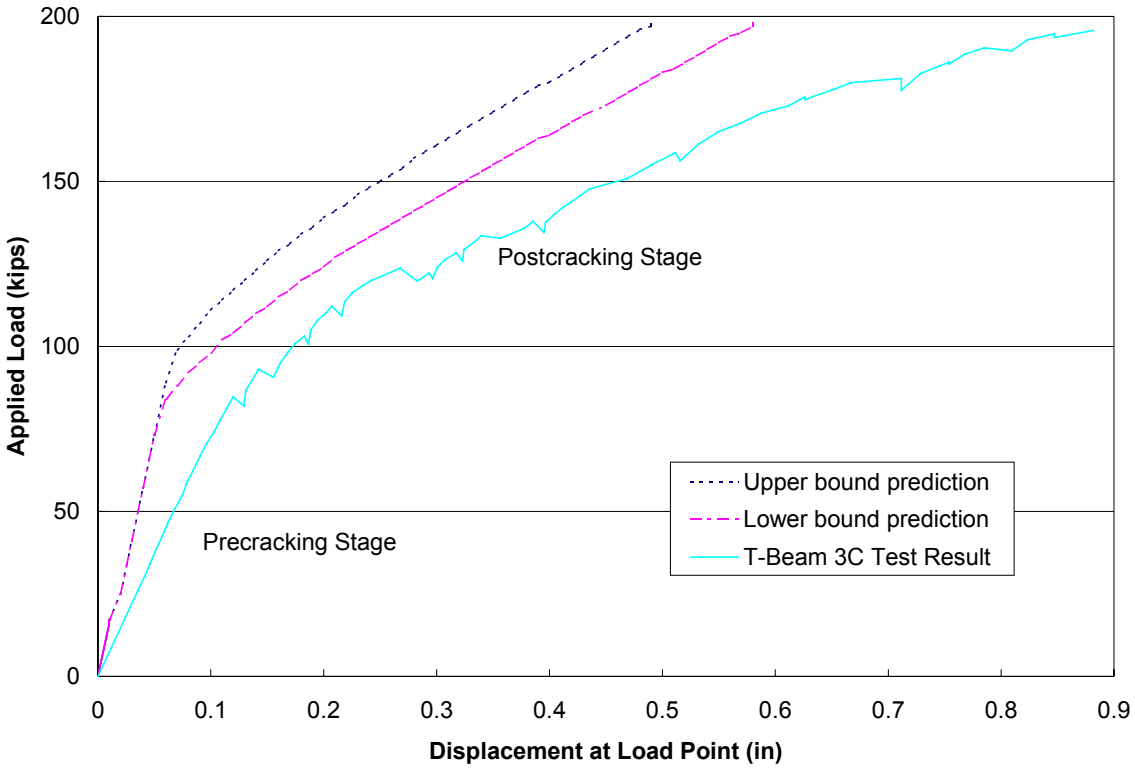

Figure 8.6: Comparison of load-displacement relationships

8.2 Comparison of the Crack Width Results from T-Beam 3W and T-Beam 3S

8.2.1 Overview of the Contribution of the CarboShear-L Stirrup Shear retrofit

The applied shear versus crack width relationships for T-Beam 3W and T-Beam 3S were monitored by the VW Crackmeter and crack gages 1 and 2 installed after testing T-Beam 3I. The installation is described in Chapter 4 and the locations are shown in Figure 4.10. The shear versus crack width relationship for each instrument during each test is shown separately in Chapter 7. These curves are compared and discussed below to evaluate the performance of the CarboShear-L stirrup retrofit system when applied over existing shear cracks.

Figure 8.7 to Figure 8.9 show the comparison of applied shear versus crack width relationship recorded by crack gages 1, 2 and the VW Crackmeter during the testing of T-Beam 3W and T-Beam 3S.

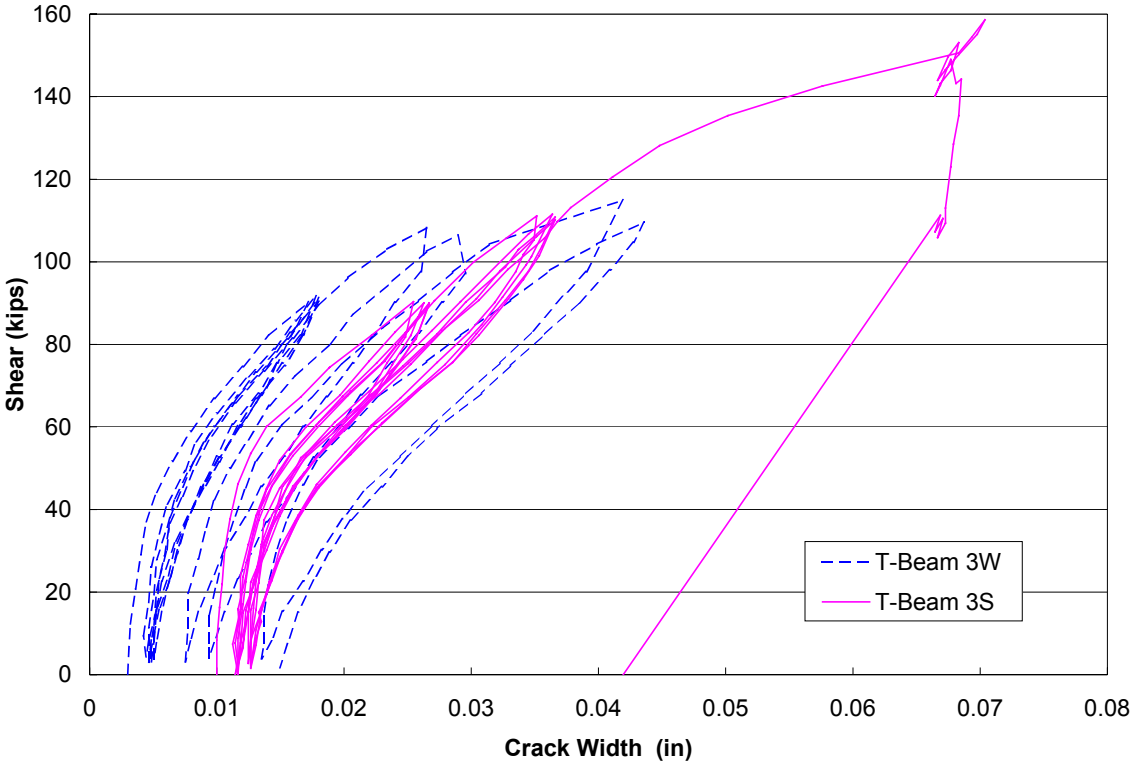

Figure 8.7: Results from crack gage 1

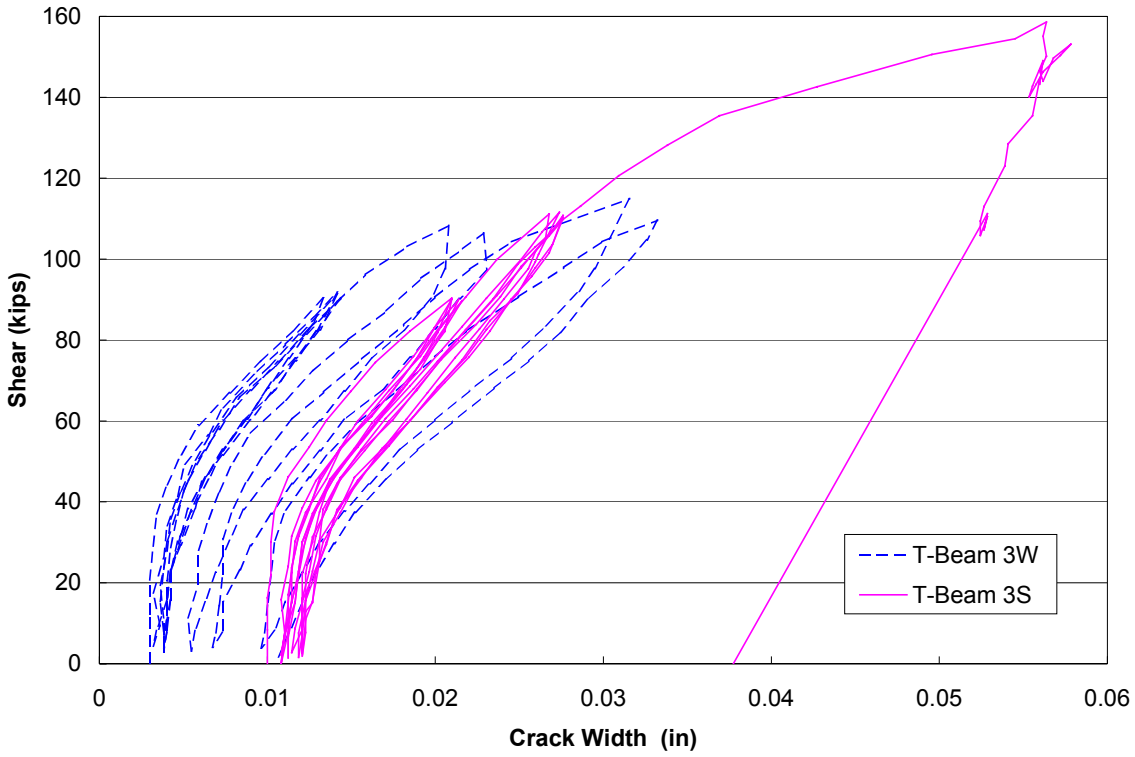

Figure 8.8: Results from crack gage 2

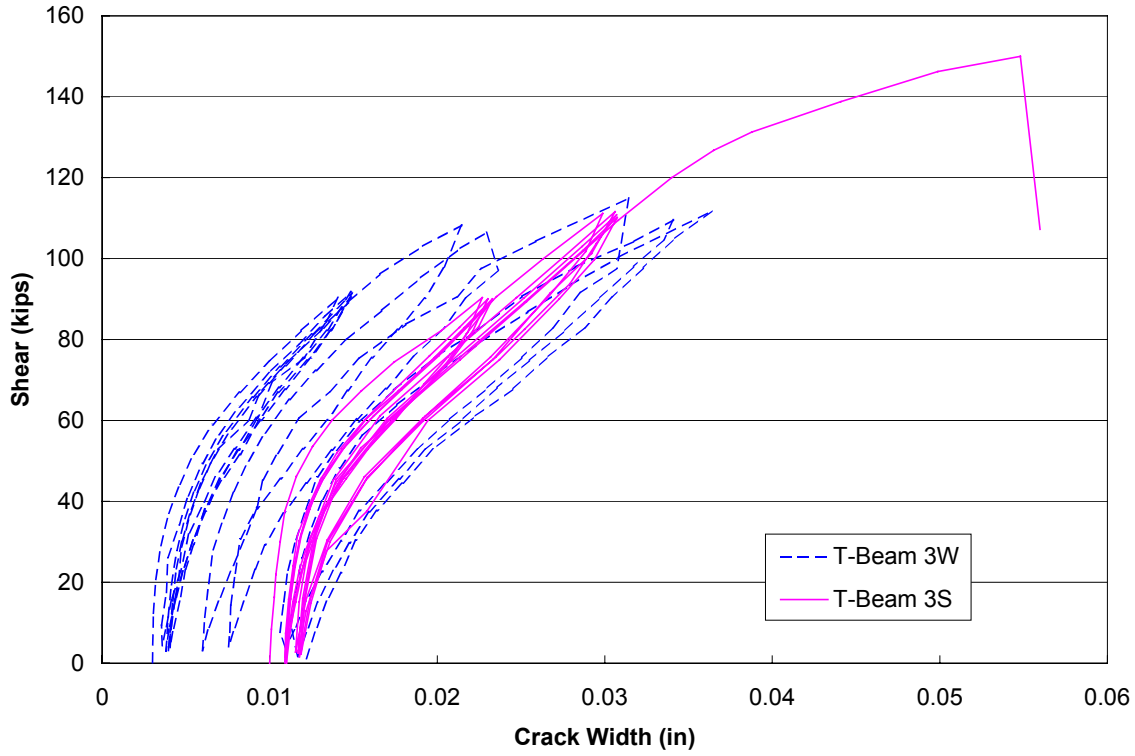

Figure 8.9: Results from VW crackmeter

From the preceding figures, the following observations were made:

1. As a result of the crack initiation test, T-Beam 3I, the existing shear crack widths on T-Beam 3W at the crack gage locations were all approximately 0.003" (0.08 mm) prior to testing.

2. Subsequent to the crack widening test, T-Beam 3W, and the time taken to install the shear retrofit, the existing crack widths on T-Beam 3S at the crack gage locations were all approximately 0.01" (0.25 mm) prior to testing.

3. During the first load cycle to the 120 kip load level, the maximum crack width and residual crack widths increased slightly for both T-Beam 3W and T-Beam 3S. However, for subsequent loading cycles to the 120 kip level, no further increase in crack width was noted for either test.

4. During the first loading cycle to the 145 kip level, the maximum crack width and residual crack width increased for both T-Beam 3W and T-Beam 3S. However, the increase in residual crack width for T-Beam 3S was only 26% of that for T-Beam 3W.

5. During subsequent cycles to the 145 kip load level on T-Beam 3W, both the maximum crack widths and the residual crack widths continued to increase. For T-Beam 3S, however, both the maximum crack widths and the residual crack widths remained constant.

6. The slope of the applied shear versus crack width relationships are greater for T-Beam 3S than for T-Beam 3W, particularly during the 145 kip loading

cycles. This confirms the improved crack control provided by the CarboShear-L stirrup retrofit system.

The above observations show that the CarboShear-L stirrups help to control crack opening. In addition, the elasticity of the CarboShear-L stirrups helps to close the cracks after unloading. By contributing to the shear capacity of the section, the CarboShear-L stirrups will have reduced the tension stresses in the internal shear reinforcement, thus preventing further growth of the crack widths under continued cycling.

Table 8-1 lists the crack widths at the start and peak of each loading cycle. Based on the values in this table, the changes in residual crack widths per cycle were computed and listed in Table 8-2. In addition, the change in crack width during each cycle was computed and listed in Table 8-3.

Table 8-1: Crack widths for T-Beam 3W and T-Beam 3S

Load Cycle	Crack gage1		Crack gage2		Crackmeter	
	3W*	3S*	3W*	3S*	3W*	3S*
Loading 120-1 start	0.0030	0.0100	0.0030	0.0102	0.0030	0.0100
Loading 120-1 peak	0.0172	0.0255	0.0134	0.0212	0.0141	0.0227
Loading 120-2 start	0.0044	0.0117	0.0032	0.0110	0.0036	0.0109
Loading 120-2 peak	0.0178	0.0263	0.0142	0.0212	0.0149	0.0230
Loading 120-3 start	0.0046	0.0117	0.0038	0.0110	0.0038	0.0110
Loading 120-3 peak	0.0180	0.0267	0.0142	0.0216	0.0149	0.0233
Loading 120-4 start	0.0048	0.0115	0.0038	0.0110	0.0039	0.0110
Loading 120-4 peak	0.0180	0.0267	0.0144	0.0218	0.0149	0.0233
Loading 145-1 start	0.0051	0.0117	0.0038	0.0115	0.0041	0.0109
Loading 145-1 peak	0.0265	0.0352	0.0208	0.0270	0.0215	0.0299
Loading 145-2 start	0.0075	0.0125	0.0055	0.0117	0.0060	0.0115
Loading 145-2 peak	0.0290	0.0364	0.0229	0.0276	0.0229	0.0306
Loading 145-3 start	0.0094	0.0127	0.0067	0.0123	0.0075	0.0118
Loading 145-3 peak	0.0419	0.0366	0.0316	0.0278	0.0314	0.0307
Loading 145-4 start	0.0135	0.0127	0.0096	0.0121	0.0109	0.0118
Loading 145-4 peak	0.0436	0.0366	0.0332	0.0278	0.0341	0.0307
Loading 145-5 start	0.0149	0.0127	0.0107	0.0125	0.0117	0.0119
Loading 145-5 peak	0.0469	0.0368	0.0355	0.0278	0.0364	0.0308

Table 8-2: Change in residual crack widths per cycle in T-Beam 3W and T-Beam 3S

load cycle	Crack gage1				Crack gage2				Crackmeter			
	3W	3S	difference	%	3W	3S	difference	%	3W	3S	difference	%
120-1	0.00144	0.00165	0.00021	14.70	0.0002	0.00083	0.00062	299.52	0.00059	0.0009	0.000305	51.61
120-2	0.00021	0	-0.00021	-100.00	0.0006	0	-0.00062	-100.00	0.00022	7E-05	-0.00014	-66.51
120-3	0.00021	-0.0002	-0.0004	-195.63	0	0	0	/	0.00014	4E-05	-0.00011	-74.83
120-4	0.00021	0.0002	-9E-06	-4.37	0	0.00043	0.000433	/	0.00011	-0.0009	-0.00101	-941.12
145-1	0.00247	0.00083	-0.00165	-66.56	0.0017	0.0002	-0.00146	-88.10	0.00193	0.0006	-0.00131	-67.58
145-2	0.00186	0.0002	-0.00166	-89.38	0.0012	0.00063	-0.00061	-49.28	0.00156	0.0003	-0.00129	-82.73
145-3	0.00412	0	-0.00412	-100.00	0.0029	-0.0002	-0.0031	-106.80	0.00339	-4E-05	-0.00342	-101.06
145-4	0.00144	0	-0.00144	-100.00	0.001	0	-0.00104	-100.00	0.00073	9E-05	-0.00064	-87.74
	Average (145-1 to 145-4)			-88.98	Average (145-1 to 145-4)			-86.04	Average (145-1 to 145-4)			-84.78

Table 8-3: Change in crack widths during each cycle in T-Beam 3W and T-Beam 3S

load cycle	Crack gage1				Crack gage2				Crackmeter			
	3W	3S	difference	%	3W	3S	difference	%	3W	3S	difference	%
120-1	0.0142	0.0155	0.0013	8.82	0.0104	0.0110	0.0006	6.11	0.0111	0.0127	0.0016	14.38
120-2	0.0134	0.0146	0.0013	9.35	0.0110	0.0102	-0.0008	-7.44	0.0113	0.0121	0.0009	7.63
120-3	0.0134	0.0150	0.0016	12.28	0.0104	0.0106	0.0002	2.31	0.0111	0.0123	0.0012	10.79
120-4	0.0132	0.0152	0.0020	15.53	0.0106	0.0108	0.0002	2.16	0.0109	0.0123	0.0014	12.62
145-1	0.0214	0.0235	0.0021	9.67	0.0170	0.0155	-0.0015	-8.63	0.0174	0.0190	0.0016	8.95
145-2	0.0214	0.0239	0.0025	11.51	0.0174	0.0159	-0.0014	-8.32	0.0169	0.0190	0.0021	12.36
145-3	0.0326	0.0239	-0.0087	-26.60	0.0248	0.0155	-0.0093	-37.57	0.0239	0.0189	-0.0050	-20.91
145-4	0.0301	0.0239	-0.0062	-20.57	0.0236	0.0157	-0.0079	-33.44	0.0232	0.0190	-0.0042	-18.16
145-5	0.0319	0.0241	-0.0078	-24.44	0.0236	0.0153	-0.0083	-35.11	0.0232	0.0189	-0.0042	-18.24

Note:
positive indicates crack width increase
negative indicates crack width decrease
/ indicates crack width remained constant

8.2.2 Residual Crack Width Comparisons

Figure 8.10 to Figure 8.12 show the comparison of cumulative changes in the residual crack width for T-Beam 3W and T-Beam 3S from each crack extensometer.

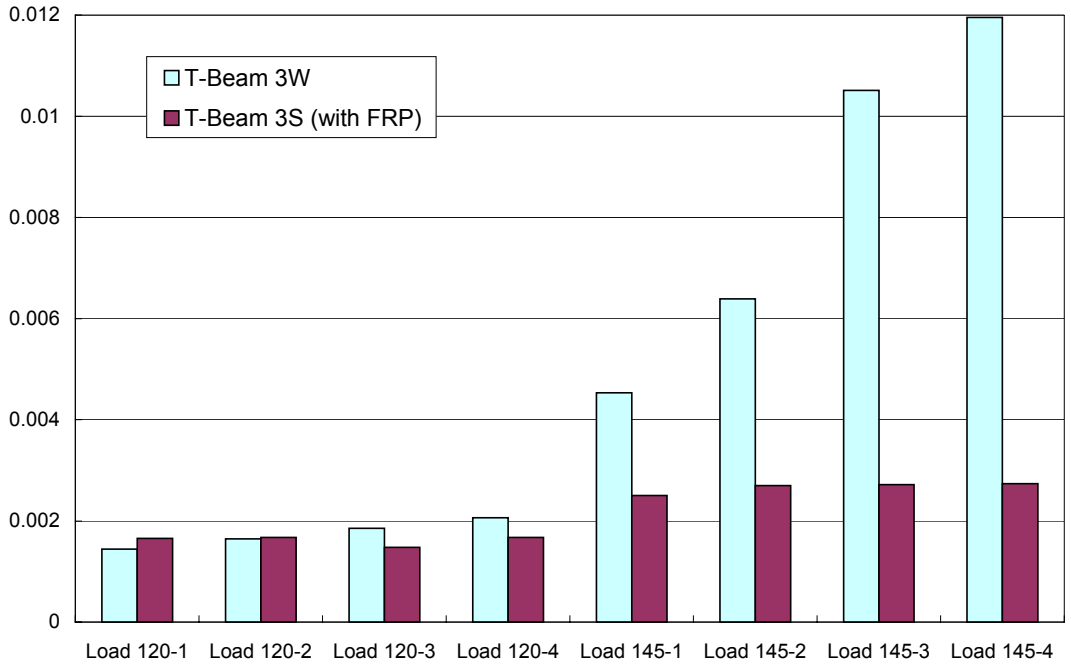

Figure 8.10: Cumulative change in residual crack width (from crack gage 1)

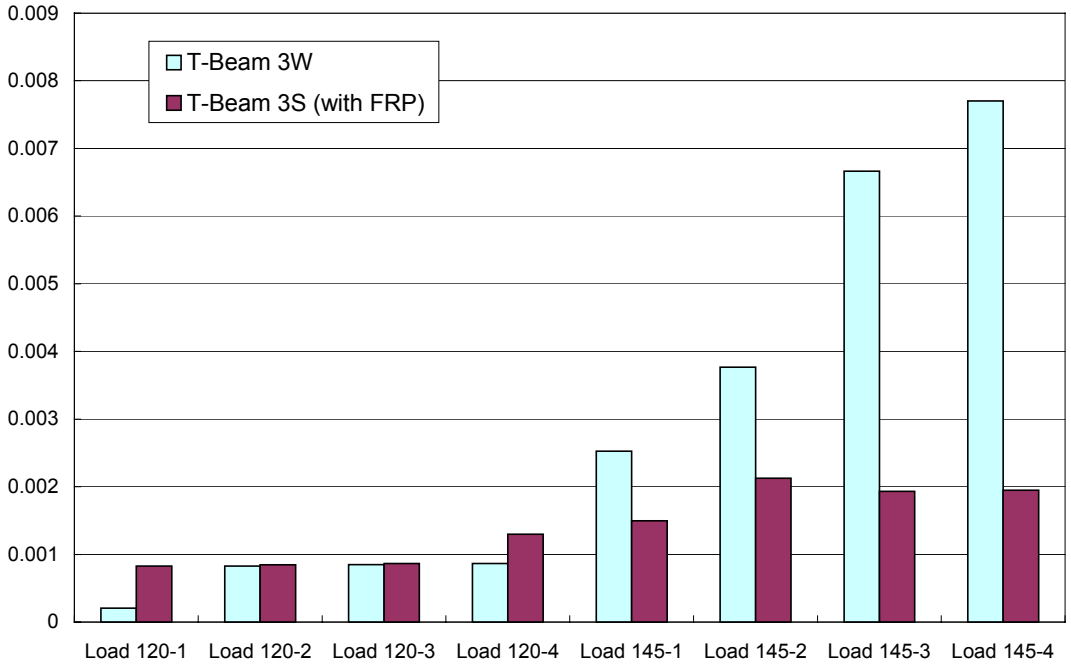

Figure 8.11: Cumulative change in residual crack width (from crack gage 2)

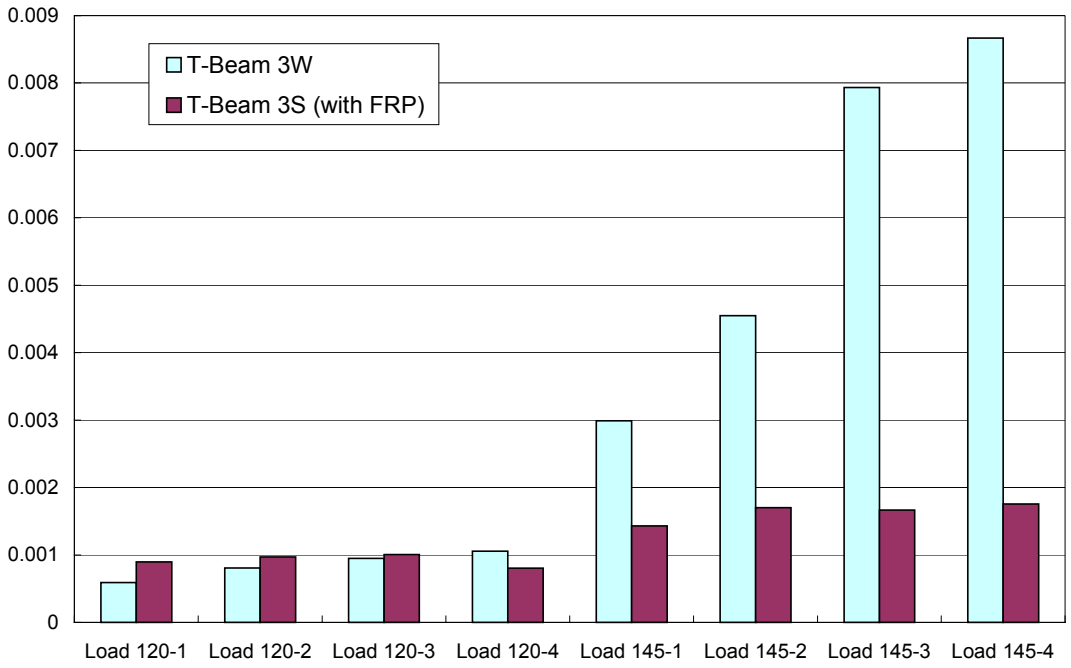

Figure 8.12: Cumulative change in residual crack width (from VW crackmeter)

In Table 8-2, changes in residual crack width per cycle in T-Beam 3W and T-Beam 3S are compared. The percentage difference for each instrument was calculated. From the figures and table, the following observations were made:

1. At the 120 kip load level, the residual crack widths were relatively constant for both T-Beam 3W and T-Beam 3S.

2. At the 145 kip load level, the residual crack widths for T-Beam 3W without CarboShear-L retrofit continued to increase with each loading cycle. The residual crack widths for T-Beam 3S, with CarboShear-L stirrups, remained relatively constant through all four cycles to the 145 kips load level.

3. Table 8-2 shows that the contribution of CarboShear-L stirrups to reduce the residual crack widths during load cycling to the 145 kip load level resulted in an average 87% decrease in the change of residual crack sizes per cycle.

4. The CarboShear-L stirrups are effective at controlling residual crack widths during cyclic loading.

8.2.3 Discussion on Crack Sizes Changes

Table 8-3 presents a comparison of the change in crack widths during each load cycle for T-Beam 3W and T-Beam 3S. The percentage difference for each instrument is also listed. During the cycles to 120 kip load, and the initial cycles to 145 kips, the CarboShear-L stirrups do not affect the crack opening under load. However, for the majority of load cycles to the 145 kip load level, the presence of CarboShear-L stirrups reduced the net crack opening under load by up to 37%. For the last three load cycles to 145 kip, the retrofit resulted in an average 26% decrease in the net crack opening.

8.3 Comparison of Strain Gages on the Same CarboShear-L Stirrups

In order to monitor the strains in the CarboShear-L stirrups, 52 strain gages (SG) were bonded to the surface of the stirrups. The strain gage locations are described in Chapter 4 and are shown in Figure 4.27. In Chapter 7, the readings from strain gages on the same stirrup were plotted together. In particular, the final loading procedure was plotted independently, with the strains zeroed at the start of this loading for better comparison. These results are discussed here with the objective to identify the initiation of stirrup delamination. Three typical stirrups are selected for this discussion and presented in section 8.3.2.

8.3.1 Maximum Strain recorded by the Strain Gages

Figure 8.13 shows the maximum strains recorded by the strain gages on the CarboShear-L stirrups during testing.

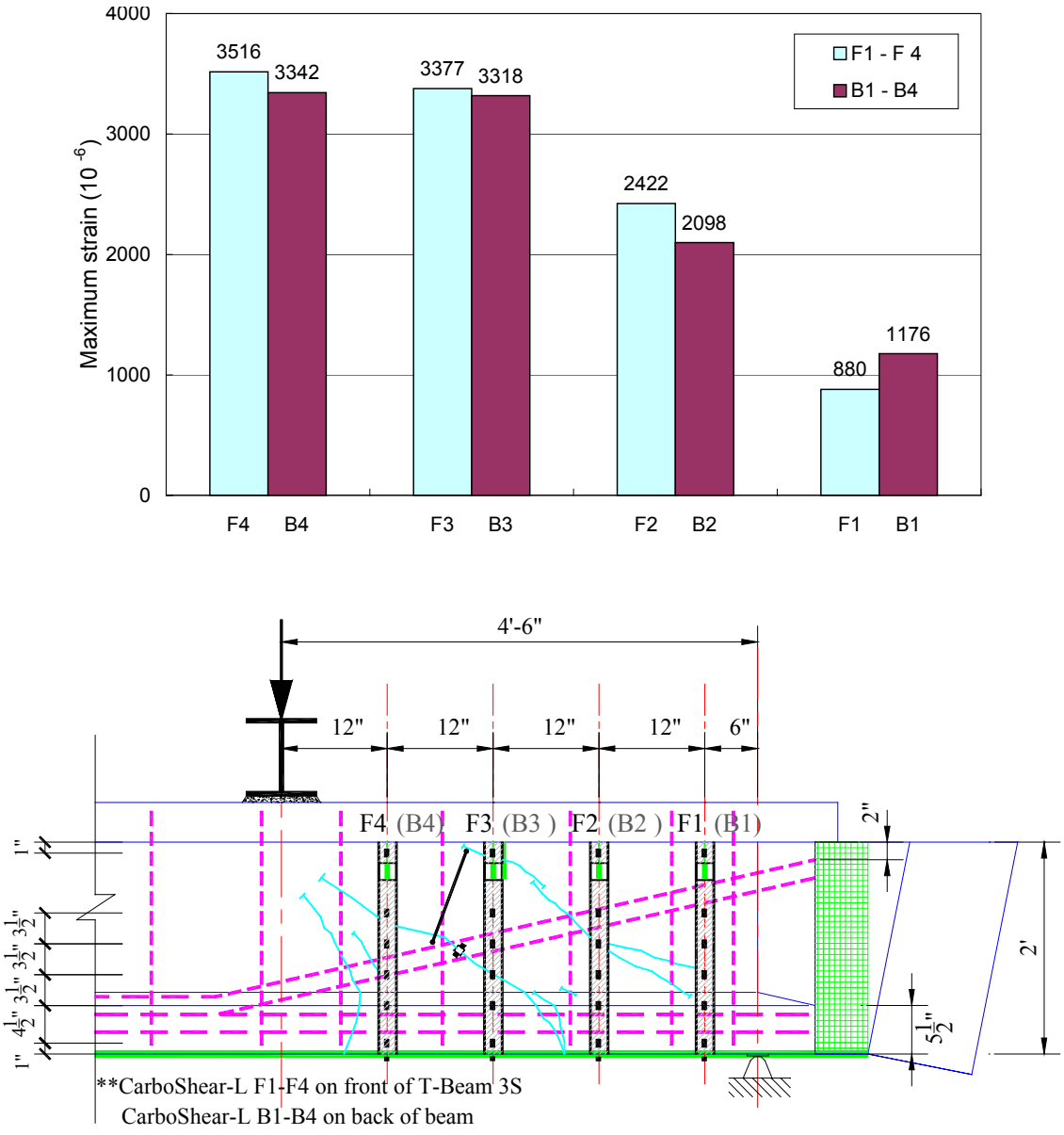

Figure 8.13: Maximum strain observed in each CarboShear-L stirrup

The CarboShear-L stirrups did not reach ultimate capacity before the flexural failure of T-Beam 3S. The maximum strain recorded in the stirrups was 0.0035, which is close to the value of 0.004 assumed in the ACI 440 shear strength calculations. It is only half of the maximum strain of 0.007 recommended by the manufacturer (Sika Corporation, 2002). If flexural failure had not occurred, it is likely that a larger strain would have developed in the stirrups.

8.3.2 Discussion of the CarboShear-L Stirrup Delamination

Case 1: Delamination of the CarboShear-L stirrup F3

Figure 8.16 shows the locations and the readings of strain gages 15-21 on the third CarboShear-L stirrup on the front of the beam.

During the first load cycle to 120 kips (90 kip shear), some of the existing cracks on the web of the beam extended through the filler blocks. For stirrup F3, these cracks occurred close to strain gages 15 and 18 resulting in increasing strains in these gages. Strain gage 19 also recorded increasing strains due to the separation between the filler block and the beam bottom bulb. Strain gages 16 and 20, which were some distance from these cracks, recorded very small strains up to a shear load of 120 kips (160 kip total load). Figure 8.14 shows the cracks formed on the filler block of stirrup F3. A red marker was used to highlight the cracks.

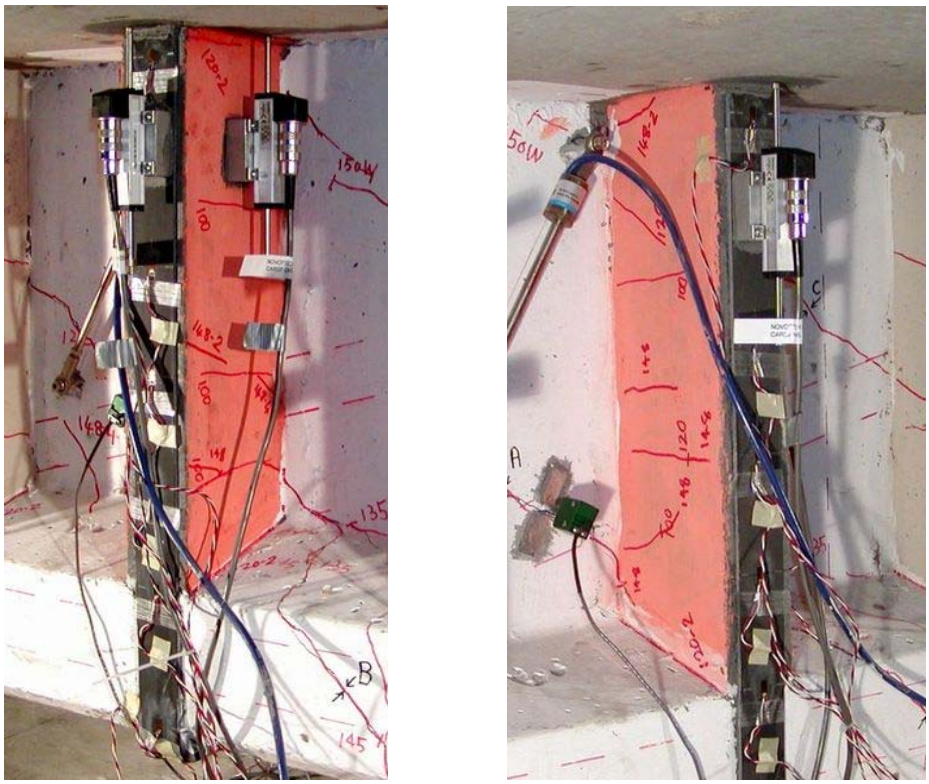

Figure 8.14: Cracks formed in the FRCC filler block of stirrup F3

At 120 kip shear load, the strain in SG16 started to increase more rapidly. At a shear load of 130 kips, the strain in SG20 suddenly increased to the same strain as the neighboring SG19 indicating that the stirrup had delaminated between these two gage locations (Figure 8.15). At 140 kip shear load, a similar jump in strain is observed for SG16 and SG17, indicating that the stirrup had delaminated over its full length.

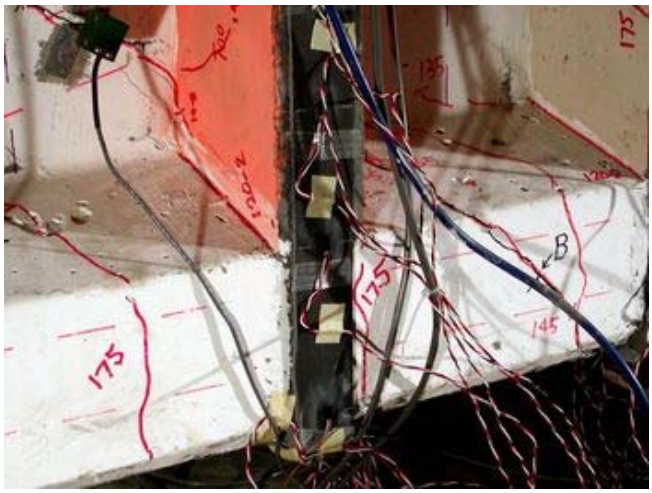

Figure 8.15: Delamination between SG 19 and SG20

Even with full delamination of the vertical leg of the stirrup, the strain in the stirrup remained high. This would indicate that the anchorage systems at both ends of the stirrup were effective at maintaining the load-carrying capacity of the stirrup. Even after delamination of the vertical stirrup leg, SG21 on the horizontal bottom leg of the stirrup recorded very small strains. This confirms that the anchorage of the CarboShear-L stirrup at the bottom of the beam was effective. The strain in SG21 eventually increased due to delamination of the Carbodur flexural retrofit strips to which the stirrups were bonded. As noted in Chapter 7, the LVDTs located at the top of each stirrup recorded no movement between the stirrup and top slab throughout the T-Beam 3S test, even subsequent to complete delamination of the vertical leg of stirrup. This confirms the effectiveness of the epoxy sleeve anchorage at the top of the stirrup.

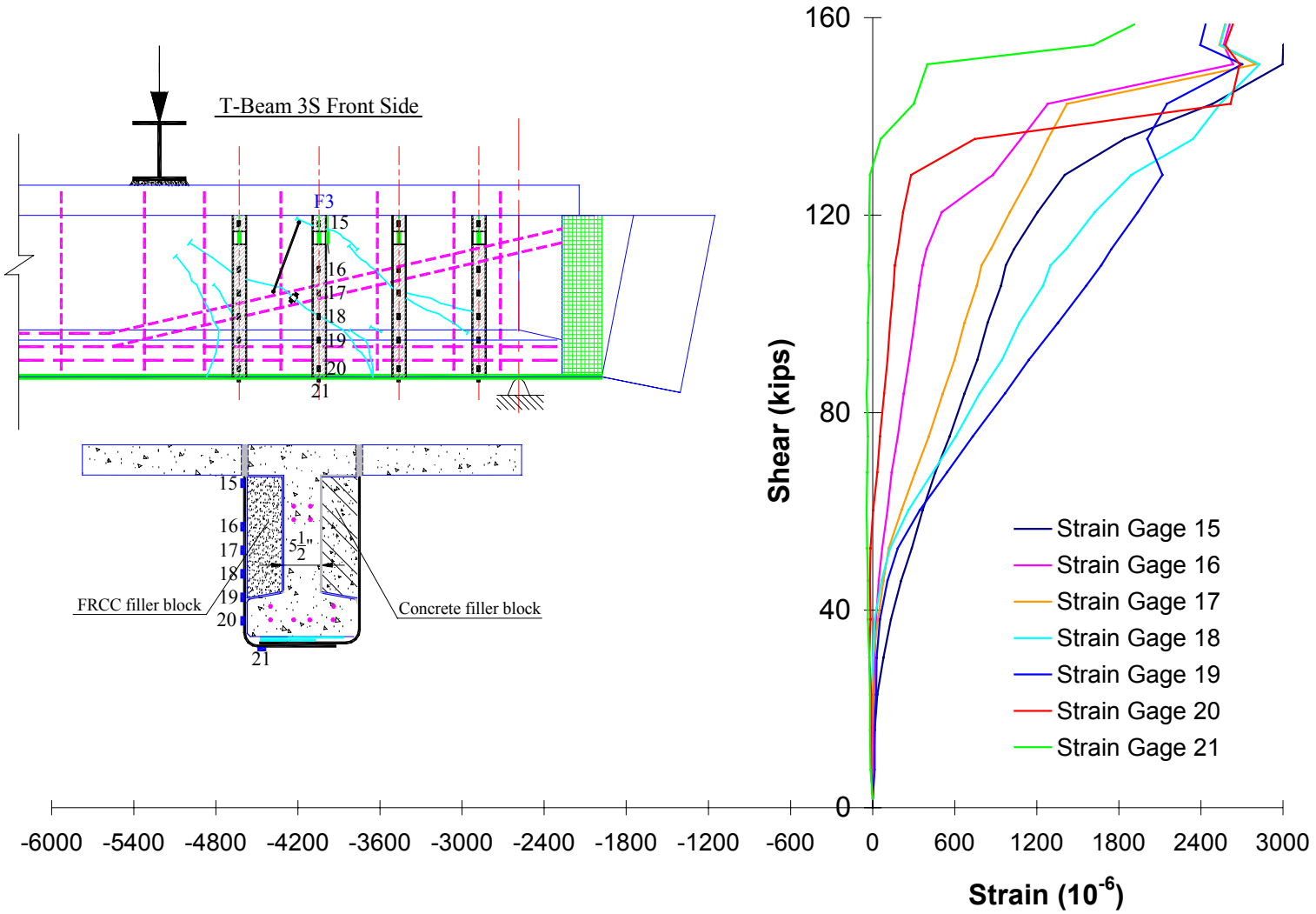

Figure 8.16: SG readings from the 3rd CarboShear-L on the front of the beam

Case 2: Delamination of the CarboShear-L stirrup B3

Figure 8.21 shows the locations and the readings of strain gages 41-46 on the third CarboShear-L stirrup on the back of the beam.

During the first load cycle to 120 kips (90 kip shear), some of the existing cracks on the web of the beam extended through the filler blocks. For stirrup B3, these cracks occurred close to strain gage 44 resulting in increasing strain in this gage. Strain gage 45 also recorded increasing strains due to the separation between the filler block and the beam bottom bulb (Figure 8.17). Strain gages 42 and 46, which were some distance from these cracks, recorded very small strains up to a shear load of 120 kips (160 kip total load). Figure 8.18 shows the cracks formed on the filler block of B3. A blue marker was used to highlight the cracks.

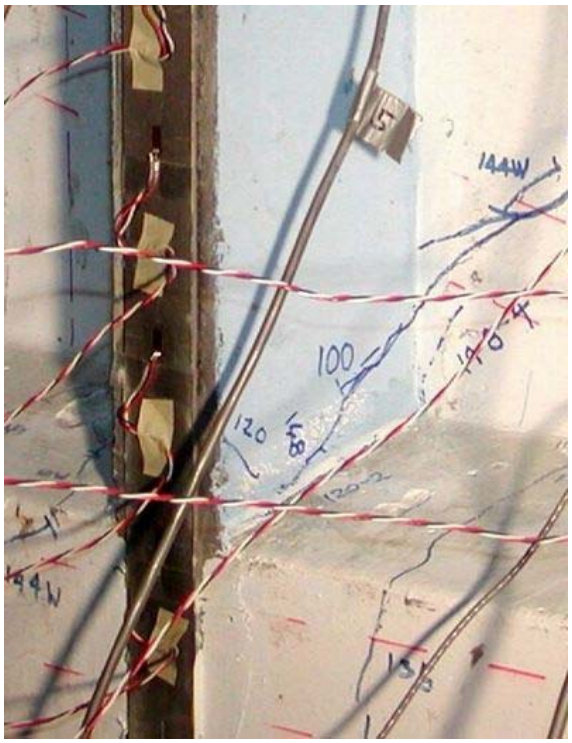

Figure 8.17: Cracks formed at the joint of the filler block

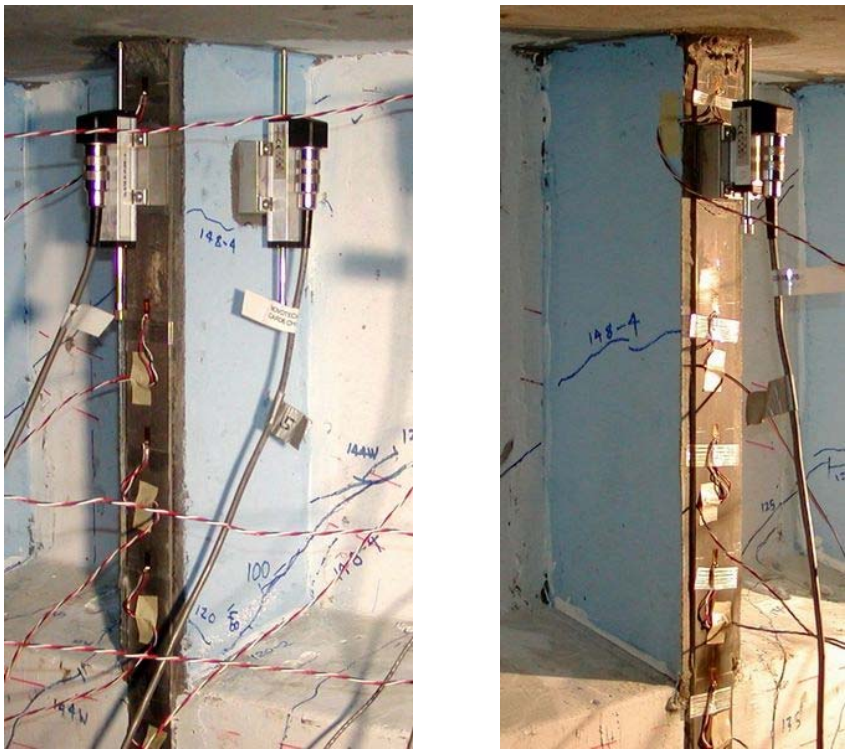

Figure 8.18: Cracks formed in the filler block of B3

At 120 kip shear (160 kips total load), SG46 suddenly increased to the same strain as the neighboring SG45 indicating that the stirrup had delaminated between these two gage locations. At 140 kip shear load, a similar jump in strain is observed for SG42 and SG43, indicating that the stirrup had delaminated over its full length (Figure 8.19).

Even with full delamination of the vertical leg of the stirrup, the strain in the stirrup remained high. As noted in Chapter 7, the LVDTs located at the top of each stirrup recorded no movement between the stirrup and top slab throughout the T-Beam 3S test, even subsequent to complete delamination of the vertical leg of the stirrup. This confirms the effectiveness of the epoxy sleeve anchorage at the top of the stirrup (Figure 8.20).

Figure 8.19: Full delamination of CarboShear-L stirrup B3

Figure 8.20: Top anchorage of stirrup B3 after delamination

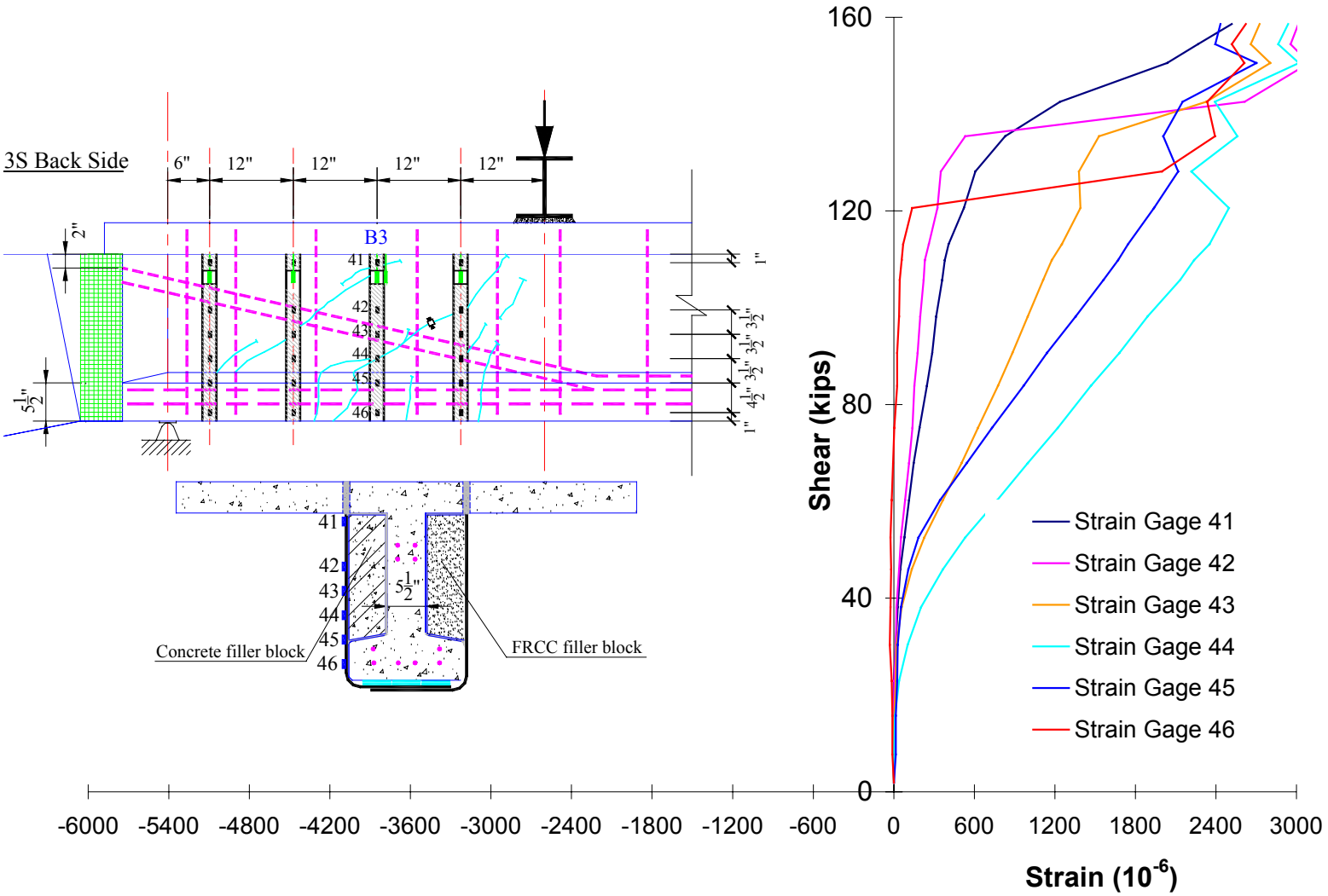

Figure 8.21: SG readings from the 3rd CarboShear-L on the back of the beam

Case 3: Delamination of the CarboShear-L stirrup F4

Figure 8.22 shows the locations and the readings of strain gages 41-46 on the third CarboShear-L stirrup on the front of the beam.

The strain results confirm that shear cracks occurred close to strain gages 22, 23, 24 and 25. Strain gage 26 recorded increasing strains because of the crack that formed between the filler block and the beam bottom bulb. Strain gages 27 and 28 recorded very small strains throughout the test until immediately prior to failure. At a shear load of 150 kips, the strain in SG27 suddenly increases to match those in other gages, indicating that the stirrup had delaminated. Strain gage 28 only recorded a slight increased in strain even though the vertical leg of the stirrup was now completely delaminated. This confirms the effectiveness of the bottom anchorage. The lack of movement between the top of the stirrup and the top slab, as confirmed by the LVDT readings, confirms that the top anchorage was also effective at maintaining stirrup integrity even after full delamination of the vertical leg.

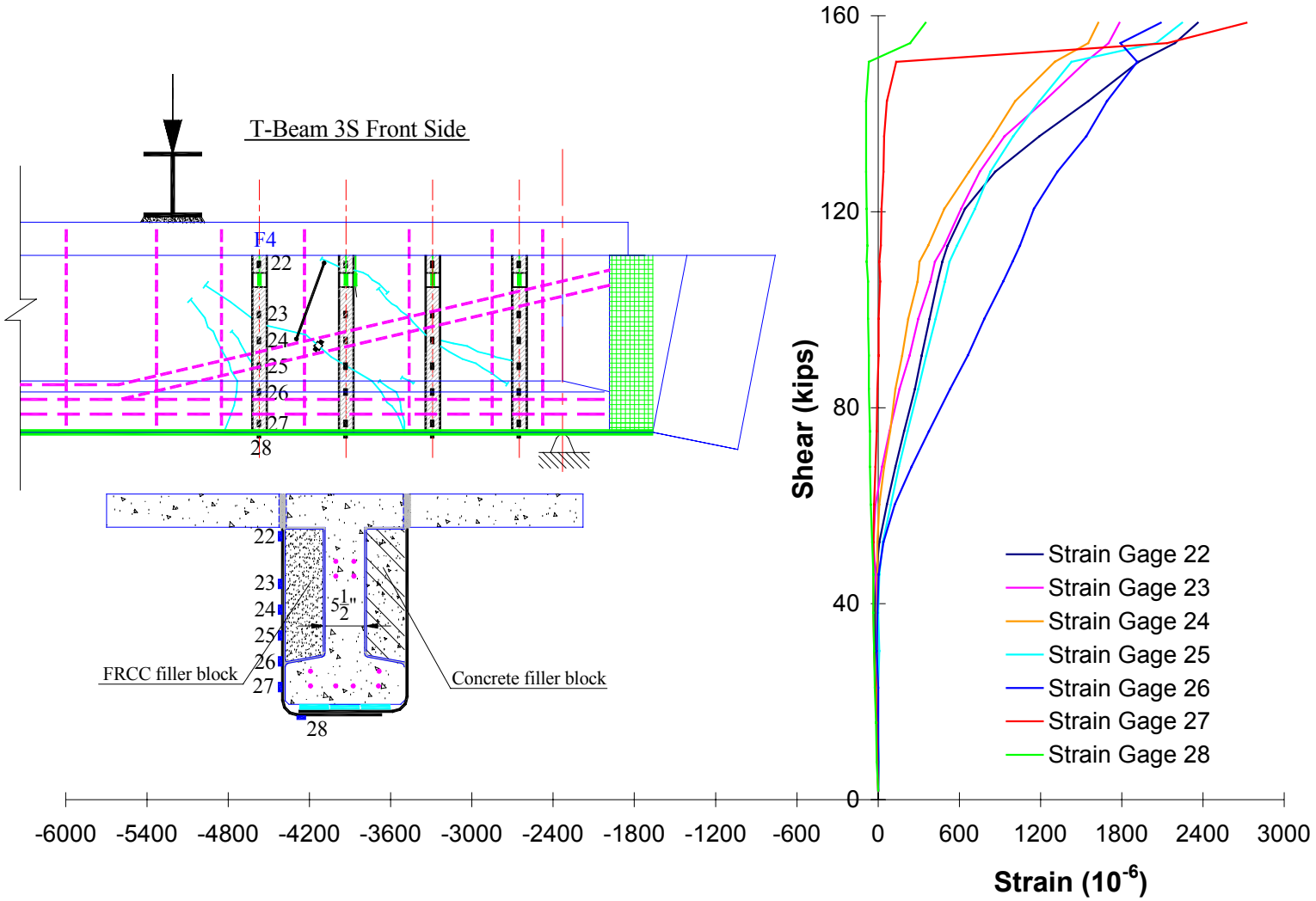

Figure 8.22: SG readings from the 4th CarboShear-L on the front of the beam

CHAPTER 9

9 SUMMARY AND CONCLUSION

9.1 Summary

This research study involved a series of tests performed on a prestressed T-Beam recovered from the Ala Moana Shopping Center Parking Structure. The objective of this study was to evaluate the performance of CarboShear-L shear stirrup retrofit applied over existing shear cracks, particularly under cyclic loading conditions. The research was performed to provide guidance for the shear retrofit to be performed on the Salt Lake Boulevard Bridge. The AASHTO prestressed girders in this bridge have inadequate shear capacity according to current AASHTO LRFD bridge design requirements. Some of these beams have shear cracks up to 0.02" (0.5mm) wide. In addition, the instrumentation system used in this study is evaluated for potential use in the field instrumentation of the Salt Lake Boulevard Bridge during and after application of the shear retrofit.

The test beam used in this study was one of three nominally identical prestressed concrete beams recovered from the Ala Moana Shopping Center Parking Garage in June 2000. Because of the low flexural strength of the original beam, flexural retrofit in the form of CFRP Carbodur strips bonded to the soffit of the beam was required to ensure shear failure.

The left end of the T-Beam was tested to determine the shear capacity of the original beam (T-Beam 3C). The nominally identical right end of the beam was then subjected to a series of shear tests. The Initial Cracking Test (T-Beam 3I) was performed monotonically to induce shear cracks in the right hand shear span. Crack width

extensometers were installed across these cracks to monitor the change in crack width during subsequent testing. The Crack Widening Test (T-Beam 3W) consisted of cyclic loading to increase the width of the residual shear cracks to the 0.02" (0.5mm) width noted in the Salt Lake Boulevard Bridge girders.

The right end of the beam was then retrofitted for shear with CarboShear-L stirrups applied over the cracked beam without epoxy injection of the existing cracks. Cementitious filler blocks were installed in the web of the beam to provide a smooth profile for installation of the vertical legs of the CarboShear-L stirrups. These blocks were made of regular concrete on the back of the web and two types of fiber reinforced cementitious composite (FRCC) on the front of the web. The final Shear Retrofit Test (T-Beam 3S) was performed to evaluate the effect of the retrofit on the crack widths under cyclic loading. The beam was then loaded monotonically to failure, which resulted from delamination of the flexural Carbodur strips bonded to the soffit of the beam. The CarboShear-L stirrups prevented shear failure in the retrofitted right end shear span.

9.2 Conclusions

9.2.1 Shear tests

Based on the shear tests performed in this study, the following conclusions were made.

- Both AASHTO and ACI 318 approaches to estimate the original shear capacity of the beam are conservative for the condition tested here, especially the prediction from the AASHTO approach.
- The CarboShear-L stirrups were relatively easy to install in laboratory conditions and the same could be expected for field conditions.

- During cyclic loading, the CarboShear-L stirrups contributed significantly to control the width of the existing shear cracks.

    1. Without CarboShear-L stirrups, the shear crack widths in test T-Beam 3W continued to increase under cyclic loading. With CarboShear-L stirrups, the crack widths in test T-Beam 3S did not increase when subjected to the same cyclic loading.

    2. On average, the CarboShear-L stirrups produced an 87% decrease in the growth of residual crack width per loading cycle.

    3. During the last three load cycles, the shear retrofit produced a 26% decrease in the net crack opening.

- The CarboShear-L stirrup retrofit system also increased the beam stiffness and reduced beam deflections.
- Cementitious filler blocks bonded into the recessed web section were effective at transferring shear in the beam web to the CarboShear-L stirrups.
- The fiber reinforced cementitious composite (FRCC) filler blocks used on the front of the web performed better than the concrete filler blocks on the back of the web. In place of single isolated cracks in the concrete filler blocks, numerous smaller cracks formed in the FRCC blocks.
- Anchorage of the CarboShear-L stirrups at the top of the beam by epoxy grouting into a slot in the top slab was effective at preventing anchorage slip even when the stirrup had fully delaminated from the web of the beam.

- Anchorage provided by the bottom leg of the CarboShear-L stirrups bonded to the bottom of the beam was effective even when the vertical leg of the stirrup had completely debonded from the face of the web.
- Repair of the existing shear cracks through epoxy injection would likely improve the beam service load performance, but did not appear to be necessary to ensure adequate performance of the CarboShear-L stirrup retrofit.
- The CarboShear-L stirrups prevented the shear failure observed in the control test, T-Beam 3C, and maintained their integrity until flexural failure of the beam. The ultimate shear capacity of the retrofit section could not be determined because the T-Beam failed in flexure upon delamination of the Carbodur strips bonded to the soffit of the beam. Further tests are planned to determine the ultimate shear strength provided by the CarboShear-L shear retrofit system.

9.2.2 Evaluation of the Instrumentation systems

- Four 4-inch long electrical resistance stain gages were used to monitor the shear in the shear span of T-Beam 3C during initial loading. This system provided an acceptable estimate of the applied shear prior to cracking of the beam. With suitable calibration, this system could be used on uncracked bridge girders in the field as a means of monitoring the shear load applied by bridge traffic.
- The crack extensometers (Vibrating Wire Crackmeter and Electrical Crack Gages) provided consistent and stable output throughout the cyclic loading and monotonic loading to failure. The crack gages can provide output at high frequency while the VW Crackmeter can only be monitored once per second. Both types of crack extensometer can be used to monitor crack widths in field conditions.

- The electrical resistance strain gages bonded to the surface of the CarboShear-L stirrups during testing of T-Beam 3S provided consistent strain readings up to 3500 microstrain without damage. The strain gage output was effective for detecting and monitoring delamination of the CarboShear-L stirrups from the concrete substrate.
- The LVDTs bonded to the top end of the CarboShear-L stirrups confirmed that there was no anchorage slip between the CFRP stirrup and the concrete top slab.

9.3 Recommendations

- Based on the results of this study and prior research outlined in the literature review, CarboShear-L stirrups are recommended for retrofit of the AASHTO girders on the Salt Lake Boulevard Bridge. Fiber Reinforced Cementitious Composite is recommended for the web filler blocks.
- Further laboratory testing should be performed on full-scale AASHTO bridge girder with CarboShear-L stirrups and FRCC filler blocks applied over existing shear cracks to verify performance of the full-scale retrofit. Tests should be performed with and without epoxy injection of the existing shear cracks to evaluate any contribution of epoxy injection.

10 REFERENCE

AASHTO (1999) "LRFD Bridge Design Specifications," American Association of State Highway and Transportation Officials, Washington, D.C.

ACI (1984) "State of the Art Report on High Strength Concrete", Report of ACI Committee 363, ACI Journal Vol. 81, No. 4 pp. 364-411.

ACI 318 (2002) "Building Code Requirements for Structural Concrete (ACI 318-02) and Commentary, (ACI 318R-02), " American Concrete Institute, Farmington Hills, MI.

ACI 440 (2002) "Guide for the Design and Construction of Externally Bonded FRP Systems for Strengthening Concrete Structures (ACI 440.2R-02), " Reported by ACI Committee 440.

Agapay, Alison A. and Robertson, Ian N. (2003) "Test of Prestressed Concrete T-Beams Retrofitted for Shear and Flexure Using Carbon Fiber Reinforced Polymers", Research Report UHM/CEE/August 2003, pp. 245.

Al-Sulaimani, G. J., Sharif, A., Basunbul, I. A., Baluch, M. H., and Ghaleb, B. N. (1994) "Shear Repair for Reinforced Concrete by Fiberglass Plate Bonding", *ACI Structural Journal Vol.91 No.4* July-August 1994, pp. 458-463.

Altin, S., Tankut, T., Anil, ö., Demirel, Y (2003). "Response of Reinforced Concrete beams with Camps Applied Externally: An Experimental Study", *Engineering Structures* July, 2003 Vol. 25, pp. 1217-1229.

Basler, M., White, D. and Desroches, M. (2003) "Shear Strengthening With Bonded CFRP L-Shaped Plates", *SP-215, Field Applications of FRP Reinforcement: Case Studies*, Editor Sami Rizkalla and Antonio Nanni, American Concrete Institute, Aug. 2003, pp. 373-384.

Chaallal, O., Nollet, M. J., and Perraton, D. (1998) "Shear Strengthening of RC Beams by Externally Bonded Side CFRP Strips", *Journal of Composites for Construction* May, 1998 Vol.2 No.2, pp. 111-113.

Chaallal, O., Shahawy, M. and Hassan, M. (2002) "Performance of Reinforced Concrete T-Girders Strengthened in Shear with Carbon Fiber-Reinforced Polymic Fabric", *ACI Structural Journal Vol.99 No.3* May-June 2002, pp. 335-343.

Czaderski, C. (2002) "Shear Strengthening with Prefabricated CFRP L-Shaped Plates", *IABSE Symposium Melbourne.*

EMPA (1998) test reports 169219E/1 and 169219E/2 "Testing of CFRP Shear Plates on Reinforced Concrete T-beams", Dübendorf, Switzerland.

Hutchinson, R. and Rizkalla, S. H. (1999) "Shear Strengthening of AASHTO Bridge Girders Using Carbon Fiber Reinforced Polymer Sheets", *SP-188, Fiber Reinforced Polymer Reinforcements for Reinforced Concrete*, Editors: C.W.Dolan, S.H.Rizkalla, and A.Nanni, American Concrete Institute, pp. 945-958.

Hutchinson, R., Tadros, G., Kroman, J. and Rizkalla, S. (2003) "Use of Externally Bonded FRP Systems for Rehabilitation of Bridges in Western Canada", *SP-215, Field Applications of FRP Reinforcement: Case Studies,* Editor Sami Rizkalla and Antonio Nanni, American Concrete Institute, Aug. 2003, pp. 239-247.

KAI Hawaii (2003), "Feasibility Study Bridge Rehabilitation at Various Locations (Salt Lake Boulevard over Halawa Stream)", company report, KAI Hawaii, Honolulu.

Khalifa, A., Tumialan, G., Nanni, A., and Belarbi, A. (1999) "Shear Strengthening of Continuous Reinforced Concrete Beams Using Externally Bonded Carbon Fiber Reinforced Polymer Sheet", *SP-188, Fiber Reinforced Polymer Reinforcements for Reinforced Concrete*, Editors: C.W.Dolan, S.H.Rizkalla, and A.Nanni, American Concrete Institute, pp. 995-1008.

Nakashima, L (2003) "Evaluation of ACI 440 Design for FRP Repair and Retrofit of Concrete Beams", M.S. Thesis, Dept. of Civil and Environmental Engineering, University of Hawaii, pp. 70.

Robertson, I.N., Agapay, A.A. and Nakashima, L.M. (2003) "Field Retrofit of Prestressed Concrete T-Beam Using CFRP", *SP-215, Field Applications of FRP Reinforcement: Case Studies,* Editor Sami Rizkalla and Antonio Nanni, American Concrete Institute, Aug. 2003, pp. 335-348.

Schuman, P., and Karbhari, V. M. (2003) "A Study On Mechanical Anchorage For Shear Rehabilitation of RC Structures", *Proceedings of the fib 2003 Symposium* Athens, Greece May 6-8, pp. 378-389.

Sheikh, S. A., DeRose, D., and Mardukhi, J. (2002) "Retrofitting of Concrete Structures for Shear and Flexure with Fiber-Reinforced Polymers", *ACI Structural Journal Vol.99 No.4* July-August 2002, pp. 451-459.

Sika Corporation (2002), "Shear Strengthening, Sika CarboDur Composite Systems", Sika AG, Switzerland.

Triantafillou, T. C. (1998) "Shear Strengthening of Reinforced Concrete Beams Using Epoxy-Bonded FRP Composites", *ACI Structural Journal Vol.95 No 2* March-April 1998 pp. 107-115.

APPENDIX

THEORETICAL BEAM SHEAR STRENGTHS

This Appendix presents shear strength predictions for the control T-Beam 3 without shear retrofit and for the retrofitted T-Beam 3. It also includes a prediction for the short-term (instantaneous) load-deflection relationship for the beam.

Notation

A_f	=	area of Carbodur Strip used for flexural retrofit
A_c	=	area of concrete on flexural tension side of the beam
A_{cp}	=	area of pre-cast prestressed concrete section
A_{cc}	=	area of composite section
$A_{fv} = 2nt_f w_f$	=	area of CarboShear-L stirrups within spacing s
$A_{No.3\ strand}$	=	area of 3/8" diameter steel reinforcing bar
A_{ps}	=	total area of prestressed strands
A_s	=	area of nonprestressed tension reinforcement
A'_s	=	area of nonprestressed compression reinforcement
$a = \beta_1 c$	=	depth of equivalent rectangular stress block
b_{eff}	=	effective flange width
b_f	=	width of the compression flange
b_v	=	effective web width
b_w (b)	=	width of the web of the T-Beam
c	=	depth of the neutral axis
cgs_c	=	center of gravity of the prestressing tendons at midspan
cgs_e	=	center of gravity of the prestressing tendons at the beam end
cgs_s	=	center of gravity of the prestressing tendons at shear span support
d_e	=	effective depth (= d_p if no mild steel is used)
d_f	=	depth of FRP shear reinforcement as defined by ACI 440
d_p	=	centroidal depth of prestressed strands measured from top of beam
d_v	=	effective shear depth (= $d_p - a/2$)
e	=	eccentricity of the prestressed tendons
e_c	=	eccentricity of the prestressed tendons at the center of the beam
e_e	=	eccentricity of the prestressed tendons at the end of the beam
e_s	=	eccentricity of the prestressed tendons at beam shear span support
E_{cs}	=	modulus of elasticity of the concrete slab
E_f	=	tensile modulus of elasticity of CFRP materials
E_{cp}	=	modulus of elasticity of prestressed concrete
E_{ps}	=	modulus of elasticity of prestressed tendons

E_s	=	modulus of elasticity of non-prestressed reinforcing steel
f_c	=	compressive strength for the pre-cast concrete T-Beam
f_{cs}	=	compressive strength for the top slab concrete
f_{ce}	=	stress due to prestress at tension fiber
f_d	=	stress due to un-factored dead load at tension fiber
f_{fe}	=	effective stress in the CFRP; stress level attained at section failure
f_{fu}	=	ultimate tensile strength of CFRP
f_{pc}	=	compressive stress in concrete at centroid of composite section
f_{pe}	=	effective prestressing stress after losses
f_{pi}	=	initial prestressing stress before losses
f_{po}	=	stress in the prestressing tendons at jacking (=0.70f_{pu}, assumed)
f_{pu}	=	ultimate strength of prestressing tendons
f_{py}	=	specified yield strength of prestressing tendons (=0.90f_{pu}, assumed)
f_r	=	modulus of rupture
f_y	=	yield strength of non-prestressed reinforcement
F_ε	=	adjustment factor when ε_x is negative
h (i.e. h_c)	=	overall thickness of member
h_f	=	thickness of the top slab
I_c	=	moment of inertia of composite section
I_{cr}	=	moment of inertia of the cracked section
I_e	=	effective moment of inertia
I_p	=	moment of inertia of pre-cast prestressed beam section
L	=	member span length
M_a	=	maximum service unfactored live load moment
M_{cr}	=	cracking moment of composite section
M_d	=	moment at section due to un-factored dead load
$M_{\max}$	=	maximum factored moment at section due to external loads
M_u	=	factored moment due to external load
n	=	number of plies of CFRP reinforcement
n_c (n_f, n_p)	=	modular ratio of elasticity
N_u	=	factored axial load normal to cross section occurring simultaneously with V_u
P (P_l)	=	externally applied load
P_{cr}	=	cracking load
P_e	=	effective prestressing force of the prestressed tendons
P_u	=	maximum applied external load
s	=	shear stirrup spacing
r	=	radius of gyration of cross section of a compression member
s_f	=	CarboShear-L stirrup spacing

$S_{bc} = \frac{I_c}{y_{bc}}$	=	bottom section modulus of the composite section
$S_{bp} = \frac{I_p}{y_b}$	=	bottom section modulus of the prestressed beam
$S_{tc} = \frac{I_c}{y_{tc}}$	=	top section modulus of the composite section
$S_{tp} = \frac{I_p}{y_t}$	=	top section modulus of the prestressed beam
t_f	=	nominal thickness of one ply of CFRP material
V_c	=	nominal shear strength provided by concrete
V_{ci}	=	nominal shear strength provided by concrete when diagonal cracking results from combined shear and moment
V_{cw}	=	nominal shear strength provided by concrete when diagonal cracking results from excessive principal tensile stress in the web
V_d	=	shear force at section due to un-factored dead load (self-weight of pre-cast and topping)
V_f	=	nominal shear strength provided by CFRP materials
V_i	=	factored shear force at section due to externally applied loads occurring with $M_{\max}$
V_n	=	nominal shear capacity
V_p	=	vertical component of effective prestress at section
V_s	=	nominal shear strength provided by steel stirrups
V_u	=	factored shear force at section
w_d	=	self-weight of prestressed beam and concrete slab
w_f	=	width of the CarboShear-L stirrups
w_u	=	factored load per unit length of the member
x	=	distance from the beam support
y	=	distance between centroid of pre-cast and composite sections
y_b	=	distance from the centroid of a prestressed beam section to the bottom of the prestressed beam section
y_{bc}	=	distance from the centroid of a composite prestressed beam section to the bottom of the composite prestressed beam section
y_t	=	distance from the centroid of a prestressed beam section to the top of the prestressed beam section
y_{tc}	=	distance from the centroid of a composite prestressed beam section to the top of the composite prestressed beam section
β	=	adjusted value used in AASHTO
β_1	=	ratio of the depth of the equivalent rectangular stress block to the

		depth of the neutral axis
δ	=	deflection under the load point
ε_{fe}	=	effective strain level in CFRP reinforcement; strain level attained in section at failure
ϕ	=	strength reduction factor
ε_x	=	strain in the tensile reinforcement
ν	=	factored shear stress
θ	=	variable angle of crack chosen by trial and adjustment in AASHTO
ψ	=	angle between the inclined tendon and the horizontal

Shear Strength of T-Beam 3 (without shear retrofit)

The original shear capacity of the T-Beam (left end of T-Beam 3) is predicted by using the AASHTO "LRFD Bridge Design Specifications" (AASHTO, 1999), as well as by using the ACI 318-02 "Building Code Requirement for Structural Concrete" (ACI318, 2002).

The T-Beam was simply supported on an 18 feet span with a single line load applied at 4.5 ft from the left support. Based on the span dimensions, the total load applied to the beam was transferred to the supports in the ratio 3 to 1. The left span (test span) therefore resisted three fourths of the total load applied to the beam.

The T-Beam was prestressed with ten 3/8" diameter seven-wire stress relieved strands. The existing internal steel stirrups were 2-leg #3 stirrups at approximately 12" spacing. Figure A.1 shows the T-Beam layout and geometrical dimensions for the original shear capacity calculation.

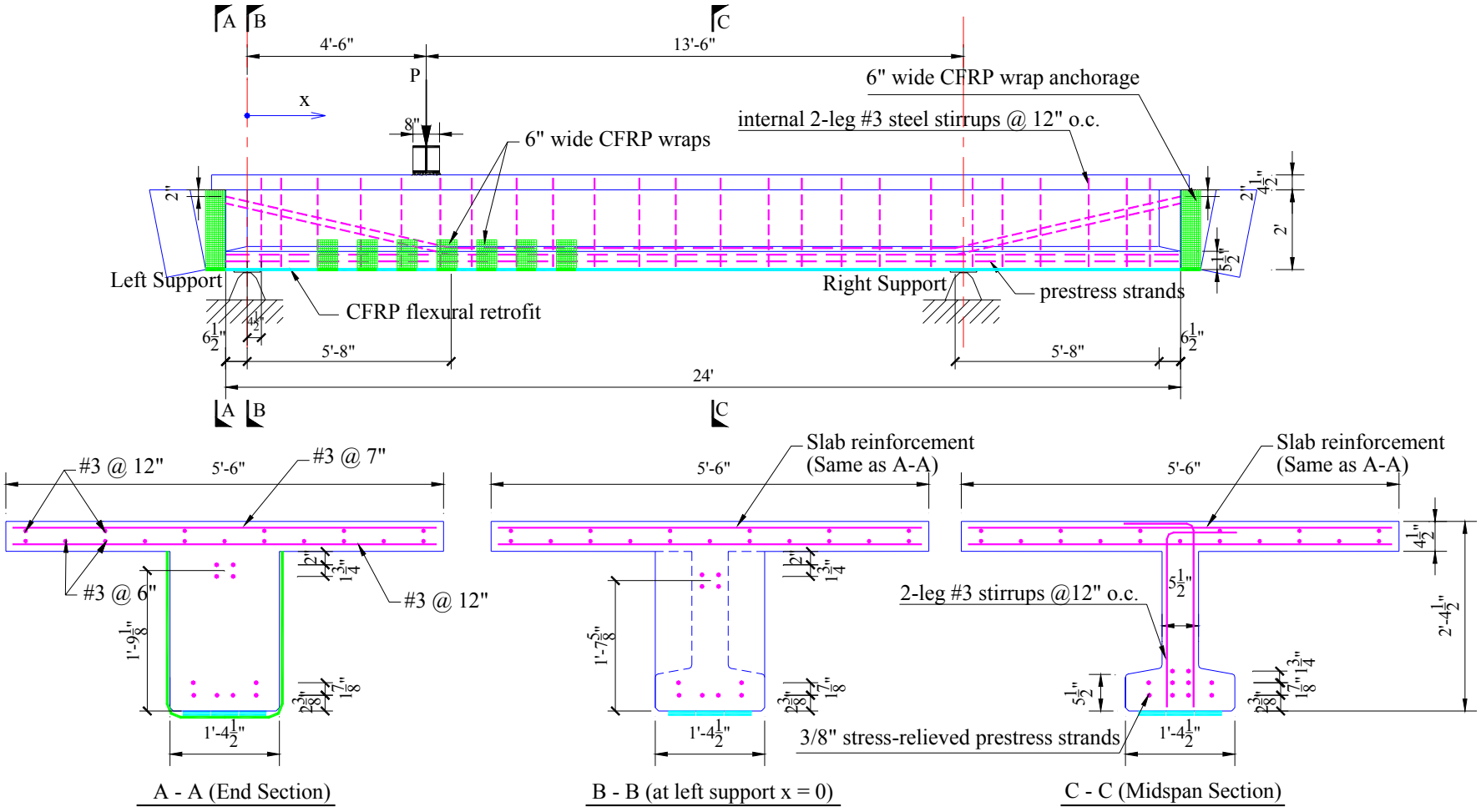

Figure A.1: T-Beam 3 layout for the control shear strength calculation

Using the AASHTO "LRFD Bridge Design Specifications" to Calculate V_n

Based on the AASHTO "LRFD bridge design specifications", V_n, the nominal shear resistance of the prestressed beam, is

$$V_{n\_AASHTO}(x) = V_p(x) + V_c(x) + V_s(x)$$

where: x = distance from the left hand end of the beam, as shown in Figure A.2

V_p = nominal shear strength provided by vertical component of the harped longitudinal tendons

$$V_p = P_e \cdot \sin\psi$$

V_c = nominal shear strength provided by the tensile stresses in the concrete

$$V_c(x) = 0.0316\beta(x) \cdot \sqrt{f_c' \cdot 10^{-3}} \cdot b_v \cdot d_v(x)$$

V_s = nominal shear strength provided by the tensile stresses in the web reinforcement

$$V_s(x) = \frac{A_v \cdot f_y \cdot d_v(x) \cdot Cot\,\theta(x)}{s}$$

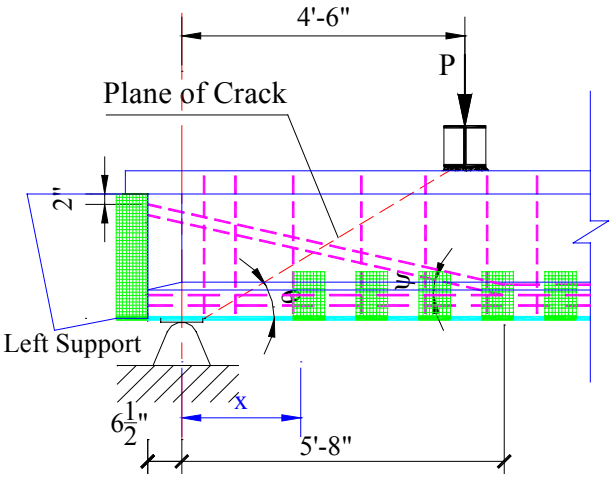

Figure A.2: T-Beam Parameters for AASHTO

In order to determine the nominal shear resistance of the prestressed T-Beam, the values β and θ are needed to compute V_c and V_s. For prestressed concrete sections, AASHTO assumes a shear crack with inclination θ to the horizontal. The crack inclination θ will change along the beam span. With the assumed θ, the strain in the tensile reinforcement, ε_x, can be obtained using

$$\varepsilon_x(x) = \frac{\frac{M_u(x)}{d_v(x)} + 0.5 \cdot N_u + 0.5 \cdot V_u(x) \cdot Cot\theta(x) - A_{ps} \cdot f_{po}}{2 \cdot \left(E_s \cdot A_s + E_{ps} \cdot A_{ps} + E_f \cdot A_f\right)}$$

With the value of ε_x, AASHTO Table 15.9 is used to check whether the angle θ is close to the one assumed in the first trial. If so, then the β value obtained from AASHTO Table 15.9 is used to compute V_c and V_s; if not, the procedure is repeated until the predicted θ is very close to the value obtained from Table 15.9. The procedure to calculate V_n using AASHTO "LRFD Bridge Design Specifications" is presented below. The calculation was performed with the help of *Mathcad 2001*.

T- Beam Section Properties :

Prestressed section:

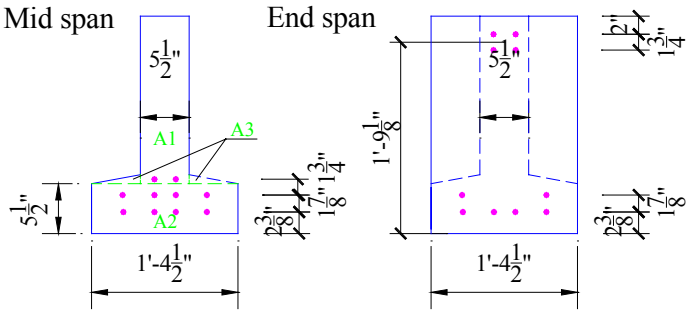

$A_{No.3strand} := 0.08$ $A_{ps} := 10 \cdot A_{No.3strand}$ $A_{ps} = 0.8\ in^2$

$A_1 := 5.5 \cdot (17 + 1.5)$ $A_2 := 16.5 \cdot 5.5$ $A_3 := \frac{1}{2} \cdot 5.5 \cdot 1.5 \cdot 2$

$A_{cp} := A_1 + A_2 + A_3$ $A_{cp} = 200.75\ in^2$

$b_w := 5.5 \quad in \qquad h := 24 \quad in \qquad L := 24 \quad ft$: L is the total length of the beam.
The T-Beam3C span is 18 ft

$$y_b := \frac{A_1 \cdot \left(\frac{17 + 1.5}{2} + 5.5\right) + A_2 \cdot \frac{5.5}{2} + A_3 \cdot \left(\frac{1.5}{3} + 5.5\right)}{A_{cp}} \qquad y_b = 9 \quad in \qquad y_t := h - y_b \qquad y_t = 15 \quad in$$

Mid span: $cgs_c := \frac{4 \cdot 0.08 \cdot 2.375 + 4 \cdot 0.08 \cdot 4.25 + 2 \cdot 0.08 \cdot 6}{10 \cdot 0.08}$ $cgs_c = 3.85$ in : from the bottom

$e_c := y_b - cgs_c \qquad e_c = 5.12$ in : Eccentricity of prestress at center

End span: $cgs_e := \frac{4 \cdot 0.08 \cdot 2.375 + 2 \cdot 0.08 \cdot 4.25 + 4 \cdot 0.08 \cdot 21.125}{10 \cdot 0.08}$ $cgs_e = 10.25$ in : from the bottom

$e_e := y_b - cgs_e \qquad e_e = -1.28$ in : Eccentricity of prestress at end

at Left support (x = 0):

$cgs_s := \frac{4 \cdot 0.08 \cdot 2.375 + 2 \cdot 0.08 \cdot 4.25 + 4 \cdot 0.08 \cdot 19.625}{10 \cdot 0.08}$ $cgs_s = 9.65$ in : from the bottom

$e_s := y_b - cgs_s \qquad e_s = -0.68$ in : Eccentricity of prestress at left support

$$I_p := \frac{5.5 \cdot (17 + 1.5)^3}{12} + A_1 \cdot (y_b - 14.75)^2 + \frac{16.5 \cdot 5.5^3}{12} + A_2 \cdot \left(y_b - \frac{5.5}{2}\right)^2 + 2 \cdot \frac{5.5 \cdot 1.5^3}{36} + A_3 \cdot (y_b - 6)^2$$

$I_p = 10115 \quad in^4 \qquad S_{bp} := \frac{I_p}{y_b} \qquad S_{bp} = 1128.16 \quad in^3 \qquad S_{tp} := \frac{I_p}{y_t} \qquad S_{tp} = 672.79 \quad in^3$

$f_c := 8405 \quad psi \qquad f_{pu} := 250000 \quad psi \qquad f_{pi} := 187500 \quad psi \qquad f_{pe} := 150000 \quad psi$

$f_{py} := 0.9 \cdot f_{pu} \qquad f_{py} = 225000 \quad psi \qquad P_e := f_{pe} \cdot A_{ps} \qquad P_e = 120000 \quad lb$

$E_{cp} := 4667$ ksi : precast concrete $\qquad E_{ps} := 28500 \quad ksi \qquad f_y := 50900$ psi : for steel stirrups

Composite section:

$b_f := 66 \quad in \qquad h_c := 28.5 \quad in \qquad h_f := 4.5 \quad in$

$E_{cs} := 3104$ ksi : Top slab concrete $\qquad f_{ct} := 5114$ psi : topping slab

$b_{trans} := \frac{\sqrt{f_{ct}}}{\sqrt{f_c}} \cdot b_f \qquad b_{trans} = 51.48 \quad in \qquad A_{cc} := A_{cp} + b_{trans} \cdot h_f \qquad A_{cc} = 432 \quad in^2$

$y_{bc} := \frac{1}{A_{cc}} \cdot (A_{cp} \cdot y_b + b_{trans} \cdot h_f \cdot 26.25) \qquad y_{bc} = 18.2 \quad in \qquad y_{tc} := h_c - y_{bc} \qquad y_{tc} = 10.3 \quad in$

$$I_c := I_p + A_{cp} \cdot (y_b - y_{bc})^2 + \frac{b_{trans} \cdot h_f^3}{12} + b_{trans} \cdot h_f \cdot (26.25 - y_{bc})^2 \qquad I_c = 42636.44 \quad in^4$$

$S_{bc} := \frac{I_c}{y_{bc}} \qquad S_{bc} = 2339.34 \quad in^3 \qquad S_{tc} := \frac{I_c}{y_{tc}} \qquad S_{tc} = 4149.86 \quad in^3 \qquad n_c := \frac{E_{cs}}{E_{cp}} \qquad n_c = 0.67$

The shear capacity profile for the beam is developed by computing V_c, V_p and V_s at 0.5 ft intervals from the left support to the right support.

Set $x := 0, 0.5 .. 18 \quad ft$

1. Compute V_u and M_u:

unit weight of concrete : 0.15 kip/ft^3

Normal weight concrete beam self weight plus top slab self weight:

$$W_d := \frac{\left(A_{cp} + b_f \cdot h_f\right)}{144} \cdot 0.15 \qquad W_d = 0.52 \quad klf \qquad W_u := 1.2 \cdot W_d \qquad W_u = 0.62 \quad klf$$

$$W := W_u \cdot L \qquad W = 14.93 \quad kips$$

The load point is 4.5 ft from the left end support, and 13.5 ft from the right end support.

$$L_1 := 4.5 \quad ft \qquad L_2 := 13.5 \quad ft$$

From T-Beam 3 control test, the maximum load applied was 198 kips, so: $P_u := 198 \quad kips$

Width of the steel spreader beam is 1 ft): $p_u := \frac{P_u}{1} \qquad p_u = 198 \quad klf$

The reactions at the right and left supports are :

$$V_R := \frac{P_u \cdot L_1 + W_u \cdot \frac{L^2}{2}}{L_1 + L_2} \qquad V_R = 59.46 \quad kips$$

$$V_L := P_u + W - V_R \qquad V_L = 153.48 \quad kips$$

Thus,

$$V_u(x) := \begin{cases} V_L - W_u \cdot x & \text{if } 0 \le x \le 4 \\ \left[V_L - W_u \cdot x - p_u \cdot (x - 4)\right] & \text{if } 4 \le x \le 5 \\ \left[-\left[V_R - W_u \cdot (24 - x)\right]\right] & \text{if } 5 \le x \le 18 \end{cases} \quad kips$$

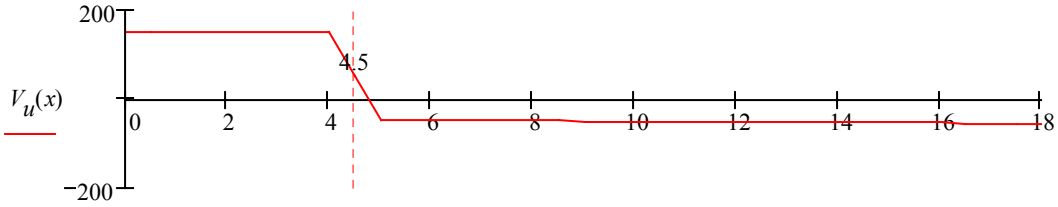

$$M_u(x) := \begin{cases} \left(V_L \cdot x - \frac{W_u \cdot x^2}{2}\right) & \text{if } 0 \le x \le 4 \\ \left[V_L \cdot x - \frac{W_u \cdot x^2}{2} - p_u \cdot \frac{(x - 4)^2}{2}\right] & \text{if } 4 \le x \le 5 \\ \left[V_R \cdot (18 - x) - \frac{W_u \cdot (24 - x)^2}{2}\right] & \text{if } 5 \le x \le 18 \end{cases} \quad kips - ft$$

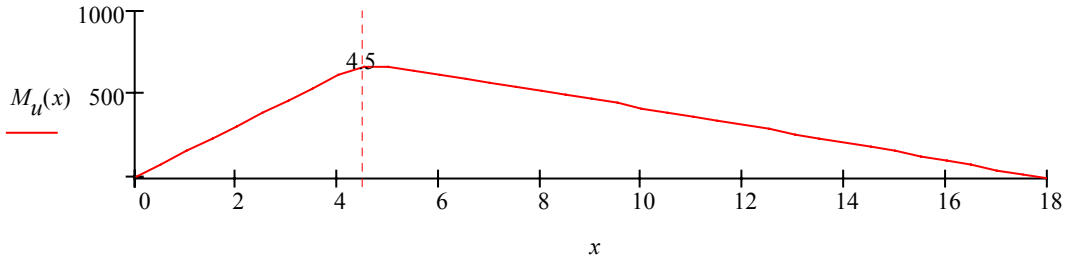

2. Compute V_p: (4 strands harped at section x = 5.67 ft from the support)

$$\sin\psi := \frac{cgs_e - cgs_c}{68} \qquad \sin\psi = 0.09$$

$$V_p(x) := \begin{cases} \left(P_e \cdot \sin\psi \cdot 10^{-3}\right) & \text{if } x \le 5.67 \\ 0 & \text{if } x > 5.67 \end{cases} \quad kips$$

3. Compute V_c:

i) ε_x:

Known: $A_s := 0$ $\quad E_s := 29000 \ ksi$ $\quad f_{po} := 0.7 \cdot f_{pu}$ $\quad f_{po} = 175000 \ psi$ $\quad N_u := 0$

$e_c = 5.12 \ in$ $\quad e_s = -0.68 \ in$

$cgs_c = 3.85 \ in$ $\quad cgs_s = 9.65$ $\quad h_c = 28.5 \ in$

Then, eccentricity along the T-Beam :

$$e(x) := \begin{cases} \left(e_s + \frac{e_c - e_s}{5.67} \cdot x\right) & \text{if } x < 5.67 \\ 5.12 & \text{if } x \ge 5.67 \end{cases} \quad in$$

d_p along the T-Beam:

$$d_p(x) := \begin{cases} \left(\frac{24.65 - 18.85}{5.67}\right) \cdot x + 18.64 & \text{if } x < 5.67 \\ 24.65 & \text{if } x \ge 5.67 \end{cases} \quad in$$

No mild steel is used, so $d_e = d_p$, so:

$d_e(x) := d_p(x)$

Other parameters:

$$k := 2 \cdot \left(1.04 - \frac{f_{py}}{f_{pu}}\right) \qquad k = 0.28 \qquad \beta_1 := 0.85 \qquad b := b_f \qquad b = 66 \ in \qquad f_y' := f_y \qquad A_s' := 0$$

Using 6 carbodur strips to retrofit the beam for flexure, then :

$A_f := 0.5642$ $\quad A_f = 1.13 \ in^2$

$f_{fe} := 177000 \ psi$ $\quad E_f := 23900 \ ksi$: refer to Apapay and Robertson (2003)

$$c(x) := \frac{A_{ps} \cdot f_{pu} + A_f \cdot f_{fe}}{0.85 \cdot f_c \cdot \beta_1 \cdot b + k \cdot A_{ps} \cdot \frac{f_{pu}}{d_p(x)}} \qquad a(x) := \beta_1 \cdot c(x)$$

$$d_v(x) := max\left[\left(d_e(x) - \frac{a(x)}{2}\right), 0.9 \cdot d_e(x), 0.72 \cdot h_c\right] \quad \phi := 0.90 \text{ for shear} \quad b_v := b_w \quad b_v = 5.5 \ in$$

Shear Stress: $$v(x) := \frac{\left|V_u(x)\right| - \phi V_p(x)}{\phi b_v \cdot d_v(x)}$$

Assume θ :

$$\theta(x) := \begin{cases} 27 & \text{if } x = 0 \\ 30.5 & \text{if } 0 < x \le 0.5 \\ 33.8 & \text{if } 0.5 < x \le 1 \\ 36.8 & \text{if } 1 < x \le 1.5 \\ 39.0 & \text{if } 1.5 < x \le 2 \\ 41 & \text{if } 2 < x \le 2.5 \\ 42.7 & \text{if } 2.5 < x \le 4.0 \\ 43.9 & \text{if } 4.0 < x \le 4.5 \\ 43.9 & \text{if } 4.5 < x \le 5 \\ 43.9 & \text{if } 5 < x \le 5.5 \\ 43.5 & \text{if } 5.5 < x \le 6 \\ 42.7 & \text{if } 6 < x \le 6.5 \\ 42.2 & \text{if } 6.5 < x \le 7 \\ 41.4 & \text{if } 7 < x \le 7.5 \\ 40.5 & \text{if } 7.5 < x \le 8 \\ 39.7 & \text{if } 8 < x \le 8.5 \\ 38.6 & \text{if } 8.5 < x \le 9 \\ 37.5 & \text{if } 9 < x \le 9.5 \\ 36.5 & \text{if } 9.5 < x \le 10 \\ 35.5 & \text{if } 10 < x \le 10.5 \\ 34.5 & \text{if } 10.5 < x \le 11 \\ 33.4 & \text{if } 11 < x \le 11.5 \\ 32 & \text{if } 11.5 < x \le 12 \\ 30.2 & \text{if } 12 < x \le 12.5 \\ 29 & \text{if } 12.5 < x \le 13 \\ 27 & \text{if } 13 < x \le 13.5 \\ 26 & \text{if } 13.5 < x \le 14 \\ 24.4 & \text{if } 14 < x \le 14.5 \\ 22.5 & \text{if } 14.5 < x \le 15 \\ 21.8 & \text{if } 15 < x \le 16 \\ 21.3 & \text{if } 16 < x \le 17 \\ 21 & \text{if } 17 < x \le 18 \end{cases}$$

$$Cot\,\theta(x) := \frac{1}{tan\left(\frac{\theta(x) \cdot \pi}{180}\right)}$$

$$\varepsilon_x(x) := \frac{\frac{M_u(x) \cdot 12}{d_v(x)} + 0.5 N_u + 0.5 \cdot \left|V_u(x)\right| \cdot Cot\,\theta(x) - A_{ps} \cdot f_{po} \cdot 10^{-3}}{2 \cdot \left(E_s \cdot A_s + E_{ps} \cdot A_{ps} + E_f \cdot A_f\right)}$$

If the value of strain ε_x at the level of the reinforcement centroid is negative, its value has to be adjusted by the factor F_ε

$$A_c := A_{cp} - b_w \cdot \left(h - \frac{h_c}{2}\right) \qquad A_c = 147.13 \ in^2$$

$$F_\varepsilon := \frac{E_s \cdot A_s + E_{ps} \cdot A_{ps} + E_f \cdot A_f}{E_{cs} \cdot A_c + E_s \cdot A_s + E_{ps} \cdot A_{ps} + E_f \cdot A_f} \qquad F_\varepsilon = 0.098$$

When x>=15.5, ε_x is negative, need adjustment:

Adjusted ε_x: $$\varepsilon_x(x) := \begin{cases} \varepsilon_x(x) & \text{if } x < 15.5 \\ \varepsilon_x(x) \cdot F_\varepsilon & \text{if } x \ge 15.5 \end{cases}$$

Also, control $\varepsilon_x(x)$ <= 0.002:

$$\varepsilon_x(x) := \begin{cases} \varepsilon_x(x) & \text{if } \varepsilon_x(x) \le 0.002 \\ 0.002 & \text{if } \varepsilon_x(x) > 0.002 \end{cases}$$

ii) Web shear strength, V_c, from $\theta - \beta$ analysis:

dis. to left (ft) $x =$	$V_u(x) =$ (kips)	$M_u(x) =$ (kips-ft)	$d_p(x) =$ (in)	$c(x) =$ (in)	$\theta(x) =$ (o)	ratio $\nu/f_c' = \frac{\nu(x)}{f_c \cdot 10^{-3}} =$	$\varepsilon_x(x) \cdot 1000 =$
0	153.48	0	18.64	0.99	27	0.168	0.11
0.5	153.17	76.66	19.15	0.99	30.5	0.168	0.35
1	152.86	153.17	19.66	0.99	33.8	0.167	0.64
1.5	152.54	229.52	20.17	0.99	36.8	0.167	0.97
2	152.23	305.71	20.69	0.99	39	0.166	1.33
2.5	151.92	381.75	21.2	0.99	41	0.164	1.69
3	151.61	457.63	21.71	0.99	42.7	0.16	2
3.5	151.3	533.36	22.22	0.99	42.7	0.156	2
4	150.99	608.93	22.73	0.99	42.7	0.152	2
4.5	51.68	659.6	23.24	0.99	43.9	0.044	2
5	-47.63	660.61	23.75	0.99	43.9	0.039	2
5.5	-47.94	636.72	24.27	0.99	43.9	0.038	2
6	-48.26	612.67	24.65	0.99	43.5	0.048	1.9
6.5	-48.57	588.46	24.65	0.99	42.7	0.048	1.79
7	-48.88	564.1	24.65	0.99	42.2	0.048	1.67
7.5	-49.19	539.58	24.65	0.99	41.4	0.049	1.56
8	-49.5	514.91	24.65	0.99	40.5	0.049	1.45
8.5	-49.81	490.08	24.65	0.99	39.7	0.049	1.33
9	-50.12	465.1	24.65	0.99	38.6	0.05	1.22
9.5	-50.43	439.96	24.65	0.99	37.5	0.05	1.11
10	-50.74	414.67	24.65	0.99	36.5	0.05	1
10.5	-51.06	389.22	24.65	0.99	35.5	0.051	0.89
11	-51.37	363.61	24.65	0.99	34.5	0.051	0.78
11.5	-51.68	337.85	24.65	0.99	33.4	0.051	0.67
12	-51.99	311.93	24.65	0.99	32	0.052	0.56
12.5	-52.3	285.86	24.65	0.99	30.2	0.052	0.47
13	-52.61	259.63	24.65	0.99	29	0.052	0.36
13.5	-52.92	233.25	24.65	0.99	27	0.053	0.28
14	-53.23	206.71	24.65	0.99	26	0.053	0.17
14.5	-53.54	180.02	24.65	0.99	24.4	0.053	0.08
15	-53.86	153.17	24.65	0.99	22.5	0.053	0.01
15.5	-54.17	126.16	24.65	0.99	21.8	0.054	-0.01
16	-54.48	99	24.65	0.99	21.8	0.054	-0.02
16.5	-54.79	71.68	24.65	0.99	21.3	0.054	-0.03
17	-55.1	44.21	24.65	0.99	21.3	0.055	-0.05
17.5	-55.41	16.58	24.65	0.99	21	0.055	-0.06
18	-55.72	-11.2	24.65	0.99	21	0.055	-0.07

Entering the values of ε_x and v/fc' into AASHTO Table 15.9, verified that the assumed θ values are O.K. Then read β values from the Table as listed on the right :

$$\beta(x) := \begin{cases} 2.55 & \text{if } x = 0 \\ 2.40 & \text{if } 0 < x \le 0.5 \\ 2.23 & \text{if } 0.5 < x \le 1 \\ 2.00 & \text{if } 1 < x \le 1.5 \\ 1.84 & \text{if } 1.5 < x \le 2 \\ 1.68 & \text{if } 2 < x \le 2.5 \\ 1.58 & \text{if } 2.5 < x \le 3 \\ 1.59 & \text{if } 3 < x \le 3.5 \\ 1.60 & \text{if } 3.5 < x \le 4 \\ 1.67 & \text{if } 4.0 < x \le 4.5 \\ 1.67 & \text{if } 4.5 < x \le 5 \\ 1.67 & \text{if } 5 < x \le 5.5 \\ 1.70 & \text{if } 5.5 < x \le 6 \\ 1.78 & \text{if } 6 < x \le 6.5 \\ 1.84 & \text{if } 6.5 < x \le 7 \\ 1.91 & \text{if } 7 < x \le 7.5 \\ 1.97 & \text{if } 7.5 < x \le 8 \\ 2.03 & \text{if } 8 < x \le 8.5 \\ 2.09 & \text{if } 8.5 < x \le 9 \\ 2.15 & \text{if } 9 < x \le 9.5 \\ 2.21 & \text{if } 9.5 < x \le 10 \\ 2.28 & \text{if } 10 < x \le 10.5 \\ 2.34 & \text{if } 10.5 < x \le 11 \\ 2.39 & \text{if } 11 < x \le 11.5 \\ 2.51 & \text{if } 11.5 < x \le 12 \\ 2.57 & \text{if } 12 < x \le 12.5 \\ 2.77 & \text{if } 12.5 < x \le 13 \\ 2.90 & \text{if } 13 < x \le 13.5 \\ 3.11 & \text{if } 13.5 < x \le 14 \\ 3.26 & \text{if } 14 < x \le 14.5 \\ 3.55 & \text{if } 14.5 < x \le 15 \\ 3.82 & \text{if } 15 < x \le 15.5 \\ 3.89 & \text{if } 15.5 < x \le 16 \\ 3.96 & \text{if } 16 < x \le 16.5 \\ 4.03 & \text{if } 16.5 < x \le 17 \\ 4.23 & \text{if } 17 < x \le 17.5 \\ 4.36 & \text{if } 17.5 < x \le 18 \end{cases}$$

Now, find V_c using :

$$V_c(x) := 0.0316\beta(x)\cdot\sqrt{f_c\cdot 10^{-3}}\cdot b_v\cdot d_v(x)$$

Also :

$$V_{c\_AASHTO}(x) := V_c(x) + V_p(x)$$

4. Find V_s:

Stirrup:Two-legs #3 @ 12 in o.c.

$$A_v := 2\cdot 0.11 \qquad A_v = 0.22 \quad in^2 \qquad s := 12 \quad in$$

Then :

$$V_s(x) := \frac{A_v\cdot f_y\cdot 10^{-3}\cdot d_v(x)\cdot Cot\,\theta(x)}{s}$$

Let :

$$V_{s\_AASHTO}(x) := V_s(x)$$

5. Find V_n, based on AASHTO:

$$V_{n\_AASHTO}(x) := V_p(x) + V_c(x) + V_s(x)$$

$$< \quad V_{n2}(x) := 0.25\cdot f_c\cdot 10^{-3}\cdot b_v\cdot d_v(x)$$

Then, use Vn, abandon Vn2:

dis. to left	$d_v(x)$	θ	β(x)	$V_c(x)$	$V_s(x)$	$V_p(x)$	$V_{n\_AASHTO}(x)$
(ft)	(ft)	(o)		(kips)	(kips)	(kips)	(kips)
$x =$	$d_v(x) =$	$\theta(x) =$	$\beta(x) =$	$V_c(x) =$	$V_s(x) =$	$V_p(x) =$	$V_{n\ AASHTO}(x)$
0	20.52	27	2.55	26.37	37.58	11.29	75.24
0.5	20.52	30.5	2.4	24.81	32.51	11.29	68.62
1	20.52	33.8	2.23	23.06	28.6	11.29	62.95
1.5	20.52	36.8	2	20.68	25.6	11.29	57.57
2	20.52	39	1.84	19.02	23.65	11.29	53.97
2.5	20.78	41	1.68	17.59	22.3	11.29	51.18
3	21.29	42.7	1.58	16.95	21.53	11.29	49.77
3.5	21.8	42.7	1.59	17.46	22.04	11.29	50.8
4	22.31	42.7	1.6	17.99	22.56	11.29	51.84
4.5	22.82	43.9	1.67	19.2	22.13	11.29	52.63
5	23.33	43.9	1.67	19.63	22.63	11.29	53.55
5.5	23.84	43.9	1.67	20.06	23.12	11.29	54.48
6	24.23	43.5	1.7	20.75	23.83	0	44.58
6.5	24.23	42.7	1.78	21.73	24.5	0	46.23
7	24.23	42.2	1.84	22.46	24.93	0	47.4
7.5	24.23	41.4	1.91	23.32	25.65	0	48.96
8	24.23	40.5	1.97	24.05	26.47	0	50.52
8.5	24.23	39.7	2.03	24.78	27.23	0	52.02
9	24.23	38.6	2.09	25.51	28.32	0	53.84
9.5	24.23	37.5	2.15	26.25	29.47	0	55.71
10	24.23	36.5	2.21	26.98	30.55	0	57.53
10.5	24.23	35.5	2.28	27.83	31.7	0	59.53
11	24.23	34.5	2.34	28.57	32.9	0	61.46
11.5	24.23	33.4	2.39	29.18	34.29	0	63.47
12	24.23	32	2.51	30.64	36.18	0	66.82
12.5	24.23	30.2	2.57	31.37	38.85	0	70.22
13	24.23	29	2.77	33.82	40.79	0	74.6
13.5	24.23	27	2.9	35.4	44.37	0	79.78
14	24.23	26	3.11	37.97	46.36	0	84.32
14.5	24.23	24.4	3.26	39.8	49.84	0	89.64
15	24.23	22.5	3.55	43.34	54.58	0	97.92
15.5	24.23	21.8	3.82	46.63	56.53	0	103.16
16	24.23	21.8	3.89	47.49	56.53	0	104.02
16.5	24.23	21.3	3.96	48.34	57.99	0	106.33
17	24.23	21.3	4.03	49.2	57.99	0	107.19
17.5	24.23	21	4.23	51.64	58.9	0	110.54
18	24.23	21	4.36	53.23	58.9	0	112.13

Using ACI 318-02 to Calculate V_n

Compared with the AASHTO code, the ACI approach to calculate the shear capacity for beams is simpler and more straightforward, without requiring a trial and adjustment procedure. Based on the ACI 318-02, "Building Code Requirements for Structural Concrete", V_n, the nominal shear resistance of the prestressed beam, is

$$V_{n\_ACI}(x) = V_c(x) + V_s(x)$$

Where: x = distance from the left hand end of the beam, as shown in Figure A.2

V_c = nominal shear strength provided by concrete section

$$V_{c\_ACI}(x) = min\left(V_{cw}(x), V_{ci}(x)\right)$$

V_s = nominal shear strength provided by steel stirrups

$$V_{s\_ACI}(x) = \frac{A_s \cdot f_y \cdot d_p(x)}{s}$$

The concrete contribution, V_c, is the lesser of V_{ci} and V_{cw}. For V_{ci}, the flexure-shear strength, the ACI code gives

$$V_{ci}(x) = 0.6 \cdot \lambda \cdot \sqrt{f_c'} \cdot b_w \cdot d_p(x) + V_d(x) + \frac{V_i(x) \cdot M_{cr}(x)}{M_{max}(x)}$$

For V_{cw}, the web-shear strength, the ACI code gives

$$V_{cw}(x) = \left(3.5\lambda \cdot \sqrt{f_c'} + 0.3 f_{pc}(x)\right) \cdot b_w \cdot d_p(x) + V_p(x)$$

The ACI 318-02, "Building Code Requirements for Structural Concrete" procedure to calculate V_n is presented below. The calculation was performed with the help of *Mathcad 2001*.

The T-Beam section properties, V_u and M_u, were presented in detail earlier in this Appendix. These values will also be used in the ACI 318-02 approach. Similar to the AASHTO approach, the shear capacity profile for the beam was developed by computing V_c and V_s at 0.5 ft intervals from the left support to the right support.

Therefore:

set: $x := 0.5, 1.. 18 \quad ft$

1. Concrete shear capacity based on flexure-shear cracking, Vci

$$d_p(x) := \begin{cases} \left(\frac{24.65 - 18.64}{5.67}\right)\cdot x + 18.64 & if \ x < 5.67 \\ 24.65 & if \ x \geq 5.67 \end{cases}$$

In the ACI code, the d_p is required to be greater than $0.8h_c$:

So, $0.8\cdot h_c = 22.8$ $\qquad d_p(x) := \begin{cases} d_p(x) & if \ d_p(x) \geq 22.8 \\ 22.8 & if \ d_p(x) < 22.8 \end{cases}$

From section 6.2.1

$W_d = 0.52 \quad klf$

$$V_u(x) := \begin{cases} V_L - W_u\cdot x & if \ 0 \leq x \leq 4 \\ \left[V_L - W_u\cdot x - p_u\cdot(x-4)\right] & if \ 4 \leq x \leq 5 \\ \left[-\left[V_R - W_u\cdot(24-x)\right]\right] & if \ 5 \leq x \leq 18 \end{cases} \quad kips$$

factored shear force at section x

For W_d only :

$V_{dL} := 4.16 \quad kips \qquad V_{dR} := 8.32 \quad kips$

Then :

$V_d(x) := V_{dL} - W_d\cdot x$ shear force at x due to un-factored dead load

$V_i(x) := \left|V_u(x)\right| - V_d(x)$ factored shear force at x due to external load

$M_d(x) := V_{dL}\cdot x - \frac{W_d\cdot x^2}{2}$ moment at x due to un-factored dead load

Also :

$$M_u(x) := \begin{cases} \left(V_L \cdot x - \frac{W_u \cdot x^2}{2} \right) & \text{if } 0 \le x \le 4 \\ \left[V_L \cdot x - \frac{W_u \cdot x^2}{2} - p_u \cdot \frac{(x-4)^2}{2} \right] & \text{if } 4 \le x \le 5 \\ \left[V_R \cdot (18-x) - \frac{W_u \cdot (18-x)^2}{2} \right] & \text{if } 5 \le x \le 18 \end{cases} \quad kips - ft$$

factored moment at x due to external load

$M_{max}(x) := M_u(x) - M_d(x)$ Maximum factored moment at section x due to external loads (not including dead load)

Eccentricity along the T-Beam :

$$e(x) := \begin{cases} \left(e_s + \frac{e_c - e_s}{5.67} \cdot x \right) & \text{if } x < 5.67 \\ 5.12 & \text{if } x \ge 5.67 \end{cases} \quad in$$

Therefore :

$f_d(x) := \frac{12000 M_d(x)}{S_{bp}}$ Stress due to unfactored dead load at section x

$f_{ce}(x) := \frac{P_e}{A_{cp}} + \frac{P_e \cdot e(x)}{S_{bp}}$ Stress due to prestress at tension fiber at section x

$M_{cr}(x) := \frac{I_c}{12000\, y_{bc}} \cdot \left(6 \cdot \sqrt{f_c} + f_{ce}(x) - f_d(x) \right)$ Cracking moment

where : $\lambda := 1.0$ normal concrete

In the ACI code, V_{ci} needs to be greater than $1.7\lambda \cdot \sqrt{f_c} \cdot b_w \cdot d_p$

and smaller than $0.5\lambda \cdot \sqrt{f_c} \cdot b_w \cdot d_p$

so:

$$V_{ci}(x) := max\left[\left(\frac{0.6 \cdot \lambda \cdot \sqrt{f_c} \cdot b_w \cdot d_p(x)}{1000} + V_d(x) + \frac{V_i(x) \cdot M_{cr}(x)}{M_{max}(x)} \right), \frac{1.7\lambda \cdot \sqrt{f_c} \cdot b_w \cdot d_p(x)}{1000} \right]$$

$< \quad 0.5\lambda \cdot \sqrt{f_c} \cdot b_w \cdot d_p(x)$ O.K.

The values of V_u, M_u, d_p, V_i, M_{cr}, and V_{ci} along the beam are listed below:

dis.from left	$V_u(x)$	$M_u(x)$	$d_p(x)$	$V_i(x)$	$M_{cr}(x)$	$V_{ci}(x)$
(ft)	(kips)	(kips-ft)	(in)	(kips)	(kips-ft)	(kips)
$x =$	$V_u(x) =$	$M_u(x) =$	$d_p(x) =$	$V_i(x) =$	$M_{cr}(x) =$	$V_{ci}(x) =$
0.5	153.17	76.66	22.8	149.27	216	442.73
1	152.86	153.17	22.8	149.21	222.7	233.16
1.5	152.54	229.52	22.8	149.16	229.66	163.31
2	152.23	305.71	22.8	149.11	236.9	128.39
2.5	151.92	381.75	22.8	149.06	244.4	107.44
3	151.61	457.63	22.8	149.01	252.17	93.47
3.5	151.3	533.36	22.8	148.95	260.21	83.5
4	150.99	608.93	22.88	148.9	268.52	76.04
4.5	51.68	659.6	23.41	49.85	277.09	30.29
5	-47.63	720.34	23.94	46.07	285.94	27.47
5.5	-47.94	694.58	24.47	46.64	295.06	28.96
6	-48.26	668.66	24.65	47.21	297.53	30.01
6.5	-48.57	642.59	24.65	47.78	296.57	30.86
7	-48.88	616.36	24.65	48.35	295.89	31.83
7.5	-49.19	589.98	24.65	48.92	295.47	32.94
8	-49.5	563.44	24.65	49.49	295.33	34.2
8.5	-49.81	536.75	24.65	50.06	295.45	35.65
9	-50.12	509.9	24.65	50.63	295.84	37.3
9.5	-50.43	482.89	24.65	51.2	296.5	39.21
10	-50.74	455.73	24.65	51.77	297.43	41.42
10.5	-51.06	428.41	24.65	52.34	298.62	43.99
11	-51.37	400.94	24.65	52.91	300.09	46.99
11.5	-51.68	373.31	24.65	53.48	301.82	50.52
12	-51.99	345.53	24.65	54.05	303.83	54.72
12.5	-52.3	317.59	24.65	54.62	306.1	59.76
13	-52.61	289.5	24.65	55.19	308.64	65.88
13.5	-52.92	261.25	24.65	55.76	311.45	73.44
14	-53.23	232.84	24.65	56.33	314.53	82.96
14.5	-53.54	204.28	24.65	56.9	317.88	95.24
15	-53.86	175.57	24.65	57.47	321.49	111.58
15.5	-54.17	146.69	24.65	58.04	325.38	134.28
16	-54.48	117.67	24.65	58.61	329.53	167.74
16.5	-54.79	88.48	24.65	59.18	333.95	221.64
17	-55.1	59.14	24.65	59.75	338.64	322.25
17.5	-55.41	29.65	24.65	60.32	343.6	574.45
18	-55.72	0	24.65	60.89	348.83	2332.66

2. Concrete shear capacity based on web shear cracking, Vcw

The shear contribution of the harped tendons is found using:

$$\sin\psi := \frac{cgs_e - cgs_c}{68} \qquad \sin\psi = 0.09$$

$$V_p(x) := \begin{cases} \left(P_e \cdot \sin\psi \cdot 10^{-3}\right) & \text{if } x \le 5.67 \\ 0 & \text{if } x > 5.67 \end{cases} \quad kips$$

Also :

$$y := y_{bc} - y_b$$

$y = 9.26 \quad in$ distance between centroid of precast and composite sections

Therefore :

$$f_{pc}(x) := \frac{P_e}{A_{cp}} - \frac{P_e \cdot e(x) \cdot y}{I_c} + \frac{M_d(x) \cdot y}{I_c}$$

$$V_{cw}(x) := \frac{\left(3.5\lambda \cdot \sqrt{f_c} + 0.3\, f_{pc}(x)\right) \cdot b_w \cdot d_p(x)}{1000} + V_p(x) \qquad \lambda = 1 \text{ normal concrete}$$

3. Shear strength of concrete, V_c :

In the ACI code, V_c is the lesser of V_{ci} and V_{cw}, therefore :

$$V_{c\_ACI}(x) := min\left(V_{cw}(x), V_{ci}(x)\right)$$

4. Shear capacity of steel stirrups, V_s:

Stirrup:Two-legs #3 @ 12 in o.c.

$$A_s := 0.22 \quad in^2 \qquad s := 12 \quad in \qquad V_{s\_ACI}(x) := \frac{A_s \cdot f_y \cdot d_p(x)}{1000\, s} \quad kips$$

5. Then, Vn based on the ACI code is:

$$V_{n\_ACI}(x) := V_{c\_ACI}(x) + V_{s\_ACI}(x)$$

The values of V_{ci}, V_{cw}, V_{c_ACI}, V_{s_ACI}, and V_{n_ACI} along the beam are listed below:

dis.from left	$V_{ci}(x)$	$V_{cw}(x)$	$V_{c\_ACI}(x)$	$V_{s\_ACI}(x)$	$V_{n\_ACI}(x)$
(ft)	(kips)	(kips)	(kips)	(kips)	(kips)
$x =$	$V_{ci}(x) =$	$V_{cw}(x) =$	$V_{c\_ACI}(x) =$	$V_{s\_ACI}(x) =$	$V_{n\_ACI}(x) =$
0.5	442.73	74.19	74.19	21.28	95.47
1	233.16	73.69	73.69	21.28	94.96
1.5	163.31	73.19	73.19	21.28	94.46
2	128.39	72.68	72.68	21.28	93.96
2.5	107.44	72.18	72.18	21.28	93.46
3	93.47	71.68	71.68	21.28	92.96
3.5	83.5	71.18	71.18	21.28	92.46
4	76.04	70.89	70.89	21.35	92.24
4.5	30.29	71.75	30.29	21.85	52.13
5	27.47	72.59	27.47	22.34	49.81
5.5	28.96	73.41	28.96	22.83	51.8
6	30.01	62.39	30.01	23	53.02
6.5	30.86	62.39	30.86	23	53.87
7	31.83	62.39	31.83	23	54.84
7.5	32.94	62.39	32.94	23	55.94
8	34.2	62.39	34.2	23	57.2
8.5	35.65	62.39	35.65	23	58.65
9	37.3	62.39	37.3	23	60.31
9.5	39.21	62.39	39.21	23	62.22
10	41.42	62.39	41.42	23	64.43
10.5	43.99	62.39	43.99	23	66.99
11	46.99	62.39	46.99	23	69.99
11.5	50.52	62.39	50.52	23	73.53
12	54.72	62.39	54.72	23	77.72
12.5	59.76	62.39	59.76	23	82.76
13	65.88	62.39	62.39	23	85.39
13.5	73.44	62.39	62.39	23	85.39
14	82.96	62.39	62.39	23	85.39
14.5	95.24	62.39	62.39	23	85.39
15	111.58	62.39	62.39	23	85.39
15.5	134.28	62.39	62.39	23	85.39
16	167.74	62.39	62.39	23	85.39
16.5	221.64	62.39	62.39	23	85.39
17	322.25	62.39	62.39	23	85.39
17.5	574.45	62.39	62.39	23	85.39
18	2332.66	62.39	62.39	23	85.39

Plot of Shear Capacity Profile for T-Beam 3

Figure A.3 shows the profile of V_c, the nominal shear strength provided by concrete. Compared to the ACI code, the AASHTO approach gives a much lower estimate of shear capacity, especially in the test shear span between the left support and the load point.

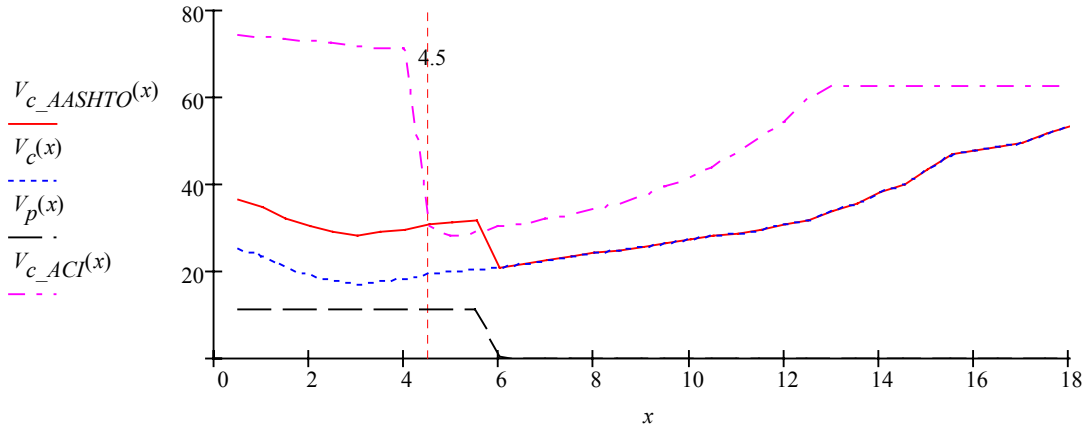

Where: $V_{c\_AASHTO}(x) := V_c(x) + V_p(x)$

Figure A.3: Shear capacity of concrete, V_c

Figure A.4 shows the profile of V_s, the nominal shear strength provided by shear reinforcement. The difference between the AASHTO and the ACI approach is that the AASHTO Code considers the crack inclination, θ, while the ACI Code assumes constant 45°. This results in a higher contribution of the steel stirrups in the AASHTO approach.

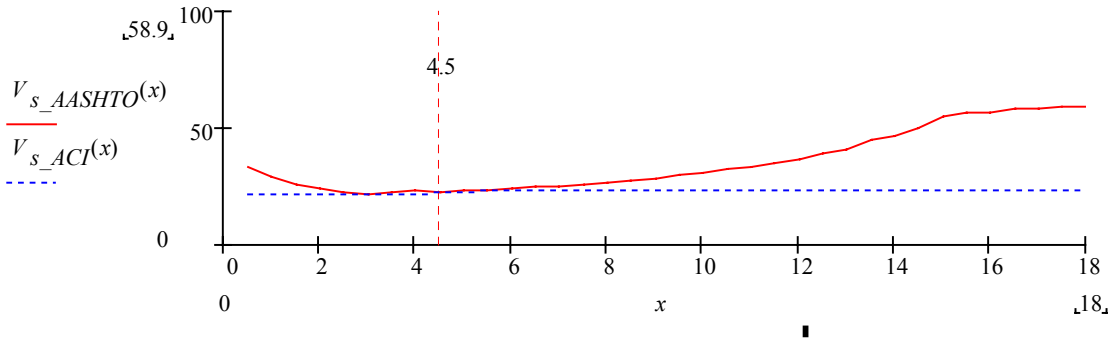

Figure A.4: Shear capacity of steel stirrups, V_s

Figure A.5 shows the applied shear diagram for T-Beam 3C at maximum load, and the shear capacity predicted by the AASHTO and ACI codes for the beam without CFRP shear retrofit.

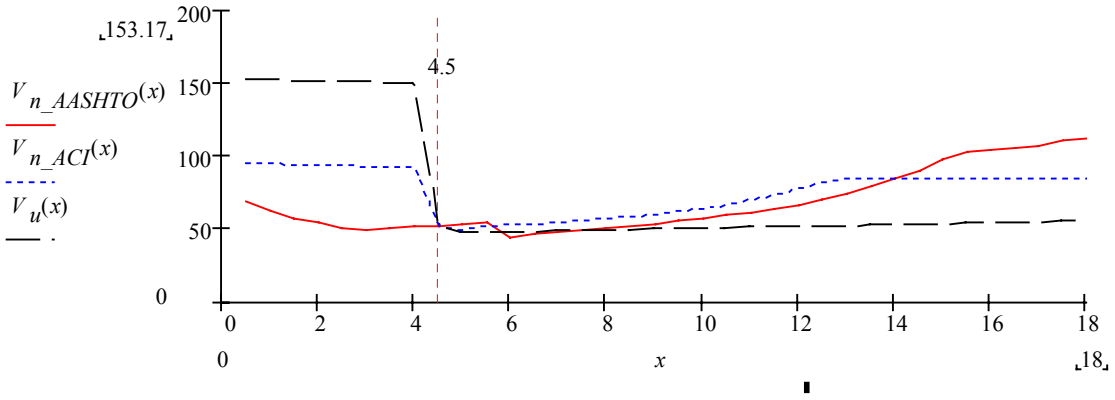

Figure A.5: Shear capacity and shear diagram of T-Beam 3C

The minimum shear capacity predicted by AASHTO code for the test span (left span) is, V_n = 49.77 kips at 3' from the left support, while the ACI code prediction is V_n = 92.24 kips at 4' from the left support. The maximum shear supported by the left shear span was 153 kips. Both codes are conservative in predicting shear capacity of the T-Beam, with more conservatism in the AASHTO prediction.

Prediction of the Short-Term Load-Deflection Relationship

In this section, the short-term load-deflection relationship of the T-Beam without retrofit is predicted based on the ACI code provisions. The calculations include 2 stages, precracking and postcracking. In the precracking stage, the uncracked member is assumed to have linear elastic behavior and ends at the initiation of the first flexural crack. In the postcracking stage the structural member develops acceptable controlled cracking in both distribution and width. Most beams lie in this region at service load.

Because of uncertainty regarding the effective prestress in the beam, and the concrete cracking strength, upper and lower bound estimates were included. The effective prestress was assumed to be between 0.7 and 0.8 f_{pi}, and the modulus of rupture was assumed to be between 6 and 7.5 $\sqrt{f_c}$. These ranges produce upper and lower bound estimates of the cracked moment of inertia. The calculation procedure is presented below.

T-Beam 3 was simply supported on an 18 feet span with a single line load applied at 4.5 ft from the left support. Here we want to find the P-Δ curve at the load point

Useful Properties

Prestressed Beam Scetion:

$f_c := 8405 \ psi$ $f_{pu} := 250000 \ psi$ $f_{pi} := 187500 \ psi$ $f_{pe} := 150000 \ psi$

$A_{ps} := 0.8 \ in^2$ $P_e := f_{pe} \cdot A_{ps}$ $P_e = 120000 \ lb$

$A_{cp} := 200.75 \ in^2$ $I_p := 10115 \ in^4$ $b_w := 5.5 \ in$ $h := 24 \ in$

$y_b := 8.97 \ in$ $y_t := 15.03 \ in$ $L := 24 \ ft$ $E_{ps} := 28500$ ksi

$S_{bp} := \frac{I_p}{y_b}$ $S_{tp} := \frac{I_p}{y_t}$ $S_{bp} = 1127.65 \ in^3$ $S_{tp} = 672.99 \ in^3$

$cgs_c := 3.85$ in from bottom $cgs_e := 10.25$ in from bottom

$e_c := y_b - cgs_c$ $e_c = 5.12$ in Eccentricity of prestresses at center

$e_e := y_b - cgs_e$ $e_e = -1.28$ in Eccentricity of prestress at support

Topping Slab: $f_{ct'} := 5114 \ psi$ $b_f := 66 \ in$ $h_c := 28.5 \ in$

CFRP Carbodur: $f_{fe} := 177000 \ psi$ $A_f := 0.5642$ $A_f = 1.13 \ in^2$

Gross Concrete Section:

$E_{cp} := 4667$ ksi : prestressed concrete $E_{cs} := 3104$ ksi : topping concrete $n_c := \frac{E_{cs}}{E_{cp}}$ $n_c = 0.67$

$E_f := 23900$ ksi : CFRP Carbodur $n_f := \frac{E_f}{E_{cp}}$ $n_f = 5.12$

transform topping to prestressed area: $A_{top} := b_f \left(h_c - h\right) \cdot n_c$ $A_{top} = 197.53 \ in^2$

Therefore, the Gross Concrete section area is : $A_{Gc} := A_{cp} + A_{top}$ $A_{Gc} = 398.28 \ in^2$

$y_{bc} := \frac{A_{cp} \cdot y_b + A_{top} \cdot (h + 2.25)}{A_{Gc}}$ $y_{bc} = 17.54 \ in$ $y_{tc} := h_c - y_{bc}$ $y_{tc} = 10.96 \ in$

$I_c := I_p + A_{cp} \cdot \left(y_{bc} - y_b\right)^2 + \frac{b_f \left(h_c - h\right)^3}{12} + A_{top} \cdot \left(h + 2.25 - y_{bc}\right)^2$ $I_c = 40345.94 \ in^4$

$S_{bc} := \frac{I_c}{y_{bc}}$ $S_{tc} := \frac{I_c}{y_{tc}}$ $S_{bc} = 2300.2 \ in^3$ $S_{tc} = 3681.27 \ in^3$

1) find Mcr:

Under the load point: $e := 3.92 \quad in \qquad d_p := 23.41 \quad in$

Also : $r := \sqrt{\frac{I_p}{A_{cp}}} \qquad r = 7.1 \quad in \qquad \lambda := 1 \qquad c_b := y_b \qquad c_b = 8.97 \ in$

Using f_{pe} = 0.8 fpi, and a modulus of rupture value of $7.5\sqrt{f_c}$

$$M_{cr\_upper} := 10^{-3} S_{bc} \cdot \left[\left(7.5 \cdot \lambda \cdot \sqrt{f_c} \right) + \frac{P_e}{A_{cp}} \cdot \left(1 + \frac{e \cdot c_b}{r^2} \right) \right]$$

$$M_{cr\_upper} = 3916.09 \quad kips - in \qquad P_{cr\_upper} := \frac{M_{cr\_upper}}{4.5 \cdot 12} \cdot \frac{4}{3} \qquad P_{cr\_upper} = 96.69 \quad kips$$

Using f_{pe} = 0.7 fpi, and a modulus of rupture value of $6.0\sqrt{f_c}$

$$P_{e2} := 0.7 \cdot f_{pi} \cdot A_{ps} \qquad P_{e2} = 105000 \quad lb$$

$$M_{cr\_lower} := 10^{-3} S_{bc} \cdot \left[\left(6.0 \cdot \lambda \cdot \sqrt{f_c} \right) + \frac{P_{e2}}{A_{cp}} \cdot \left(1 + \frac{e \cdot c_b}{r^2} \right) \right]$$

$$M_{cr\_lower} = 3307.95 \quad kips - in \qquad P_{cr\_lower} := \frac{M_{cr\_lower}}{4.5 \cdot 12} \cdot \frac{4}{3} \qquad P_{cr\_lower} = 81.68 \quad kips$$

2) find Icr :

$b_{eff} := b_f \ n_c \qquad b_{eff} = 43.9 \quad in \qquad n_p := \frac{E_{ps}}{E_{cp}} \qquad n_p = 6.11$

assume : $x := 1$

$$Given \qquad \left[\left[A_{ps} \cdot n_p \cdot \left(d_p - x \right) + A_f \ n_f \left(h_c - x \right) \right] - b_{eff} \cdot \frac{x^2}{2} \right] = 0$$

$Find(x) = 3.33$ (abandon the negative root x = - 3.36) So : $x := 3.33$ in within the flange, then O.K.

$$I_{cr} := \frac{b_{eff} \cdot x^3}{12} + b_{eff} \cdot x \cdot \left(\frac{x}{2} \right)^2 + A_{ps} \cdot n_p \cdot \left(d_p - x \right)^2 + A_f \ n_f \left(h_c - x \right)^2 \qquad I_{cr} = 6169.73 \quad in^4$$

3) find $I_{effective}$:

$P := 1 .. 198 \quad kips \qquad M_a(P) := 4.5 \cdot 12 \cdot 0.75 \cdot P$

$$I_{e\_upper}(P) := \left(\frac{M_{cr\_upper}}{M_a(P)} \right)^3 \cdot I_c + \left[1 - \left[\left(\frac{M_{cr\_upper}}{M_a(P)} \right)^3 \right] \right] \cdot I_{cr}$$

$$P_l := 1..198 \quad kips \qquad M_{a\_l}(P_l) := 4.5 \cdot 12 \cdot 0.75 \cdot P_l$$

$$I_{e\_lower}(P_l) := \left(\frac{M_{cr\_lower}}{M_{a\_l}(P_l)}\right)^3 \cdot I_c + \left[1 - \left[\left(\frac{M_{cr\_lower}}{M_{a\_l}(P_l)}\right)^3\right]\right] \cdot I_{cr}$$

4) find δ(P) :

$$\delta_{upper}(P) := \begin{cases} \left(68 \cdot 12^3 \cdot \frac{P}{E_{cp} \cdot I_c}\right) & \text{if } M_a(P) \le M_{cr\_upper} \\ \left(68 \cdot 12^3 \cdot \frac{P}{E_{cp} \cdot I_{e\_upper}(P)}\right) & \text{if } M_a(P) > M_{cr\_upper} \end{cases} \quad in$$

$$\delta_{lower}(P_l) := \begin{cases} \left(68 \cdot 12^3 \cdot \frac{P_l}{E_{cp} \cdot I_c}\right) & \text{if } M_{a\_l}(P_l) \le M_{cr\_lower} \\ \left(68 \cdot 12^3 \cdot \frac{P_l}{E_{cp} \cdot I_{e\_lower}(P_l)}\right) & \text{if } M_{a\_l}(P_l) > M_{cr\_lower} \end{cases} \quad in$$

Figure A.7 shows the prediction for the short-term load-deflection relationship of the T-Beam 3C without retrofit based on the ACI code.

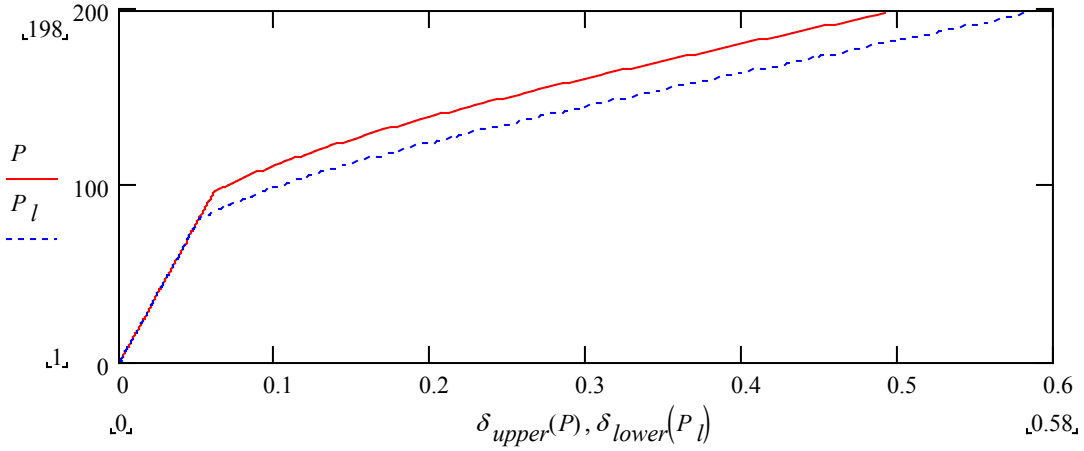

Figure A.7: Short-term load-deflection relationship prediction